Rapid, Accurate, Precise and Reproducible Binding Affinity Calculations using Ensembles of Molecular Dynamics Simulations

Agastya Prakash Bhati

A dissertation submitted in partial fulfillment

of the requirements for the degree of

Doctor of Philosophy

of

University College London.

Department of Chemistry

University College London

April 30, 2018

I, Agastya Prakash Bhati, confirm that the work presented in this thesis is my own. Where information has been derived from other sources, I confirm that this has been indicated in the thesis.

Bhagwad Gita - Chapter 2, verse 47

कर्मण्येवाधिकारस्ते मा फलेषु कदाचन।
मा कर्मफलहेतुर्भूर्मा ते सङ्गोऽस्त्वकर्मणि॥ २-४७

(You have the right to work only but never to its fruits. Let not the fruits of action be your motive, nor let your attachment be to inaction.)

Dedication

I dedicate this thesis to my parents Dr. Om Prakash and Dr. Praveena Bhati. This is another milestone in the journey. With your blessings, I hope to continue making progress in life.

Abstract

The accurate prediction of the binding affinities of ligands to proteins is a major goal in drug discovery and personalised medicine. The use of *in silico* methods to predict binding affinities has been largely confined to academic research until recently, primarily due to the lack of their reproducibility, as well as unaffordably longer time to solution. In this thesis, I mainly describe the ensemble based molecular dynamics approaches, ESMACS and TIES, that provide a route to reliable predictions of free energies meeting the requirements of speed, accuracy, precision and reliability. The performance of both these methods when applied to a diverse set of protein targets and ligands is reported. The results are in very good agreement with experimental data while the methods are repeatable by construction. Statistical uncertainties of the order of 0.5 kcal/mol or less are achieved. These methods have been further extended to incorporate enhanced sampling techniques based on replica exchange (also known as parallel tempering) to handle situations where conformational sampling is difficult using standard molecular dynamics. A critical assessment of free energy estimators like MBAR has been made for their application in binding affinity prediction. The methodologies described are shown to have a positive impact in the drug design process in the pharmaceutical domain as well as in personalised medicine, with concomitant potential major industrial and societal impact. Finally, our automated workflow, comprising the Binding Affinity Calculator (BAC) together with the FabSim are described. These tools and services help us complete the entire execution in 8 hours or less, depending on the high performance architecture and hardware available.

Impact Statement

Classical molecular dynamics (MD) simulations have been in use to simulate proteins for about 4 decades now. Over the last couple of decades, there has been a lot of advancement in the development of techniques based on classical MD simulations to calculate free energy, which is a thermodynamic property, of biomolecular systems. In spite of such tremendous progress, such techniques suffer from the issue of non-reproducible results, due to the practice of performing only a single insufficiently long simulation, making them unreliable. It has been well acknowledged in the literature that the predicted free energies yielded by such techniques vary by non-negligible values on simply repeating the calculation. In this work, I have recognised the underlying cause of this problem and developed protocols to overcome it. I have introduced the concept of "ensemble simulation" and developed two new methods namely, "thermodynamic integration with enhanced sampling (TIES)" and "enhanced sampling of molecular dynamics with approximation of continuum solvent (ESMACS)", based on it. In this thesis, I have provided sufficient evidence to show that TIES and ESMACS yield accurate, precise and reproducible free energies rapidly for a variety of biomolecular systems. In this way, I have successfully addressed a fundamental issue in the field of MD-based free energy calculations. This has attracted great attention from my peers (as of now, my research article introducing TIES has been cited 16 times in the short time of 16 months). The aforementioned methods have direct applications in important areas like drug design and precision medicine as highlighted below.

I have shown in my work that even the improved MD-based free energy methods, that accelerate the convergence of results using better sampling techniques and statistically optimal free energy estimators, exhibit a similar variation in their results on repeating the calculations. This observation will be of great interest to all the researchers working in the field of free energy calculations.

TIES and ESMACS constitute complex computational workflows and implementing them manually is quite tedious and error-prone. Therefore, in order to make them easily usable, I developed an automation toolkit comprising of the "Binding Affinity Calculator (BAC)" and "FabSim". It provides an error-proof way of implementing these workflows and helps perform the calculations rapidly, which further enhances their applicability as explained in the following paragraph.

There is a huge scope for the pharmaceutical companies to employ MD-based free energy methods in the initial stages of drug discovery, which would help them cut down both the cost and time required to develop new drugs. In the case of precision medicine, these methods can be used as a tool to predict the effect of clinically observed mutations on the affinity of drugs (a common cause of the development of drug resistance). However, the lack of reliability and the long time-to-solution of free energy methods had been limiting their application in both these areas. TIES and ESMACS are not constrained by such limitations and have been successfully employed in my collaborations with two pharmaceutical companies, GlaxoSmithKline and Pfizer.

Acknowledgements

The long journey of my PhD could have not been possible without the support, motivation and help from several people. I would like to express my thankfulness to all these people.

First of all, I would like to thank my supervisor Professor Peter V. Coveney, whose guidance always kept me going in the right direction. He granted enough room for my own ideas but also advised me whenever needed, which led me to accomplish my research work. He always motivated me and it has been fun working under his supervision. I would also like to extend my sincere gratitute to Shunzhou and Dave for all the useful scientific discussions, which helped me progress quickly with my research. I learnt several technicalities from them, without which my progress would have been much slower. I am thankful to Derek for his support and advice in the development of FabBioMD, which provided momentum to my work.

I take this opportunity to thank all my present and past colleagues at CCS (in no particular order: James, Robin, Hugh, Emily, Ulf, Stefan, Sebastian, Alex, Fouad, Maxime, Kristoff, Charlotte, Laura), who made my working hours joyful and provided a healthy working atmosphere. A special thanks to Serge and Robbie for being great PhD fellows and friends.

I cannot forget to thank all my friends Anuj, Aditya, Shiv Charan, Zulkifli, Tiago and Harshvardhan, who have been my companions in good and bad times for the last few years and have always been there in the hour of need. A special mention of Priyal is necessary to express my gratitude for her being a great company throughout.

Nothing is possible without financial resources. I would like to acknowledge UCL and Inlaks Shivdasani Foundation for providing me scholarships. I am thankful to the department of Chemistry at UCL for providing me infrastructure. I acknowledge the use of ARCHER, UK's national High Performance Computing Service, HPC facilities of the STFC's Hartree Centre and those of the Leibniz Research Centre for all the work presented in this thesis.

No acknowledgement would ever adequately express my gratitude to my family. I would like to specially mention Dr. Om Prakash, Dr. Praveena and Aditya Bhati for always believing in me. Their moral support has always boosted my confidence and their teachings have always enabled me to progress in life.

Publications

The following publications and presentations have arisen from this thesis.

Publications

- D. Groen, A. P. Bhati, J. Suter, J. Hetherington, S. Zasada, and P. V. Coveney. "FabSim: facilitating computational research through automation on large-scale and distributed e-infrastructures." *Computer Physics Communications*, 207, 375385 (2016), DOI:10.1016/j.cpc.2016.05.020.

- A. P. Bhati, S. Wan, D. Wright, P. V. Coveney. "Rapid, accurate, precise and reliable relative free energy prediction using ensemble based thermodynamic integration." *Journal of Chemical Theory and Computation*, 13(1), 210-222 (2017), DOI: 10.1021/acs.jctc.6b00979.

- S. Wan, A. P. Bhati, S. J. Zasada, I. Wall, D. Green, P. Bamborough, P. V. Coveney. "Rapid and Reliable Binding Affinity Prediction of Bromodomain Inhibitors: a Computational Study." *Journal of Chemical Theory Computation*, 13(2), 784-795 (2017), DOI: 10.1021/acs.jctc.6b00794.

- S. Wan, A. P. Bhati, S. Skerratt, K. Omoto, V. Shanmugasundaram, S. Bagal, P. V. Coveney. "Evaluation and Characterization of Trk Kinase Inhibitors for the Treatment of Pain: Reliable Binding Affinity Predictions from Theory and Computation.", *Journal of Chemical Information and Modelling*, 57(4), 897-909 (2017), DOI: 10.1021/acs.jcim.6b00780.

- A. P. Bhati, S. Wan, Y. Hu, B. Sherborne, P. V. Coveney. "Uncertainty Quantification in Alchemical Free Energy Methods.", *Journal of*

Chemical Theory Computation, Just Accepted Manuscript (2018), DOI: 10.1021/acs.jctc.7b01143.

Oral Presentations

- "Rapid, accurate, precise and reliable relative free energy prediction using ensemble based thermodynamic integration", *11^{th} European Conference on Theoretical and Computational Chemistry (11EuCOTCC)*, September 2017, Institute for Catalan Studies, Barcelona, Spain.

- "Rapid, accurate, precise and reliable relative free energy prediction using ensemble based thermodynamic integration", *4^{th} Scientific and Industrial Conference by PRACE - PRACEDays17*, May 2017, Polytechnic University of Catalonia, Barcelona, Spain.

- "Rapid, precise and reproducible binding affinity calculations for drug-protein interactions", *15^{th} European Conference on Computational Biology (ECCB 2016)*, September 2016, World Forum Convention Centre, The Hague, Netherlands.

- "Computing ligand-protein free energies using multiscale methods", *Solvay workshop on "Bridging the gap at the PCB interface"*, April 2016, Université libre de Bruxelles, Brussels, Belgium.

- "Rapid, precise and reproducible binding affinity calculations for drug-protein interactions", *2^{nd} workshop on High Throughput Molecular Dynamics*, November 2015, Barcelona Biomedical Research Park (PRBB), Barcelona, Spain.

Poster Presentations

- "Rapid, accurate, precise and reliable relative free energy prediction using ensemble based thermodynamic integration", *Computational Molecular Science 2017 conference*, March 2017, University of Warwick, United Kingdom.

- "Rapid, Accurate and Reproducible Binding Affinity Calculations for Drug-Protein Interactions", *CCP5 Summer School 2015*, July 2015, University of Manchester, United Kingdom.

- "Rapid, Accurate and Reproducible Binding Affinity Calculations for Drug-Protein Interactions", *Exascale Applications and Software Conference (EASC) 2015*, April 2015, University of Edinburgh, United Kingdom.

Contents

List of Figures

List of Tables

Chapter 1

Introduction

Reproducibility is an intrinsic characteristic of any scientific result, whether experimental or computational. A method cannot be reliable if it does not yield the same result when performed by others. However, the lack of reproducible results in the published literature is a rising concern in the scientific community[1]. This is true for all fields of research and for both computational and experimental methods. It was recently revealed through a survey by *Nature* that more than 70% of researchers failed to reproduce another researcher's results, while more than half were unable to reproduce their own[2]. In the case of experiments, non-reproducible results can be an artifact of factors ranging from mixed up chemicals, through confirmational bias[3, 4], fluctuations in the environment to variations in the experimental setup[5, 6]. In the case of computer-based methods, the reasons may lie in the theory or the model used, convergence of the calculations, reliability of the software, and so on[7].

The use of computer models and simulations to understand natural systems has become widespread, encompassing many diverse disciplines in academia as well as industry. The systems studied can be as small as sub-atomic particles and as large as the universe itself. The biggest advantage of computational modelling is that it provides insight into the underlying mechanisms of the processes studied, which are often inaccessible experimentally, within the limits of the approximations in the model and the theory concerned. Computer simulations can be performed under conditions at which it is impossible to conduct

experiments, for instance, at very high pressures and temperatures. In addition, one can argue that computational techniques may cut down both time and cost as well as help the environment by reducing chemical waste in processes like drug design. Due to such advantages, computer-based techniques are becoming increasingly popular among researchers from all backgrounds, and are being adopted as routine techniques by a large section of the scientific community. The relentless improvement in performance of computers is another contributor to the increasing adoption of computer-based methods in sciences during the last few decades.

Given the growing popularity of computational techniques, it is all the more necessary to ensure that the results and conclusions from these techniques are reproducible. Only when the results from a computational technique are repeatable irrespective of its user, time and place, can it be relied upon for taking actionable decisions and become a standard technique applicable in a scientific research, industrial or clinical context. The terms "reproducibility" and "repeatability" in the context of this thesis refer to the ability of a technique to yield the same results within the expected uncertainty on repeating the calculation with and without any variation in its implementation, the software and/or the hardware employed, respectively. This work is dedicated to improving the precision of free energy methods such that the results from two independent calculations are the same within the reported uncertainties making such methods more reliable.

In this thesis, I confine my studies to the field of free energy calculation methods based on classical molecular dynamics (MD) simulations and biomolecular systems. A systematic account of the variation in the results of *in silico* free energy calculations from independent short simulations and an explanation for its occurrence is provided. A solution to this problem is provided including substantial evidence of its ability to control the uncertainties in results. It should be noted that observations made regarding the variation in results through the work presented here are general and applicable to all methods based on

classical MD simulations when running a single short simulation. Before discussing more about the free energy calculation methods, below I mention their important applications and current shortcomings which I overcome using the methods presented in this thesis.

Applications of *In Silico* Free Energy Prediction

A ligand is any substance that binds reversibly and specifically to a biomolecule (a protein in the context of this thesis) and alters its activity. It is often a compound with low molecular weight and these are the ligands we consider here. Binding affinity is the change in the free energy associated with the binding event. The magnitude of the binding affinity is a measure of how strong the interaction is between the ligand and the protein, and hence it is often directly related to the potency of the ligand (in the case which the ligand is a drug).

The measurement of ligand-protein binding affinity is of importance in the fields of drug design and personalised medicine. It can be used as a virtual screening tool in drug design or as a clinical tool to tailor a patient's medication based on his/her genetic makeup. Computer-aided drug design (CADD) is an extremely active field of research[8]. In addition, rapid and accurate binding affinity predictions can be useful in health-related applications like design of medicines with reduced side-effects and drug resistance. Thus, the use of *in silico* techniques to predict binding affinities has grown immensely in the last few decades[9]. However, it should be noted that these applications of *in silico* binding affinity prediction are subject to their short time to solution and reliable predictions. The time needed to make a prediction should be shorter than that required by the experimentalists in industrial and clinical settings in order to influence decision making while, it is needless to say, the predictions should be reliable. Presently, both of these factors restrict the application of *in silico* methods in real-world scenarios.

Origin of the Variation in Results of Classical MD Based Methods

As mentioned earlier, several factors can lead to the variation in results between independent calculations in the case of methods based on short molecular simulation. For the classical MD based methods, such a variation in results from two independent short runs exists even on getting rid of all other sources of variation like the differences in force field parameters, MD engine, and so on. As we will discuss in detail in chapter 2, the prediction of macroscopic properties such as the Gibbs free energy using MD simulations requires ensemble averaging over microscopic states as dictated by the theory of statistical mechanics. Given the sensitivity of Newtonian dynamics to initial conditions, the trajectories from two different MD simulations diverge rapidly over time no matter how close their initial conditions[10]. This is true for essentially all MD simulations of complex systems. It is worth mentioning here that the equivalence of time average and the ensemble average via the ergodic theorem, which is a key assumption in all current classical MD based methods, holds in the limit of Poincaré recurrence time, which is extremely long and unapproachable on compute resources available today[10]. Thus, short trajectories may not be able to visit all relevant conformations and hence may lead to unconverged thermodynamic averages. This is also known as the "time-scale" problem.

Proposed Solution to Overcome the Variation in Results of Free Energy Methods

A possible solution to the problems mentioned above is to perform ensemble simulation as proposed in this thesis, breaking away from the traditional practice of performing a one-off simulation. Ensemble simulation in this context means performing multiple replicas of MD simulations, where each replica is an independent calculation initiated from a random initial condition. The results from ensemble simulations are accurate, precise and repeatable as will be

evident in the following chapters. It should be noted that the term "accuracy" in this thesis refers to the closeness of the results to the corresponding experimental values and it has been achieved within the limitations of the force field employed. Importantly, ensemble simulations provide a route to quantify the statistical uncertainties associated with the results. In addition, given the large size of modern high performance computing resources, all of the replicas can be run in parallel and hence the ensemble simulation can be run in the same wall-clock time as needed for running a single replica. This leads to a rapid outcome which is essential for improved applicability of free energy methods. The appropriate number of replicas and the duration of simulation for each replica are adjustable parameters which are dependent on the choice of system studied and the level of precision desired.

Considerable effort has been invested into the development of new sampling protocols in order to accelerate phase space sampling[11–16]. Among these, the most popular in the case of biomolecular simulations is the Hamiltonian-replica exchange (H-REMD)[17] and its variants - replica exchange with solute tempering (REST2)[18] and FEP/REST[19] - which have all been discussed in detail in Chapter 2. In addition, a free energy estimator called multistate Bennett acceptance ratio (MBAR)[20] is also becoming increasingly popular. Sometimes it is argued that the implementation of the "best" accelerated sampling protocol and the "best" free energy estimator, such as the ones mentioned here, may overcome the problem of the variation in results between independent short runs. In this work, the credibility of such claims has been evaluated by performing ensemble simulations using these so-called best practices (refer to chapter 4). Unsurprisingly, it is observed that, even in such cases, a single replica generates large variation and so the results obtained are non-repeatable. Moreover, I have demonstrated that running a single replica for extended duration (such that its total simulation time is equal to that of the ensemble of short simulations) also does not help and cannot be an alternative to ensemble simulation.

Brief Outline of the Thesis

The focus of the research presented in this thesis is to develop methods to calculate rapid and reliable free energies based on classical MD simulations which will overcome the problems of variation in results between independent short runs and long time to solution, and enhance the applicability of such methods in the context of drug design and personalised medicine. Chapter 2 provides the theoretical basis for calculating free energy computationally and an overview of the popular methods available for the same. It also describes the ensemble averaging approach employed in this work and how it leads to repeatable binding affinity predictions. Chapter 3 describes an approach based on alchemical free energy methods using ensemble simulations called thermodynamic integration with enhanced sampling (TIES)[21]. As the name suggests, TIES is based on the free energy method called thermodynamic integration (described in Chapter 2) and involves performing ensemble simulations at several intermediate points along the alchemical path followed by the stochastic integration of the potential energy derivative along that path to calculate the free energy and associated uncertainty. The successful application of TIES to a range of biomolecular systems has been demonstrated. The results are accurate and repeatable, and the method is able to capture important chemical properties of the systems studied. I have also provided a comparison of TIES results for the same biomolecular system from two different sources using different software and hardware along with some other variations in the calculations. They agree quite well indicating that TIES approach is reproducible too. Chapter 4 provides an account on the application of the TIES approach to the accelerated sampling methods, REST2[18] and FEP/REST[19], along with the employment of the free energy estimator MBAR[20] (all detailed in Chapter 2). The replicawise variation in results from short trajectories has been shown to exist irrespective of the sampling method and the free energy estimator employed. Evidence is provided to show that a single extended simulation (such that its total simulation time is equal to that of the ensem-

ble of short simulations) cannot be an alternate to the ensemble simulation. Chapter 5 describes another approach based on ensemble simulation called enhanced sampling of molecular dynamics with approximation of continuum solvent (ESMACS), which involves approximations while calculating the different components of free energy unlike TIES. The ESMACS approach is based on a free energy method called MMPBSA (described in detail in Chapter 2) and also involves calculating the entropic component using the normal mode analysis (detailed in Chapter 2). Different versions of ESMACS, namely 1-, 2- and 3-trajectory, have been employed and their results compared for different biomolecular systems. Chapter 6 contains the details of the software toolkit employed to automate the complex computational workflows of TIES and ESMACS. Chapter 7 provides conclusions for all the work presented and an outlook on the future directions of research based upon it.

TIES and ESMACS methodologies have been employed in our collaborative studies with two pharmaceutical companies, GlaxoSmithKline and Pfizer, yielding accurate and precise binding affinities. The results from both these studies have been published[22, 23], which exhibits the suitability of these approaches in drug design context as a reliable virtual screening tool. These results have been discussed in this thesis; TIES related discussion has been included in Chapter 3, while ESMACS related discussion in Chapter 5.

Chapter 2

Binding Affinity Prediction with Classical Molecular Dynamics

Proteins are complex macromolecules which constitute a substantial portion of human body mass and play an important role in the functioning and regulation of our cells and tissues. They are classified based on the functions they perform. An enzyme is a protein that acts as a catalyst in a chemical reaction taking place in the cell, while a receptor is one which receives a specific chemical signal (by selectively binding to the signalling molecule specific to it) to initiate a cellular or tissue response. The signalling molecule that binds to a receptor is termed ligand. It can be a protein, a peptide or any small organic molecule, for example a pharmaceutical drug, for which the receptor has high specific affinity. A ligand is called an agonist if it activates the receptor on binding resulting in a biological response, while it is called an antagonist if it does not activate the receptor on binding but blocks the binding site for any agonist, thereby inhibiting the latter's biological response. A cell's functions are encapsulated by the chemical reactions it carries out, which in turn, are controlled by regulating protein activity through the binding of agonists and antagonists. Thus, the phenomenon of molecules binding to proteins has great importance in our metabolism. Most drug molecules are antagonists which inhibit the biological response triggered by a disease's causative agent.

Binding affinity is a property used to quantify the extent of binding between a ligand and a protein. Section 2.1 describes binding affinity, a few experimental methods for its determination and the theory from statistical mechanics which forms the basis for its determination using computational methods. Section 2.2 briefly describes the theory and the implementation of classical molecular dynamics. Section 2.3 provides an overview of the available *in silico* methods based on classical MD simulations for determination of binding affinity, detailing the ones relevant for this thesis. Section 2.4 introduces the concept of ensemble simulation employed throughout this thesis to perform ensemble averaging and Section 2.5 provides its relationship to the repeatability of free energy predictions made using the *in silico* methods described in this chapter.

2.1 Binding Affinity

Binding affinity is a measure of the strength of interaction between a protein and a ligand. A stronger interaction leads to better binding. The binding affinity can be determined either experimentally or theoretically and there are several methods available in each category as described below. Each method quantifies the binding affinity in terms of different physical or physico-chemical quantities. Before describing a few popular methods, the underlying theory is discussed.

Consider a solution containing fixed concentrations of protein, P, and ligand, L. The reaction between them can be written as:

$$[P] + [L] \underset{k_{off}}{\overset{k_{on}}{\rightleftharpoons}} [PL] \tag{2.1}$$

where [P] and [L] denote the concentrations of the protein and ligand respectively, whereas [PL] denotes the concentration of their bound complex. k_{on} and k_{off} represent the association and dissociation rate constants measured in $M^{-1}s^{-1}$ and s^{-1}, respectively. At equilibrium:

$$K_d = \frac{[P]_{eq}[L]_{eq}}{[PL]_{eq}} = \frac{k_{off}}{k_{on}} = \frac{1}{K_a} \tag{2.2}$$

where $[..]_{eq}$ denotes the equilibrium concentration; K_d and K_a are the dissociation and association constants respectively. If $[P]_i$ is the initial concentration of protein, then $[P]_{eq} = [P]_i - [PL]_{eq} \implies [P]_i = [P]_{eq} + [PL]_{eq}$. It can be seen from Equation 2.2 that when $K_d = [L]_{eq}$, $[P]_{eq} = [PL]_{eq} = [P]_i/2$. Thus, the dissociation constant is the concentration of ligand at which half of the total available binding sites of protein are occupied by ligand at equilibrium. Therefore, the lower the value of K_d, the smaller concentration of ligand is sufficient to occupy the available binding sites, which in turn, can be related to higher level of attraction between the ligand and the protein. Consequently, K_d is a measure of binding affinity. When the ligand, L, is an inhibitor (that is, if binding reduces or eliminates protein activity), the dissociation constant of protein-inhibitor reaction is usually denoted as K_i. Equation 2.2 can be rearranged as:

$$\frac{[PL]_{eq}}{[P]_{eq}} = K_a[L]_{eq} \tag{2.3}$$

It can be seen from Equation 2.3 that the ratio of concentrations of bound and free protein is proportional to the association constant. Thus, the larger the value of K_a, the larger the probability of binding is, and hence, K_a is another measure of binding affinity.

Thermodynamics provides an alternate measure of binding affinity in terms of the change in appropriate thermodynamic potential depending on the reaction conditions such that it is minimised during the course of reaction. Standard experiments are conducted in open vessels with constant room pressure and temperature conditions (constant NPT). For such conditions, the appropriate thermodynamic potential is the Gibbs free energy (G). For Equation 2.1, the net change in G is given by:

$$\Delta G = G(PL) - G(P) - G(L) \tag{2.4}$$

The binding of P and L will only occur spontaneously if it leads to a net loss of G, that is, if the ΔG is negative. The more negative the ΔG, the stronger the

binding. Therefore, ΔG provides another measure of the binding affinity. It can also be related to the association constant, K_a, by the *van't Hoff* equation:

$$\Delta G = -RT \ln K_a = RT \ln K_d \tag{2.5}$$

where R and T are the universal gas constant and the temperature, respectively, and ΔG is the standard binding affinity.

2.1.1 Experimental Determination

Experimentally, quantitative *in vitro* analysis of the binding reaction is undertaken to determine the binding affinity. For this, a number of methods have been developed which detect and monitor the concentration of ligand and/or protein, including NMR spectroscopy, dynamic light scattering, fluorescence cross-correlation spectroscopy, affinity capillary electrophoresis, isothermal titration calorimetry, surface plasmon resonance and many more[24, 25]. In some experiments, the association and dissociation rate constants, k_{on} and k_{off} respectively, of the protein-ligand reaction (as shown in Equation 2.1) are measured based on which they report the binding affinity in terms of K_d (or K_i, when the ligand is an inhibitor). Isothermal titration calorimetry (ITC)[26] is a calorimetric approach which measures the heat loss or gain during the course of the reaction between protein and ligand based on which ΔG is reported. In the case of competitive antagonists (the ones which compete with the agonists to bind with the receptor), experiments usually report the half maximal inhibitory concentration known as IC_{50}. IC_{50} is defined as the concentration of inhibitor which reduces the receptor activity by half, that is, when half of the agonist bound to the receptor is replaced by the inhibitor (antagonist). It is not a direct measure of binding affinity, but is related to the binding affinity through the Cheng-Prusoff equation[27]:

$$K_i = \frac{IC_{50}}{1 + \frac{[S]}{K_m}} \tag{2.6}$$

where K_i and K_m are the dissociation constants of inhibitor and agonist for the receptor respectively, [S] is the agonist concentration. The dependence of IC_{50} on [S] and K_m implies that it can only be used to compare different inhibitors binding to the same receptor, but not same inhibitor binding to different receptors. When [S] is low, IC_{50} can be approximated as K_i, and Equations 2.5 and 2.6 give:

$$\Delta G \approx RT \ln(IC_{50}) \tag{2.7}$$

Due to this approximation ΔG values derived from IC_{50} values are considered to be less accurate than those from more direct sources such as ITC.

2.1.2 Determination Using Computational Methods

Computational methods usually take the thermodynamic route to measure binding affinity in terms of ΔG. They are commonly based on molecular level simulations, where a single molecule of protein-ligand complex is simulated to yield ΔG, which is macroscopic thermodynamic property. Statistical mechanics provides the link between microscopic simulations and macroscopic properties estimated. This section is dedicated to a brief discussion of some important concepts from statistical mechanics relevant for the determination of binding affinity using computer-based methods. For more details, refer to standard texts[28].

In classical statistical mechanics, the canonical partition function (Q) for a system of N indistinguishable molecules is defined as:

$$Q = \frac{1}{N!h^{3N}} \int \int exp\left(-\frac{E(\mathbf{p},\mathbf{r})}{k_B T}\right) d\mathbf{r} d\mathbf{p} \tag{2.8}$$

where k_B is Boltzmann's constant, T is absolute temperature, h is the Planck constant and $E(\mathbf{p},\mathbf{r})$ is the total energy of the system which depends on its coordinates ($\mathbf{r}$) and momenta ($\mathbf{p}$). The total energy of the system can be taken to be the sum of its kinetic and potential energies and the partition function

can be rewritten as:

$$
\begin{aligned}
E(\mathbf{p},\mathbf{r}) &= \sum_{i=1}^{3N} \frac{p_i^2}{2m} + U(\mathbf{r}) \\
Q = \frac{1}{N!h^{3N}} \left[\int \dots \int exp\left(-\frac{\sum p_i^2}{2mk_BT} \right) dp_1 \dots dp_{3N} \right] & \left[\int exp\left(-\frac{U(\mathbf{r})}{k_BT} \right) d\mathbf{r} \right] \\
&= \frac{Z}{N!h^{3N}} \left[\int_{-\infty}^{+\infty} exp\left(\frac{-p^2}{2mk_BT} \right) dp \right]^{3N} \\
&= \frac{Z}{N!} \left(\frac{2\pi mk_BT}{h^2} \right)^{3N/2} \\
Z &= \int exp(-\frac{U(\mathbf{r})}{k_BT}) d\mathbf{r}
\end{aligned}
\tag{2.9}
$$

where, $U(\mathbf{r})$ is the potential energy of the system, m is the molecular mass and Z is the configurational integral. The partition function can be used to calculate the measurable properties of a system, and hence, provides a link between its microscopic states and macroscopic variables. For example, the Helmholtz free energy (A) of a system with partition function (Q) is given by:

$$A = -k_BT \ln Q \tag{2.10}$$

As mentioned earlier, the binding reaction is driven by the need of minimising an appropriate thermodynamic potential depending on the conditions of the reaction. In case of constant number of particles (N), volume (V) and temperature (T), also known as canonical ensemble, the appropriate potential is Helmholtz free energy (A), while in case of constant NPT (P is the pressure), also known as isothermal-isobaric ensemble, the Gibbs free energy (G) is the appropriate quantity. These two state functions are related as follows:

$$G = A + PV \tag{2.11}$$

where, P and V are pressure and volume. For condensed phase system, such as biomolecules in aqueous solutions, the contribution to free energy from

change in volume in isothermal-isobaric ensemble is negligible, and hence can be neglected. On doing this, $G \equiv A$, and hence, a unified notation (G) will be used for free energy henceforth.

If we want to calculate the free energy difference between two well-defined states 1 and 2, it can be expressed in terms of a ratio of the two partition functions corresponding to each state. Let Q_1 and Q_2 be the partition functions for states 1 and 2 respectively, the difference in their free energies is given by:

$$\Delta G = G_2 - G_1 = -k_B T \ln \left(\frac{Q_2}{Q_1} \right) \tag{2.12}$$

The ratio of partition functions can be simplified as:

$$\frac{Q_2}{Q_1} = \left\langle exp \left(\frac{-(E_2 - E_1)}{k_B T} \right) \right\rangle_1 \tag{2.13}$$

where $\langle \rangle_1$ denotes that the average of the enclosed quantity is evaluated from a thermodynamic ensemble for state 1, which essentially means that the term $exp(-(E_2 - E_1)/k_B T)$ for a particular configuration is weighed directly proportional to the probability of occurrence of that configuration in the ensemble of configurations of state 1. Thus, the free energy difference between two states can be computed from an ensemble average of the energy difference between a reference state and a perturbed state, as follows:

$$\Delta G = G_2 - G_1 = -k_B T \ln \left\langle exp \left(\frac{-(E_2 - E_1)}{k_B T} \right) \right\rangle_1 \tag{2.14}$$

It is worth mentioning here that, theoretically, E in Equation 2.14 is the total energy of the system. However, as shown in Equation 2.9, the kinetic energy component factorises out as the product of Gaussian integrals over momenta. Therefore, the momentum contribution to the free energy difference is zero.

All the methods for *in silico* binding affinity determination as described in the following sections will be derived from the above theory, more specifically from Equations 2.10 and 2.14. The key point to be noted here is that to calculate ΔG

in silico, one needs to compute the ensemble average of microscopic properties. Thus, the basic requirement for determining binding affinity is the generation of an ensemble of conformations for the microscopic system. Molecular dynamics is the method most commonly used to generate an ensemble of conformations as discussed in the next section.

2.2 Molecular Dynamics

Molecular dynamics (MD) provides a way of modelling the complex motion of biomolecules governed by their chemical interactions. Classical MD is based on classical mechanics and is popularly used for modelling protein dynamics given the large number of atoms in proteins. It should be noted here that classical MD is only a tool to study the temporal evolution of the simulated system. However, as discussed in the previous section, ensemble averaging over microstates needs to be performed in order to compute the macroscopic properties of a system like the Gibbs free energy. According to the ergodic theorem, the ensemble average is equal to the time average only in the limit of "long" time. Thus, a single short simulation cannot be used to compute ensemble averages. Nonetheless, the practice has been so. The reliability of such a practice is discussed in Section 2.4 and in the later chapters of this thesis. In the remainder of this section, classical MD is described briefly. The details on it can be found in standard texts like Leach[29], Frenkel and Smith[30] or Allen and Tildesley[31].

2.2.1 Implementation of Molecular Dynamics

In MD simulations, the smallest unit of the molecule is taken to be atom. Therefore, no sub-atomic level description of the system studied is possible using MD. All atoms are considered to be point masses with a given partial charge. The interactions between atoms are modelled using force field parameters as described in Section 2.2.2. All atoms in a system of interest are assigned initial positions and velocities and its trajectory is determined by numerically solving the Newton's equation of motion using an integrator. An important

criterion which an integrator should satisfy is energy conservation. There are several integrators available but the most commonly used ones are the Verlet-style algorithms like Verlet method[32], velocity Verlet method[31]. The latter is employed by the NAMD code used for all simulations in this work.

2.2.2 Force Fields

In classical molecular dynamics, the potential energy of a molecular system for a given set of nuclear coordinates is approximated as a parametric function of nuclear coordinates. The set of parameters and the function form used to model the system's energy is termed force field. Since the smallest unit of the molecular system in any force field is atom, the bonding information of the system must be explicitly provided. The functional form of a typical molecular mechanics force field (AMBER [33]) is as follows:

$$\begin{aligned} U = \sum_{bonds} K_R(r - r_0)^2 + \sum_{angles} K_\theta(\theta - \theta_0)^2 \\ + \sum_{dihedrals} \frac{V_n}{2}[1 + cos(n\phi - \gamma)] \\ + \sum_{i<j} \left(\frac{A_{ij}}{R_{ij}^{12}} - \frac{B_{ij}}{R_{ij}^{6}} + \frac{q_i q_j}{4\pi\epsilon R_{ij}} \right) \end{aligned} \tag{2.15}$$

In this equation, the first two terms treat bond stretching and angle bending by harmonic oscillator approximations, where r_0 and θ_0 are the equilibrium values of bond lengths and angles respectively, and K_R and K_θ are the force constants of bond and angle respectively. The third term accounts for bond torsions (dihedrals) due to bond rotation, where V_n represents the n-fold barrier to rotation (dihedral angle ϕ) about a bond with a phase angle of γ. The last term includes the non-bonded interactions in terms of van der Waals forces through the Lennard-Jones potential and electrostatic contribution through the Coulomb's potential. R_{ij} represents the interatomic distance between a pair of atoms i and j, A_{ij} and B_{ij} are Lennard-Jones parameters, q_i and q_j are the atomic point charges, and ϵ is the dielectric constant of the medium.

It is clear from Equation 2.15 that force field potential function contains many parameters such as force constants, equilibrium geometric parameters, Lennard-Jones parameters, atomic charges and so on. These parameters are obtained by fitting its potential function to experimental data or high-level quantum calculations and hence the potential energy calculated using force fields is said to be empirical. Some common force fields are AMBER [33], CHARMM[34], MMFF[35], GROMOS[36], OPLS[37], CEDAR[38], MM2[39] and MM3[40]. It should be noted that the force field functional form as well as parameters may differ depending on the physical conditions used for their parameterisation. AMBER employed in all the simulations performed for this thesis is parameterised to be suitable for studying proteins.

The force field formalism involves several assumptions. The functional form used to calculate the potential energy is itself an approximation. Another important one is transferability, that is, assuming that the parameters fitted for a relatively small set of molecules will remain valid for any molecule. For instance, it is generally assumed in all force fields that the equilibrium bond length and the harmonic force constant for the carbon-carbon single bond is the same for all molecules. An important limitation of force fields is that the number of atom combinations used for parameterisation is limited. Therefore, although the atom combinations in all amino acids have been parameterised, this may not be true for all molecules of interest. The General AMBER force field[41] has been developed to extend parameterisation to nearly all known atom combinations in organic molecules and has been used for ligand molecules in all simulations for this thesis.

2.2.3 Thermostats and Barostats

Experiments are generally performed at constant pressure and temperature conditions. Therefore, it is often desirable to perform simulations sampling conformations from isothermal-isobaric ensemble. A method which maintains the temperature of the system at a pre-defined value is known as thermostat, while one which maintains the pressure of the system at a fixed value a

barostat. There are a variety of thermostats and barostats available for MD simulations. Below we discuss the Langevin thermostat[42, 43] and Berendsen barostat[44] which have been employed in all simulations performed for this thesis.

The Langevin theromstat is analogous to the system of interest being embedded in a sea of small fictional particles. These smaller fictional particles create a damping force to the momenta of real atoms and give random kicks to the atoms by virtue of their motion. The equations of motion for MD simulations are replaced by the Langevin equation[42] which includes two additional terms corresponding to the damping force and the randomly fluctuating force which are related to each other such that the desired ensemble with constant temperature is recovered.

The Berendsen barostat involves coupling the simulating system with an external pressure bath. The extent of coupling is determined by a coupling parameter. Pressure is maintained by scaling the coordinates of the atoms and hence adjusting the volume of the system at each time step. The scaling factor is derived from the difference between the instantaneous pressure of the system and that of the external bath, the isothermal compressibility of the system and the coupling parameter.

2.2.4 Improving Computational Efficiency

There are several techniques employed in MD simulations to improve the computational efficiency of simulations while enhancing the simulation model's resemblance to real experimental system. A few of them are mentioned below.

MD simulations are usually performed using just a single molecule of the system of interest contained in a solvent buffer of a few tens of angstroms. In order for it to mimic the real experimental system and yield the bulk properties of the system, periodic boundary conditions are employed which increase the effective size of the system. The idea is to have an infinite array of replicates, called images, of the simulation box in all directions. The number of particles in the simulation box are conserved by allowing any particle leaving the

simulation box from one side be replaced by its image entering the box from the opposite side. The employment of periodic boundary conditions enables getting bulk properties by simulating a relatively small number of atoms.

The calculation of non-bonded energy terms is computationally much more expensive than that of the bonded energy terms as, unlike non-bonded interactions, the bonded interactions are limited to a few neighbouring atoms. A common strategy to reduce the computational cost for calculation of non-bonded energies is to introduce a cut-off distance beyond which all non-bonded energies are set to zero[29, 45]. Conventionally, the cut-off distance for periodic systems is set to a value smaller than half the length of the shortest edge of the simulation box so that each atom just interacts with only one image of any other atom. However, this scheme is effective only for the short range Lennard-Jones potential which tails off quickly with distance. Electrostatic interactions are long range and have considerable values even at long distances and hence this scheme is inaccurate for them.

In the case of periodic systems, the electrostatic potential can be evaluated more efficiently using the Ewald summation[46] or its improved variant particle-mesh Ewald (PME)[47]. These schemes assume that the periodic boundary conditions have been employed and compute the electrostatic potential energy as the sum of short range and long range terms. The short range terms are calculated using the standard Coulomb formula in real space while the long range terms are computed using Fourier transforms in reciprocal space. PME employs Fast Fourier Transform to compute the long range terms and hence is more efficient computationally. To further reduce the computational cost, the long-range electrostatic potential is sometimes not computed at every time step in the simulation but less frequently. Such an approach is referred to as a multiple time stepping algorithm[48].

The vibrational motion of hydrogen atoms bound to heavy atoms is usually the fastest motion in the simulated system, necessitating the use of a timestep of 1 fs. However, there are cases when these vibrations do not contribute sig-

nificantly to the overall dynamics of the system. In such cases, the lengths of these bonds can be constrained which in turn allows using a larger timestep (typically 2 fs in protein simulations). Several constraint algorithms are available for this purpose: SHAKE[49], RATTLE[50], SETTLE[51], M-SHAKE[52] and so on.

2.3 Methods for *In Silico* Determination of Binding Affinity

As detailed in the previous section, MD provides a tool to collect microstates of the biomolecule of interest. Thereafter, the theory of statistical mechanics can be applied to get the macroscopic thermodynamic properties G or ΔG from the ensemble of microstates. The statistical framework for macromolecular free energy calculations was first described by Zwanzig [53], Kirkwood [54], and Valleau and Torrie [55], but it could not be actually implemented until the advent of fast computers in the early 1980s. The first macromolecular free energy calculations were performed about three decades ago [56–59]. The methods so developed were used to calculate relative free energies for the binding of several ligands to a common receptor [59] and also to compute the binding affinity for a single ligand and receptor [60]. Later that decade, free energy studies started yielding exciting results and became very popular. Several excellent reviews in this field are available [61–79]. Today, there exist several methods to calculate the binding affinity based on non-biased MD simulations. Some of the popular ones, in order of decreasing speed and increasing accuracy, are:

- Empirical scoring methods, based on simplified energy functions representing different contributions to binding affinity [80–83].

- Linear interaction energy (LIE) method, where electrostatic part of the binding affinity is estimated using the linear response approximation, while the non-electrostatic contributions are derived using empirical

parameters[84].

- Molecular mechanics Poisson-Boltzmann surface area (MMPBSA) method, a semi-empirical method, where the solvent is approximated to be a continuum [85].

- Free energy perturbation (FEP)[53] and thermodynamic integration (TI)[86, 87].

Broadly, methods to calculate free energies can be classified into three classes based on the part of phase space sampled: (i) end-point methods, which sample just the bound and unbound states of protein-ligand complex, (ii) methods based on sampling along an alchemical thermodynamic pathway, and (iii) methods based on calculating free energy along a reaction coordinate, known as the potential of mean force (PMF). Another classification of free energy methods could be: "exact" and "approximate". The former are based directly on equations from statistical mechanics, while the latter start with statistical mechanics, but then incorporate some assumptions and approximations into those equations. One can logically conclude that the former are more accurate than latter. But there exists a trade-off between accuracy and speed, therefore, the former are computationally more expensive and time consuming than latter. In the rest of this section, the methods relevant to this thesis are described in more detail.

2.3.1 End-point Methods

End-point methods consider only the end states of the system, for example bound and unbound states of the protein-ligand complex, and calculate their absolute binding affinities. Methods like linear interaction energy (LIE)[84], linear response approximation (LRA)[88], molecular mechanics/Poisson-Boltzmann surface area (MM/PBSA)[85] and molecular mechanics/generalised Born surface area (MM/GBSA)[89]. Here, we describe the latter two.

MMPBSA is often considered to be the best compromise between the speed and accuracy of calculations. It is the most accurate among the approximate

methods and relatively less computationally expensive than exact methods. Being an end-point method, MMPBSA considers only the two end states of interest, that is, the protein and ligand in free and bound states and calculates their absolute free energies. The binding affinity is subsequently calculated as the difference of absolute free energies as shown below:

$$\Delta G = \langle G_{complex,aq} \rangle - \langle G_{receptor,aq} \rangle - \langle G_{ligand,aq} \rangle \tag{2.16}$$

However, in solvated systems the majority of contributions to free energy come from solvent-solvent interactions, resulting in large fluctuations. Therefore, each of the above absolute free energies is decomposed into several components as shown below[90–92]:

$$\langle G_{aq} \rangle = \langle G_{vac} \rangle + \langle G_{sol} \rangle \tag{2.17a}$$

$$\langle G_{vac} \rangle = \langle U_{MM} \rangle - T\langle S_{MM} \rangle \tag{2.17b}$$

$$\langle G_{sol} \rangle = \langle G_{polar} \rangle + \langle G_{np} \rangle \tag{2.17c}$$

where, $\langle ... \rangle$ denotes averaging over an ensemble of conformations, $\langle G_{aq} \rangle$ is free energy in solvated state, $\langle G_{vac} \rangle$ is free energy in vacuum, $\langle G_{sol} \rangle$ is free energy of solvation, which is the free energy change associated with taking a molecule from vacuum into solvent. $\langle U_{MM} \rangle$ represents the mean enthalpic energy of the solute and $\langle S_{MM} \rangle$ the mean solute entropy. $\langle G_{polar} \rangle$ is the polar solvation free energy and $\langle G_{np} \rangle$ the non-polar solvation free energy. It is worth mentioning here that the terms $\langle G_{polar} \rangle$ and $\langle G_{np} \rangle$ include both energetic and entropic components of solvent free energy and hence $\langle S_{MM} \rangle$ is the configurational entropy associated with solute motion only. In practice, a MD simulation is performed using explicit solvent and counter ions to get an ensemble of conformations for each state in Equation 2.16 and the different energy components are then calculated in the post processing step. The remainder of this section briefly describes the method of evaluating all the components of MMPBSA.

2.3.1.A Calculation of the Solute Enthalpic Contribution

The solute enthalpic term $\langle U_{MM} \rangle$ is calculated as the ensemble average of the molecular mechanical force field terms for the solute. It consists of

$$U_{MM} = U^{elec} + U^{vdW} + U^{int}, \tag{2.18}$$

where U^{elec} is the electrostatic energy, U^{vdW} is the van der Waals energy and U^{int} is the internal energy of the solute molecule. U_{int} can generally be decomposed into bond, angle and dihedral terms of the force field.

2.3.1.B Calculation of the Solvation Free Energy

In order to calculate the solvation free energy, $\langle G_{sol} \rangle$, the explicit solvent molecules and counter ions are removed from the MD trajectories and replaced by a continuum solvent. As mentioned above, $\langle G_{sol} \rangle$ has two components, one due to electrostatic interactions ($\langle G_{polar} \rangle$) and another due to non-polar interactions ($\langle G_{np} \rangle$).

The polar solvation free energy $\langle G_{polar} \rangle$ measures the energy corresponding to the presence of the solute's charge distribution in the continuum dielectric. It is calculated either by numerical solution of the linearised Poisson-Boltzmann (PB) equation[85, 93] or generalized-Born (GB) analysis [89, 94], which is a faster approximation to full PB model, for the snapshots from the MD trajectory. For typical biomolecules, the dielectric constants of solute and water are commonly chosen to be 1.0 and 80.0 respectively for PB calculations.

The non-polar contribution $\langle G_{np} \rangle$ accounts for the hydrophobic effect which promotes the association of non-polar surfaces of the receptor and ligand [95]. It is determined using an equation involving solvent accessible surface area (A)[96] and empirically derived parameters γ and b as shown in the equation below[97].

$$\langle G_{np} \rangle = \gamma A + b \tag{2.19}$$

The coefficient γ is taken to be positive which leads to higher (unfavourable) energy for conformations with more surface area (as it displaces more solvent

and hence needs more energy), and hence, it favours the binding which reduces surface area. The method has been named MMPBSA due to contributions from molecular mechanics (MM), Poisson-Boltzmann (PB) and surface area (SA) terms. It is called MMGBSA if the generalized-Born solvation energy is used instead of Poisson-Boltzmann.

It is important to mention here that MMPB(GB)SA involves taking the difference of large numbers (the absolute free energies are of the order of hundreds to thousands of kcal/mol) to determine relatively small binding affinity (of the order of tens of kcal/mol). Thus, it is important that the average absolute free energies converge to values invariant of simulation length and also have relatively low variances.

2.3.1.C Calculation of Configurational Entropy

The configurational entropy term $\langle S_{MM} \rangle$ can be calculated using quasi-harmonic analysis[98], normal-modes analysis [90] or restraint release approach[99]. However, due to complications involved in its calculation, it is often neglected for convenience. Here, we describe one of the most popular methods for calculating configurational entropy - normal mode analysis.

Normal mode analysis method is based on the assumption that translational, rotational and vibrational motions are independent from each other [100], and also that the potential energy for the 3N-6 mutually orthogonal vibrational degrees of freedom are harmonic with frequencies ω_i. The total entropy can then be calculated using the standard statistical mechanics formulae [28] as follows:

$$
\begin{aligned}
S_{vib} &= k_B \left[\sum_{i=1}^{3N-6} \frac{\alpha_i}{exp(\alpha_i) - 1} - \ln(1 - exp(-\alpha_i)) \right] \\
S_{rot} &= k_B \ln \left[\frac{\sqrt{\pi}}{\sigma} \left(\frac{T^3}{\Theta_A \Theta_B \Theta_C} \right)^{1/2} e^{3/2} \right] \\
S_{trans} &= k_B \ln \left[\left(\frac{2\pi m k_B T}{h^2} \right)^{3/2} \frac{V}{N} e^{5/2} \right]
\end{aligned}
\tag{2.20}
$$

where $\alpha_i = \hbar\omega_i/k_BT$, $\Theta_i = \hbar^2/2I_ik_B$ is the rotational temperature, I_i is one of the 3 principal moment of inertia I_A, I_B, I_C and σ is the symmetry number. Now, the problem of calculating conformational entropy of the molecule is essentially reduced to determining its harmonic vibrational frequencies. This can be done by diagonalizing the Hessian matrix **H** (a square matrix of order 3N with elements H_{ij}) of the system's potential energy (U) defined as follows:

$$H_{ij} = \left(\frac{\partial^2 U}{\partial x_i \partial x_j}\right) \tag{2.21}$$

where x_i and x_j are the i^{th} and j^{th} component of the 3N dimensional configuration of the system. In a normal mode analysis, the elements of the Hessian matrix are constructed from a single conformation of the solute molecule. To get the correct normal modes, the system needs to be at the minimum potential energy, that is, $\partial U/\partial x_i = 0$ and $\partial^2 U/\partial x_i \partial x_j > 0$ for each i and j [101–103]. Thus, first of all an energy minimization is performed in the normal mode analysis, followed by construction of the Hessian matrix and its diagonalization to get the normal mode frequencies. Finally, Equation 2.20 is applied to get the entropy. In practice, this procedure is applied on a selection of conformations from the MD trajectories to get an ensemble of S_{MM} and their average is the final solute configurational entropy $\langle S_{MM}\rangle$.

Swanson et al. [104] proposed the notion of free energy of association (referred to as ΔG_{Assoc} hereafter) to improve the validity of the binding affinity calculated using MMPB(GB)SA method. It accounts for the fact that a free molecule at standard concentration of 1-M has translational freedom of 1660 $\mathring{A}^3$ and rotational freedom of $8\pi^2$. On binding, the solute molecule loses these freedoms while solvent molecules gain an equivalent freedom. ΔG_{Assoc} can be seen as alternate way to compute the ΔS_{trans} and ΔS_{rot}. We use it in the following way to get the final binding affinity:

$$\Delta G = \langle U_{MM}\rangle + \Delta G_{Assoc} - T\langle S_{MM,vib}\rangle + \langle G_{solv}\rangle + \langle G_{np}\rangle \tag{2.22}$$

ΔG_{Assoc} is evaluated using quasiharmonic model from Equation 2.23. For more details about the method, refer to the literature [104, 105].

$$\Delta G_{Assoc} = -RT \ln \left(\frac{C^0 z_{ligand}^{trans} z_{ligand}^{rot}}{8\pi^2} \right) \tag{2.23}$$

where C^0 is the standard concentration 1 M, z_{ligand}^{trans} and z_{ligand}^{rot} are ligand translational and rotational configurational integrals, respectively.

2.3.1.D Single and Multiple Trajectory Approaches

As per Equation 2.16, in order to get the binding affinity, we need to calculate $G_{complex,aq}$, $G_{receptor,aq}$ and $G_{ligand,aq}$. The conformations of the complex, receptor and ligand can be extracted either from separate MD trajectories for each species, or all from a single MD trajectory of the protein/ligand complex, leading to multiple and single trajectory versions of MMPB(GB)SA. More precisely, the former is 3-trajectory, while the latter is 1-trajectory approach. The 1-trajectory approach has an advantage that contributions from parts of the system that do not affect binding exactly cancel as the same coordinates are used for the components both as part of the complex and separated. If separate trajectories are used then this exact cancellation of errors does not occur as each trajectory is free to explore different conformations, and hence, convergence of free energy might be difficult. On the other hand, the 1 trajectory approach is unable to account for alterations in the conformations available to the protein or ligand induced during binding and consequently may ignore important contributions to the overall binding affinity.

2.3.2 Alchemical Methods

A range of methods are based on calculating the free energy along a non-physical thermodynamic pathway, usually referred to as alchemical pathway, to yield free energy difference between its two end points. Such methods are termed as alchemical methods. The alchemical pathway usually corresponds to transformation of one chemical species at one end into a different chemical species at the other end of the pathway. In practice, this transformation is

defined as the function of a coupling parameter, λ, ranging between 0 (corresponding to the initial state) and 1 (corresponding to the final state). In the intermediate λ-states, the force field parameters are transformed from those of the initial state to those of the final state in a smooth fashion, if not linearly. The Hamiltonian of the system is defined in terms of λ such that it satisfies the above mentioned properties. For example, one commonly used function is:

$$E(\lambda, \mathbf{p,r}) = (1-\lambda)E_1(\mathbf{p,r}) + \lambda E_2(\mathbf{p,r}) \tag{2.24}$$

where E_1 and E_2 are the Hamiltonians of the initial and final states of the alchemical transformation respectively. At each intermediate λ-state, a MD simulation is performed to sample the conformations available to the system. After this, there are several ways to calculate the free energy difference between the two end states of the alchemical transformation. In the remaining of this section, some important methods to do so are described.

2.3.2.A Thermodynamic Integration

Using Equations 2.8 and 2.10, we can derive the following:

$$\begin{aligned}
\frac{\partial G}{\partial \lambda} &= \frac{\partial(-k_B T \ln Q)}{\partial \lambda} \\
&= \frac{-k_B T}{Q}\frac{\partial Q}{\partial \lambda} \\
&= \frac{-k_B T}{Q}\frac{1}{N!h^{3N}}\int\int \frac{-1}{k_B T} exp\left(\frac{-E(\lambda, \mathbf{p,r})}{k_B T}\right)\frac{\partial E(\lambda, \mathbf{p,r})}{\partial \lambda} d\mathbf{r}d\mathbf{p} \\
&= \left\langle \frac{\partial E}{\partial \lambda} \right\rangle_\lambda
\end{aligned} \tag{2.25}$$

where $\langle ... \rangle_\lambda$ denotes ensemble average over state λ. If λ is taken to be the coupling parameter ranging from 0 to 1, the free energy difference between the two end points is given by:

$$\Delta G_{0\to 1} = \int_0^1 \frac{\partial G}{\partial \lambda} = \int_0^1 \left\langle \frac{\partial E}{\partial \lambda} \right\rangle_\lambda \tag{2.26}$$

Computing free energy difference using Equation 2.26 is termed as Thermodynamic Integration (TI). In practice, the ensemble average of $\partial E/\partial\lambda$ is taken at a few discrete values of λ and the free energy difference is calculated by numerical integration of the integrand using standard methods like trapezoidal rule.[106] The appropriate number of λ points depends on the curvature of the $\langle\partial E/\partial\lambda\rangle$ function. For smooth and monotonic curves of $\langle\partial E/\partial\lambda\rangle$, TI is expected to be quite accurate even using a small number of points.

2.3.2.B Free Energy Perturbation

Free energy perturbation (FEP) is one of the oldest methods to calculate the free energy difference between two states. It was first proposed by Zwanzig[53] and is described by Equation 2.14. It is also known by some other names in the literature, such as, exponential averaging (EXP) and Zwanzig relation. Equation 2.14 is precise only when the potential energy difference between the two states is less than $2k_BT$ which is often not the case. If the two states do not have much phase-space overlap, the convergence of results is difficult using FEP. In such cases, a series of non-physical intermediate states are defined in terms of the coupling parameter, λ, and the free energy difference between the end states is given by the sum of free energy differences between consecutive intermediate λ-points as follows:

$$\begin{aligned}\Delta G_{\lambda(i-1)\rightarrow\lambda(i)} &= -k_BT\ln\left\langle exp\left(\frac{-[E(\lambda(i),\mathbf{p},\mathbf{r})-E(\lambda(i-1),\mathbf{p},\mathbf{r})]}{k_BT}\right)\right\rangle_{\lambda(i-1)}\\ \Delta G &= \sum_i \Delta G_{\lambda(i-1)\rightarrow\lambda(i)}\end{aligned} \tag{2.27}$$

where $\lambda(i)$ refers to the i^{th} point in the series of λ values chosen, starting from $\lambda = 0$ and ending at $\lambda = 1$. The number of intermediate λ-points depends on the type of alchemical transformation. For significant chemical changes during the transformation, a larger number of intermediate points are required.

2.3.2.C Bennett Acceptance Ratio

Bennett proposed an acceptance ratio estimator to calculate the free energy difference between two ensembles sampled using two different Hamiltonians[107]. His original formulation was based on the following form of free energy difference:

$$\Delta G_{1\to 2} = k_B T \ln \frac{Z_1}{Z_2} = k_B T \ln \frac{\langle \alpha(\mathbf{r}) exp[-\beta U_1(\mathbf{r})] \rangle_2}{\langle \alpha(\mathbf{r}) exp[-\beta U_2(\mathbf{r})] \rangle_1} \tag{2.28}$$

where $\langle ... \rangle_i$ denote ensemble average over state i with potential energy U_i and configurational integral Z_i, $\beta = (k_B T)^{-1}$ is the inverse temperature, $\alpha(\mathbf{r})$ is an arbitrary weight function which is finite for all coordinates $\mathbf{r}$. Equation 2.28 is valid for any function $\alpha(\mathbf{r})$. Thereafter, variational calculus is applied to find $\alpha(\mathbf{r})$ such that the variance of the free energy is minimized. This gives an implicit function of $\Delta G_{1\to 2}$ which can be solved numerically. This method of calculating free energy difference is called the Bennett acceptance ratio (BAR). BAR has been shown to have lower bias and smaller variance than EXP. [108, 109]

2.3.2.D Weighted Histogram Analysis Method

Histogram weighing techniques first introduced by Ferrenberg and Swendsen[110] provide a route to calculate the entropy or free energy as a function of a macroscopic parameter (X) at any desired value of X's conjugate (Y) using the probability distribution of X. Multiple distributions of X from ensembles at different values of Y can also be combined to get statistically optimal estimate of free energy. For example, Helmholtz/Gibb's free energy as a function of internal energy/enthalpy can be derived given multiple probability distributions of internal energy/enthalpy from independent simulations at different temperatures. The weighted histogram analysis method (WHAM) is an extension of these histogram weighing techniques which allows computation of free energy differences or potential of mean force (PMF) using data from multiple simulations with varying temperatures and/or potentials, usually controlled by a parameter λ[111]. In addition, it allows one to calculate the expectation of any observable at the desired state for the system. WHAM has been

applied in the analysis for alchemical free energy methods to compute free energy differences (for FEP) or their derivatives (for TI) at any desired value λ using data from all the intermediate λ states[112, 113]. WHAM is a very efficient free energy estimation method as it extracts the maximum possible information from available simulation data and is optimised to minimise the statistical error in its estimates. Recently, two modified versions of WHAM have been published, namely STWHAM and PTWHAM, for applications in simulated tempering and parallel tempering approaches which are both accelerated sampling techniques as described in Section 2.3.4[114].

2.3.2.E Multistate-Bennett Acceptance Ratio

In case of alchemical free energy methods, MD simulations are run at several intermediate states and a more efficient free energy estimate can be obtained by using information from all the states. The multistate Bennett acceptance ratio (MBAR) is a free energy estimator which uses samples from multiple equilibrium states to estimate free energy.[20] It is an extension of BAR. The basic equation for MBAR is a modified form of Equation 2.28 as follows:

$$\sum_{j=1}^{K} \frac{Z_i}{N_i} \sum_{n=1}^{N_i} \alpha_{ij}(\boldsymbol{r_{in}}) exp[-\beta U_j(\boldsymbol{r_{in}})] = \sum_{j=1}^{K} \frac{Z_j}{N_j} \sum_{n=1}^{N_j} \alpha_{ij}(\boldsymbol{r_{jn}}) exp[-\beta U_i(\boldsymbol{r_{jn}})] \tag{2.29}$$

where N_i is the number of samples from state i, α_{ij} is a weighing function. For $i = 1, 2, ..., K$, Equation 2.29 gives a set of K equations parametrised with functions α_{ij}. The choice of α_{ij} functions is made such that the variance of free energies is minimised for all states. With such choice of α_{ij}, the following expression yields the free energy of i^{th} state:

$$G_i = -\beta^{-1} \ln \sum_{k=1}^{K} \sum_{n=1}^{N_k} \frac{exp[-\beta U_i(\boldsymbol{r_{kn}})]}{\sum_{k'=1}^{K} N_{k'} exp[\beta G_{k'} - \beta U_{k'}(\boldsymbol{r_{kn}})]} \tag{2.30}$$

For $i = 1, 2, ...K$, it gives a set of K equations which is solved self-consistently for G_i. It should be noted that the free energies are determined uniquely only

up to an additive constant and hence only their differences are meaningful. The above MBAR formulation can also be used to determine the equilibrium expectation of an observable, for instance $\partial G/\partial\lambda$, at any desired state. MBAR is considered to be the lowest variance estimator.[20] It is noteworthy that MBAR (Equation 2.30) is equivalent to WHAM in the limit of histograms comprised of zero width bins.

2.3.2.F End-point Catastrophes

In cases where atoms are created or annihilated during an alchemical transformation, points of singularities in $\partial E/\partial\lambda$ or numerical instability may occur close to the end-points using classical force fields. This can happen when the suddenly appearing atom overlaps or is very close to an existing atom leading to 0 or very small interatomic distance between the two atoms. The Lennard-Jones (LJ) and Coulomb terms used in classical force fields to describe the non-bonded interactions will tend to infinity, or very large repulsive forces in such situation. The former leads to singularities while the latter is the reason of numerical instability during the simulation, which collectively may be referred to as end-point catastrophes. To avoid them, a soft-core potential is used which scales and shifts the non-bonded interaction such that the repulsion between two atoms approaches a finite value at very short distances.[115–117] A softcore potential can be used either just for van der Waals interaction[115] or for both van der Waals and electrostatic interactions.[116] In the former case, the coupling of non-softcore electrostatic interactions can be deferred until the softcore van der Waals interactions have got rid of all unwanted overlaps, after which its safe to couple the electrostatic interactions too. A new version of the softcore potential has recently been proposed[117].

2.3.3 Relative and Absolute Binding Affinity Calculation

All the alchemical methods described in the previous section yield ΔG between the two end-points of the alchemical transformation. However, the quantity of

real interest is the free energy difference between free and bound states of the protein-ligand system, that is, their binding affinity. To calculate binding affinity using alchemical methods, a thermodynamic cycle approach is employed as shown in Figure 2.1. It can be used to calculate absolute (Figure 2.1(a)) or relative (Figure 2.1(b)) binding affinity. Two calculations are required in such approaches. The first calculation corresponds to the alchemical transformation of ligand 1 to 2 in aqueous phase, whose free energy change is ΔG_{alch1}, while the second calculation corresponds to the same alchemical transformation in a protein environment with accompanying free energy change as ΔG_{alch2}. In the case of absolute binding affinity calculation, the end-point, $\lambda = 1$, corresponds to fully decoupled ligand 1, while in case of relative binding affinity calculation, it corresponds to full decoupled ligand 1 and fully coupled ligand 2. Therefore, in the former case, $\Delta G_2 = 0$ as can be seen in Figure 2.1(a). The following equations give the corresponding binding affinities:

$$\begin{aligned} \Delta\Delta G &= \Delta G_1 - \Delta G_2 = \Delta G_{alch1} - \Delta G_{alch2} \\ \Delta G_1 &= \Delta G_{alch1} - \Delta G_{alch2} \quad (\text{when } \Delta G_2 = 0) \end{aligned} \tag{2.31}$$

This approach can be employed to calculate the relative binding affinities between two ligands associating with a protein or between two different proteins bound to the same ligand.

The approach shown in Figure 2.1(a) to calculate the absolute binding affinity of a ligand-protein interaction is termed as the double annihilation method (DAM)[118]. However, this approach when applied directly has the problems of ignoring the standard state dependence and slow convergence due to large amount of sampling required, both of which can be overcome by the double decoupling method (DDM), where the decoupled ligand is restrained to the binding position[119]. Subsequently, several potentials restraining different degrees of freedom and strategies to calculate absolute binding affinity have been developed[120–122].

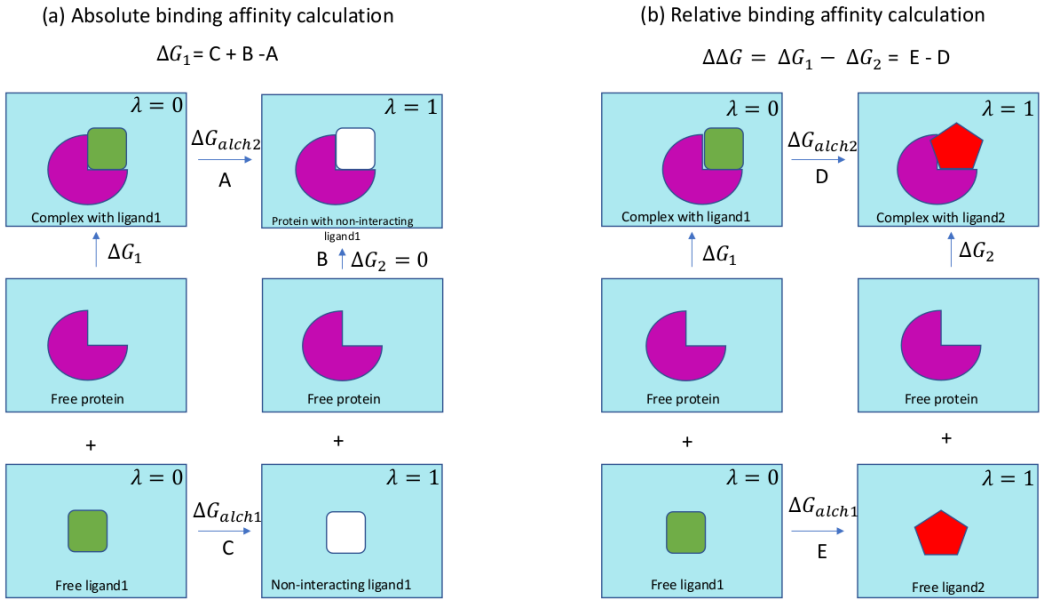

Figure 2.1: Thermodynamic cycles for calculation of binding affinities using alchemical methods. Protein is shown in magenta; ligand 1 is shown in green and white while interacting and not interacting with the environment respectively; ligand 2 is shown in red. (a) Calculation of absolute binding affinity of ligand 1 (ΔG_1), (b) calculation of relative binding affinity of ligands 1 and 2 ($\Delta\Delta G$).

2.3.4 Accelerated Sampling Techniques

One thing which is common to all the methods to calculate free energy of biomolecular systems is the need for proper conformational sampling which is important for robust results. The motion of biomolecular systems is governed by a rugged energy landscape with several local minima connected by high energy barriers[123]. It is not uncommon to have situations where the ligand and/or protein are flexible and have interconvertible conformations (corresponding to two local minima) through an energy barrier which is significantly higher than the kinetic energy of molecules at room temperature (k_BT). Sometimes, large conformational changes are important for protein activity, for example during catalysis or membrane transport. In such cases, conventional MD simulations may take up to as long as a few microseconds to swap between the two minima[124] or they might even get trapped into one of the local minima indefinitely[13, 125] leading to their inability to sample the conformational space of the protein-ligand system appropriately. Such trapping of molecules

in local minima slows down the conformational sampling of the molecule. To overcome such problems, several accelerated sampling techniques have been proposed. These include umbrella sampling[126], metadynamics[127], tempering approaches[12, 14], steered molecular dynamics[128, 129], blue moon sampling[130], adaptive biasing force algorithm[131], slow growth[132], fast growth[133] and Gaussian accelerated MD[134] to name a few. A lot of good reviews are available in the literature on different popular approaches[11–16, 135]. Broadly, these techniques can be divided into two categories: tempering approaches and those based on biasing potential. In the remainder of this section, a few popular methods taken from these categories are discussed.

2.3.4.A Biasing Potential Based Approaches

Such approaches involve adding biasing terms to the Hamiltonian in order to smooth out the energy landscape so as to facilitate the sampling of otherwise unapproachable areas of the phase-space. The most popular method in this category is umbrella sampling (US)[126]. It involves adding harmonic constraints to the original potential centered at different fixed values of a predefined reaction coordinate. An example of such a reaction coordinate is the binding (or unbinding) pathway of a ligand to protein. This allows the sampling of higher energy configurations relevant for the process of binding which would otherwise remain unsampled. The complete potential of mean force (PMF) along the reaction coordinate is calculated using weighted histogram analysis method (WHAM)[111]. WHAM uses the biased probability distributions of reaction coordinates from individual US simulations to yield the optimal estimate of the unbiased probability distribution function which allows the calculation of the potential of mean force (PMF). The total unbiased probability function is taken to be the weighted mean of the individual unbiased probability functions from each simulation, where the weights are evaluated so as to minimise the statistical error in the total probability function. Souaille and Roux[136] demonstrated that US in combination with FEP could be advantageous compared to the standard FEP or TI through the judicious use of

a biasing potential.

Another biasing potential method, popularly known as metadynamics, is where the biasing potential is adaptively built by periodic addition of perturbing terms with time in order to flatten the potential energy surface of the system along the reaction coordinate[127]. The biasing potential in this case is history-dependent, disfavouring configurations already visited in the space of reaction coordinate. This allows efficient exploration and determination of the energy surface with respect to the reaction coordinate. Many examples of its application to study ligand binding are available in the literature[137–140].

2.3.4.B Tempering Based Approaches

Tempering methods involve increasing the temperature of the MD simulation so as to facilitate crossing of energy barriers inaccessible at room temperature. These methods form a subset of a class of methods which involve performing a simulation in the *generalised ensemble* based on artificial, non-Boltzmann probability distribution allowing a random walk in the potential energy space[141, 142]. There are two types of tempering methods based on the way higher temperature is introduced into the system. First is simulated tempering (ST), also referred to as the method of expanded ensemble, where a single MD simulation accesses different temperatures by performing a free 1D random walk in the temperature space[143, 144]. ST, like some other methods based on the *generalised ensemble* simulation, uses non-Boltzmann weight factors which are not known *a priori* and need to be determined by short trial simulations. This task is tedious for biomolecular systems with multiple minima. A solution to this problem is given by the second type of tempering method called parallel tempering, also popularly known as the replica-exchange method[145]. Replica exchange is discussed in more detail in the following sections as it forms the basis of Chapter 4 in this thesis.

2.3.4.C Replica Exchange Molecular Dynamics

The replica exchange simulation method was first used by Swendsen and Wang[146] as a replica Monte Carlo method in 1986. Thereafter, further de-

velopment and application of this approach by several people[147–149] led to its current implementation in MD proposed by Okamoto and Sugita[145] in 1999. The basic idea of replica exchange molecular dynamics (REMD) is to simulate M independent replicas of the system in the canonical ensemble with each replica at a different temperature, some at low and others at high temperatures. The high temperature replicas are able to span much larger volumes of the phase space and frequent exchanges of configurations between different replicas allows better sampling of the phase space. The low temperature replicas may be able to access several local minima, separated by high energy barriers, due to such exchanges of configurations with high temperature replicas. Since all the M replicas are simulated in canonical ensemble, they are based on Boltzmann probability function, and hence, the problem of unknown weight factors associated with other *generalised ensemble* methods, does not exist in case of REMD. While the exchanges are attempted regularly with neighbouring replicas, their acceptance probability is determined by the standard Metropolis criterion[150] which ensures the satisfaction of the detailed balance condition[151] and convergence to an equilibrium distribution[145].

The implementation of REMD requires one to decide the optimal number of replicas, temperature range and the highest temperature. The aim is to get the best possible sampling done with minimum possible computational expense. The maximum temperature should be high enough to cross the energy barriers one is concerned with so as to avoid trapping of any replica in local minima. For a given maximum temperature, the number of replicas and temperature spacing between neighbouring replicas need to be tuned such that each replica spends equal amounts of time at each temperature[152]. This means that the temperature of each replica has to be chosen such that the temperature spacing between adjacent replicas allows a reasonable acceptance ratio and this ratio should be equal for all adjacent pairs of replicas. Since the acceptance probability decreases exponentially with the energy difference as well as the temperature difference[145], the temperature spacing of neigh-

bouring replicas should allow overlap in corresponding energies[153]. Several schemes for optimal temperature distribution over replicas have been suggested in the literature[17, 152, 154–156]. One way is to impose the condition that the energy fluctuation of a replica should be of the same order as the difference between the mean energy of that replica and that of its neighbouring replica, which results in an exponential rule for the temperature distribution over replicas[17]. It has also been shown that in some cases, minimisation of the round trip time between the lowest and the highest temperatures is a better estimate of mixing between states than the acceptance ratio[157]. Various studies have arrived at different numbers as the optimal acceptance ratio for the most efficient performance of REMD[152, 154, 158]. However, it turns out that there is no strict rule and anything between 0.20-0.50 is deemed good enough.

2.3.4.D Generalised Replica Exchange Methods

In the previous section, the original replica exchange method was introduced where all the independent replicas differ only in their temperatures and the rest of the properties of the system are identical for all replicas. However, the replica exchange technique need not be confined to a random walk in temperature space alone. Several generalisations have been reported in the literature. The first ever application of parallel tempering with multiple swapping variables was reported by Yan and Pablo[159, 160]. Thereafter, a multidimensional replica exchange method (MREM) was introduced soon after the original REMD where, along with temperatures, the Hamiltonians of the replicas were also modified[161]. In MREM, a one-to-one correspondence is defined between replica m and its corresponding parameter set, $\Lambda_m \equiv (T_m, \lambda_m)$ where T_m is the temperature and λ_m is another parameter on which the Hamiltonian depends for replica m. MREM provides a framework to combine REMD with umbrella sampling[126] and FEP[53], in which λ_m can be used as the biasing potential parameter in the former and the alchemical coupling parameter in the latter case. It is to be noted that, in MREM, the temperature may or may

not be varied across replicas; that is, one can also have $\Lambda_m \equiv \lambda_m$ with same T for all replicas. Replica exchange umbrella sampling (REUS), a combination of REMD and US where λ is varied between different replicas of US with and without temperature exchanges, has been reported as an example[161, 162] and has been shown to improve sampling in free energy calculations. FEP/λ-REMD, a combination of FEP and REMD where λ is exchanged between replicas, was reported by Jiang *et al.* as a scheme to calculate the absolute hydration energy and binding affinity with improved convergence of their results[163]. Multicanonical versions of replica exchange have also been reported by adding some features of other *generalised ensemble* methods to the original REMD with improved performance[141, 164–169]. There are a lot of other improved versions of the original REMD available in literature[170–175]. In the light of these developments, the original REMD is also referred to as T-REMD, as temperature is the only swapping parameter in that case.

As shown by Fukunishi *et al.*, the optimal number of replicas required in REMD for a given temperature range is proportional to $\sqrt{f}$, where f is the total number of degrees of freedom of the system[17]. This imposes a severe restriction on the applicability of such methods to solvated biomoleculear system with large number of degrees of freedom as the number of replicas required would be very high for them. Since most of the total degrees of freedom of such systems are from the solvent, a large number of exchanges using REMD would be uninteresting and waste CPU time. The solution to this problem was proposed by Fukunishi *et al.* in the form of Hamiltonian replica exchange method (H-REMD)[17]. In this approach, each replica differs in its interactions, that is Hamiltonian, rather than temperature. It should be noted that even MREM allows the use of different Hamiltonians at the same temperatures across replicas like H-REMD. However, the advantage of H-REMD over MREM is that the former allows one to modify the Hamiltonian only for a few selected degrees of freedom which we are interested in across replicas. This reduces the required number of total replicas thereby reducing the computa-

tional cost of the calculation. In terms of thermodynamics, potential scaling is equivalent to scaling of the inverse temperature β, and hence, T-REMD is a special case of H-REMD. However, from a practical point of view, H-REMD has several advantages over T-REMD. First of all, since it allows scaling/modifying a part of the Hamiltonian, it is possible to avoid the wastage of CPU time by excluding all uninteresting degrees of freedom from the scaled part of the Hamiltonian. This substantially reduces the required number of replicas. In addition, since all the replicas are run at the same temperature, there is no need to reinitialise velocities after every successful exchange of configurations like in T-REMD. The acceptance probability (A) between replicas i and j in H-REMD is given by:

$$A = \min\{1, exp[-\beta([U_i(\mathbf{r}') + U_j(\mathbf{r})] - [U_i(\mathbf{r}) + U_j(\mathbf{r}')])]\} \tag{2.32}$$

where U_i and U_j are the potential energies of replica i and j, $\mathbf{r}$ and $\mathbf{r}'$ are the configurations of replicas i and j, respectively, prior to the exchange attempt. The advent of H-REMD widely expanded the realm of application of replica exchange methods. Thereafter, several variants of H-REMD have been developed[176–181]. Jiang *et al.* proposed a method called FEP/H-REMD[182], which is an extension to their previous method FEP/λ-REMD[163], to calculate absolute ligand binding affinity. In this method, H-REMD is implemented along two orthogonal axes, along one of which the alchemical parameter λ varies, while along the other the boosting parameter controlling the boosting potential set to accelerate sampling varies.

An important variant of H-REMD is called replica exchange with solute tempering (REST)[183] where the total potential energy is divided into solute-solute (SS), solute-solvent (SW) and solvent-solvent (WW) interactions and the latter two are scaled by some factor along the replica ladder. It should be noted that although a different system temperature is used for each replica, like in T-REMD, scaling part of the Hamiltonian makes it equivalent to increasing the temperature of solute only (the molecule of interest) while keeping

the solvent effectively cold across replicas. The acceptance probability of an exchange attempt is dependent only on the degrees of freedom of the solute (f_p) in this method reducing the required number of replicas for optimal performance which scales as $\sqrt{f_p}$. However, REST was not found to be very effective for large biomolecules[184]. Therefore, some variants of the REST methodology have been published like replica exchange with flexible tempering (REFT)[185] and the one by Terakawa *et al.*[186]. In the latter, the SS and SW interactions are scaled with a scaling factor < 1 which results in a higher effective temperature for the solute on climbing the replica ladder while all replicas are run at the same temperature unlike the original REST. Soon after that, Wang *et al.* proposed REST2[18] where they used the potential scaling scheme proposed by Terakawa *et al.* Indeed, the two schemes differ only in the way they define the effective solute inverse temperature ($\beta_m = 1/k_B T_m$) for an intermediate replica m which in turn defines the potential scaling factor for that replica. It is important to note that the "solute" region in these methods need not be the entire biomolecule. It may well be a small part of it. The following is the expression of potential energy used in REST2:

$$U_m(\mathbf{r}) = \frac{\beta_m}{\beta_0} U_{SS}(\mathbf{r}) + \sqrt{\frac{\beta_m}{\beta_0}} U_{SW}(\mathbf{r}) + U_{WW}(\mathbf{r}) \tag{2.33}$$

where U_{SS}, U_{SW} and U_{WW} are the components of the total potential energy comprising of solute-solute, solute-solvent and solvent-solvent interactions, respectively. $\beta = 1/k_B T$ is the inverse temperature with T_m as the desired effective solute temperature for replica m and T_0 being the system temperature at which all replicas are simulated.

2.3.4.E Replica Exchange for Alchemical Free Energy Calculations

Exchanges between intermediate states of an alchemical calculation, even if all replicas remain at a fixed temperature, may prevent trapping of sampled states and hence can improve covergence. Therefore, replica exchange seems to be an attractive accelerated sampling method for alchemical free energy calculations.

The original idea of using replica exchange with FEP was proposed (although not implemented) by Sugita *et al.* as a special case of MREM[161]. Later, Woods *et al.* reported an improvement in the performance with the H-REMD versions of both FEP and TI, called REFEP and RETI, respectively[112, 187], where the usual simulations at the intermediate states for these calculations were run accompanied with exchange of configurations between neighbouring simulations. This was followed by several other similar reports of quicker convergence and improved sampling when alchemical methods were combined with H-REMD[188–192]. In all these applications, none of the replicas were heated. Rick demonstrated the implementation of T-REMD with TI and reported better convergence[113]. Jiang *et al.* reported FEP/λ-REMD[163] to calculate absolute hydration and binding affinity using a combination of FEP and REMD. They extended this method to propose a 2-dimensional replica exchange scheme for absolute ligand binding affinity calculation based on H-REMD, called FEP/H-REMD[182], where there is a two-dimensional grid of simulations with the alchemical parameter varying in one direction while the boosting potential parameter varying in the other and the exchanges are attempted in both directions. Replica exchange has also been employed for absolute binding affinity calculation[193, 194].

All the methods described above either introduce exchanges in the alchemical space alone, or if they involve exchanging in the temperature or Hamiltonian space, it is orthogonal to the exchanges in alchemical space. However, Wang *et al.* recently proposed a method, called FEP/REST[19], combining the ideas of MREM[161] and REST2[18]. It is basically a two dimensional H-REMD[†] where both REST2 potential scaling factor, β, as well as the alchemical coupling parameter, λ, vary and are exchanged across replicas such that the effective temperatures of the end-point replicas corresponding to $\lambda = 0$ or 1 are set to the room temperature, while it gradually increases for the intermediate λ values attaining a maximum in the middle. This scheme provides the advantages

[†]Two-dimensional only in the sense that two parameters vary across replicas. It does not need a two-dimensional grid of simulations like FEP/H-REMD.

of both tempering as well as exchanging in the alchemical space and also is computationally less expensive as compared to its conceptually equivalent method, FEP/H-REMD[182]. This method has been implemented to calculate the free energies for a large number of biomolecular systems[195, 196].

2.4 Ensemble Averaging to Determine Thermodynamic Properties

As noted earlier in this chapter, statistical mechanics provides the formalism to evaluate macroscopic thermodynamic properties like the Gibbs free energy from the molecular simulations via ensemble averaging over microscopic samples (see Equation 2.14). However, it is a common practice to replace ensemble average with time average performed in a single simulation relying on the ergodic theorem. Time averaging self-evidently makes no sense when studying non-equilibrium systems. It should be noted that the ergodic theorem holds only in the limit of Poincaré recurrence time, which is usually extremely long for ligand binding[10]. Moreover, the Newtonian dynamics are very sensitive to the initial conditions and hence two different MD trajectories diverge rapidly over time no matter how close their initial conditions[10]. The key point is that, for systems which exhibit an equilibrium thermodynamic state, the microscopic dynamics must be at least mixing in the language of ergodic theory, hence chaotic[10]. Therefore, the practice of performing a short one-off MD simulation to calculate free energy of a system should be replaced with ensemble simulation. An ensemble simulation in this context means performing multiple replicas of MD simulations, where each replica is an independent calculation initiated from a randomly selected initial condition. Several different approaches to vary the initial conditions of replicas have been reported including varying only the initial velocities[21, 105, 197–204] or the initial velocities in combination with other properties like the intial structures, the protonation states, the solvation boxes, the intial conformations, the ligand charges, and so on.[203, 205–209] In this thesis, all the replicas have identical initial con-

figurations while their initial velocities are randomly drawn from a Maxwell-Boltzmann distribution. Ensemble averages can be computed by running a sufficiently large number of replicas, an approach applicable for systems in as well as out of equilibrium. The appropriate number of replicas in an ensemble simulation is determined by the control of the error in the free energy predictions that ensue. There is no general theory to determine this number which needs to be assessed for each case under investigation[10]. In this thesis, it is determined through the rule that the addition of one further replica to a set N of replicas does not have a significant effect on the prediction. In practice, there is a trade-off between the desired level of precision and the associated computational cost. The number of replicas required may vary with the size and the flexibility of the biomolecule studied as well as the free energy method employed. For instance, in this thesis, I have used 5 replicas for all the relative binding affinity calculations, but 25 replicas for all the absolute binding affinity calculations (these choices have been justified in the following chapters). Ensemble simulation also provides a route to quantify the statistical uncertainty associated with the calculated free energy.

2.5 Ensemble Averaging and Repeatability of *In Silico* Binding Affinity Predictions

A reliable prediction of binding affinity has several important applications as mentioned in Chapter 1. Drug design and personalised medicine are two important areas where such predictions can have a great deal of positive impact. However, a prediction method can be relied upon only if one can confidently get the same answer for a given system on repeating the process. A major drawback of the methods described in the previous section (when running only a single short MD simulation) is the variability in results on repeating the calculation. This means that the studies reported by one group (which might yield results in good agreement with experiment) do not yield the same results when repeated by others[1, 2]. This lack of repeatability in the free

energy predictions obtained from the single short trajectory based versions of these methods makes them unscientific as well as unsuitable for application in any real world context, including in academic setting. This is one of the key reasons why MD based methods have not been widely used in pharmaceutical industry in the past. Other key reasons include high computational costs, limited accuracy of force fields and technical challenges in the implementation of free energy calculations.

The underlying causes of the variability in results of these methods is the assumption that the ensemble average is equal to the time average of a single (often insufficiently long) trajectory, and the sensitivity of MD trajectories to the initial conditions as mentioned in Section 2.4. This shortcoming has been recognised and reported in the literature where various published works indeed demonstrate compellingly that multiple short simulations yield much more accurate binding affinities than a single extended simulation, both in end-point methods[201, 203, 210] and alchemical methods[200, 202, 204, 211]. Recently, two systematic approaches have been published which provide a solution to this problem - enhanced sampling of molecular dynamics with approximation of continuum solvent (ESMACS) and thermodynamic integration with enhanced sampling (TIES)[21, 105, 199, 212–214]. These approaches have been successful in making accurate, precise and repeatable predictions of binding affinities for a variety of biomolecular systems including blind case studies with pharmaceutical companies[22, 23]. TIES forms the basis of Chapters 3 and 4 of this thesis, while ESMACS is the main focus of Chapter 5.

Chapter 3

Thermodynamic Integration with Enhanced Sampling

In Chapter 2, several methods available for *in silico* binding affinity predictions were mentioned. The importance of the ability to make reliable predictions of binding affinities for ligand-protein complexes in real-world was mentioned in Chapter 1. However, as noted in Chapter 2, the free energy methods based on classical MD simulations suffer from the problem of variability in results when running a single short simulation by virtue of the sensitivity of MD trajectories to the initial conditions. Ensemble simulation can be used to overcome this problem. In this chapter, a new method called thermodynamic integration with enhanced sampling (TIES) is described, which utilises the idea of ensemble simulation to yield accurate, precise and repeatable relative binding affinities. TIES is based on one of the "exact" free energy methods, thermodynamic integration (TI), described in Chapter 2. Based on calculating ensemble averages, it allows quantification of statistical uncertainties associated with the results. TIES has been shown to perform well for a wide range of target proteins and ligands.

As has been emphasised in Chapter 1, reliable binding affinity predictions need to be made on time scales comparable to, if not shorter than, the experimental ones in order to have any impact in drug design. In the case of personalised medicine, *in silico* methods should be able to make reliable predictions in a

few hours to be useful in clinical context. Therefore, the time to solution is another important factor influencing the applicability of computational methods in real-world. Currently, the wall-clock time requirements for predictions by TIES (∼6-8 hours; reduced by a factor of 3-5 with GPUs) fulfil these requirements given the availability of sufficient computer resources. In fact, the TIES approach has been employed in collaborative studies with two pharmaceutical companies (GlaxoSmithKline and Pfizer), yielding accurate and precise relative binding affinity predictions[22, 23].

A method called independent trajectory TI (IT-TI)[204] has been reported in the literature, and attempts to use multiple independent trajectories to improve the accuracy of calculated free energies. Genheden *et al.* have also shown that performing several independent trajectories yields better estimates of free energies[215]. However, TIES involves a systematic application of the concept of ensemble simulation for "exact" free energy calculations which is different from the act of merely repeating the calculation a small number of times as will be shown later in this chapter. The TIES methodology and most of the results included in this chapter have been published and some figures and tables have been reproduced from the published articles[21–23].

3.1 Ensemble Simulation Based Thermodynamic Integration

TIES is based on the "exact" free energy method TI which was described in Section 2.3.2. TI involves numerically integrating the potential energy derivative with respect to λ ($\partial E/\partial\lambda$), where λ is the alchemical coupling parameter (see Equation 2.26). Therefore, to get a reliable free energy change $\partial E/\partial\lambda$ values should be accurate, precise and repeatable which is not achievable using a single short MD simulation at each λ-window. TIES involves running an ensemble simulation at each λ-window. All replica simulations of the ensemble have identical initial conditions except their initial velocities, which

are randomly drawn from a Maxwell-Boltzmann distribution.* This allows the calculation of ensemble average of $\partial E/\partial\lambda$ values for each λ-window. The frequency distribution of the ensemble of $\partial E/\partial\lambda$ values are characteristic of a Gaussian random process as shown in Figure 3.1. Thus, the integral in Equation 2.26 is interpreted as a stochastic integral and the average of the distribution of $\partial E/\partial\lambda$ is used to evaluate it using the trapezoidal rule. The uncertainties in $\partial E/\partial\lambda$ are also propagated to the final result according to the stochastic calculus as described in Section 3.3.

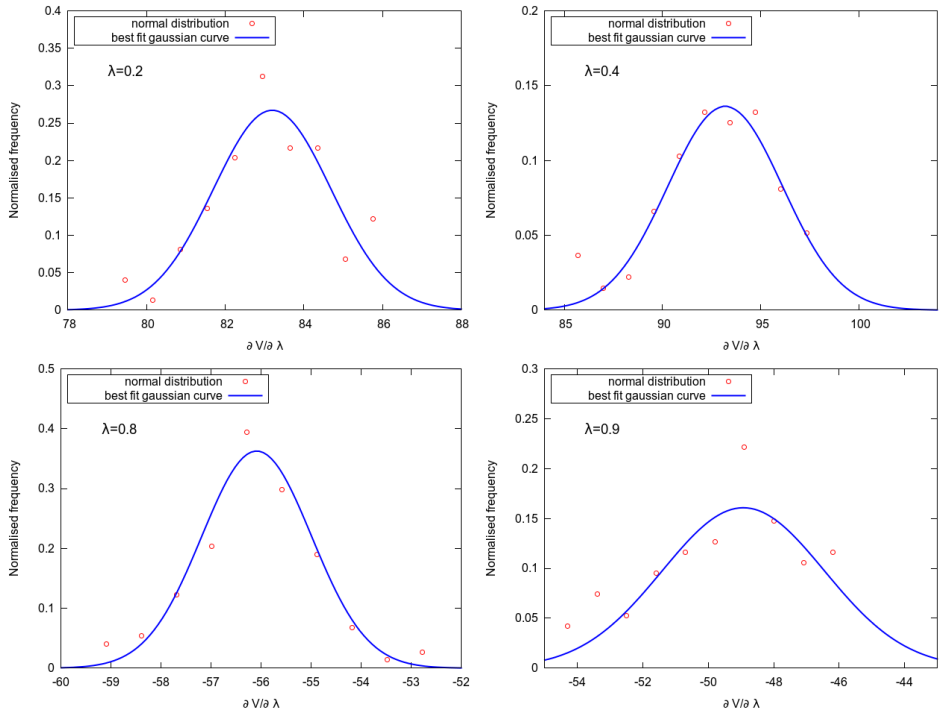

Figure 3.1: Normalized frequency distribution of ensembles of $\partial E/\partial\lambda$ values for 4 different intermediate alchemical states (λ=0.2, 0.4, 0.8, 0.9), fitted to Gaussian distributions for the transformation from ligand L1Q to ligand LI9 binding to CDK2.

3.2 Ligand-Protein Systems Studied

In this study, TIES has been applied to a large set of ligands bound to seven different target proteins namely: cyclin-dependent kinase 2 (CDK2), thrombin, tyrosine kinase 2 (TYK2), myeloid cell leukemia 1 (MCL1), protein tyrosine phosphatase 1B (PTP1B), bromodomain-containing protein 4 (BRD4)

*It should be noted here that performing non-biased MD simulations while using the same initial structure may not be able to overcome large energy barriers. In such cases, enhanced sampling protocols may be useful as shown in the next chapter.

and tropomyosin receptor kinase A (TRKA). All of them are different types of proteins with varying functions in the human body and are all important therapeutic targets. Research is ongoing to develop their inhibitors. CDK2 has an essential role in the eukaryotic cell-cycle and its overexpression can lead to unregulated cell growth[216]. The serine protease thrombin is a key enzyme involved in the coagulation cascade and regulates hemostasis and thrombosis whose increased activation can cause severe thromboembolic disorders[217]. TYK2 is involved in some signalling pathways in the cell, which have been found to have implication in the pathogenesis of chronic inflammatory disorders of skin and gastrointestinal tract and colon; its inhibition has been recognised as an effective therapeutic strategy in their treatment[218, 219]. The overexpression of MCL1 prevents the apoptosis of cancerous cells. Moreover, it has developed resistance against the existing inhibitors and hence the need of the development of new inhibitors[220]. PTP1B regulates the insulin and leptin receptor pathways and hence is an attractive therapeutic target for diabetes and obesity[221]. BRD4 is known to have roles in pathologies ranging from inflammation to cancer, and the development of their inhibitors is an area of ongoing research[22]. TRKA is the receptor of a nerve growth factor neuropeptide which has a crucial role in pathogenesis of pain; TRKA inhibitors have been shown to reverse the effect of such pain transduction[23]. The structures of all the proteins studied are shown in Figure 3.2.

3.3 Method

This section contains the details of the standard TIES protocol employed for all the free energy calculations in this study, along with the details on simulation setup and force field parameters. The statistical analyses which form the basis of the choice of the values for parameters like the ensemble size, simulation length and the intermediate λ values used for this protocol are described. It is worth noting that although the standard protocol described below is applicable to all of the ligand-protein systems studied here, it may need to be modified

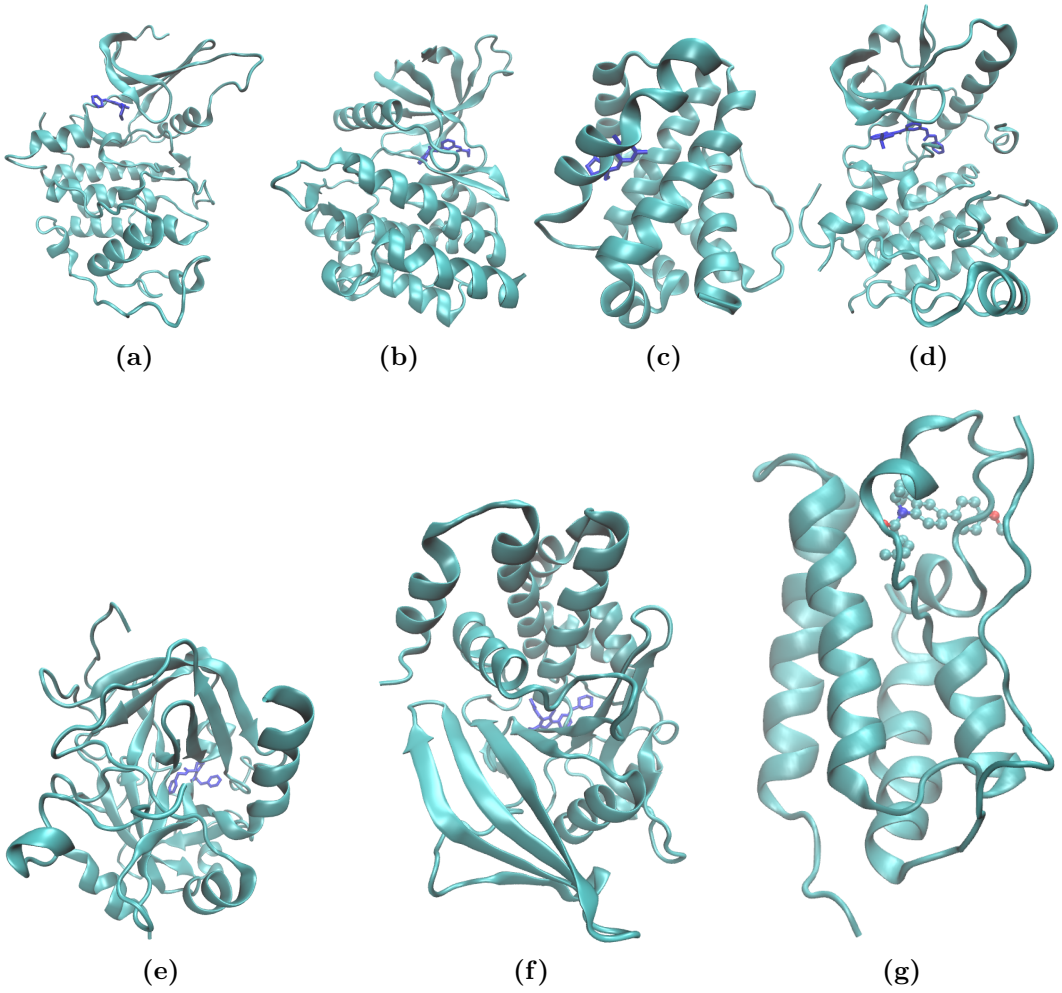

Figure 3.2: Structures of all the seven target proteins (ribbon representation) studied in each case shown bound to a ligand (stick representation): (a) cyclin-dependent kinase 2 (CDK2); PDB:1H1Q, (b) tyrosine kinase 2 (TYK2); PDB:4GIH, (c) myeloid cell leukemia 1 (MCL1); PDB:4HW3, (d) tropomyosin receptor kinase A (TRKA); PDB:5JFV, (e) thrombin; PDB:2ZFF, (f) protein tyrosine phosphatase 1B (PTP1B); PDB:2QBS and (g) bromodomain-containing protein 4 (BRD4); PDB:4BJX. Structures of all ligands (which are all drawn from congeneric series) are provided in the Appendix.

in some situations.

3.3.1 Initial Structures and Simulation Protocol

The starting structures for all proteins were downloaded from the Protein Data Bank (PDB)[222]. The corresponding PDB IDs are 4BJX for BRD4, 5JFV for TRKA, 2ZFF for thrombin, 4HW3 for MCL1, 2QBS for PTP1B, 4GIH for TYK2 and 1H1Q for CDK2. In the case of thrombin, a different PDB (code:

2ZC9) was used as the starting structure while studying the transformation of unsubstituted benzylamine to meta-substituted benzylamide as the water molecule initially present in the S1 pocket of the protein get displaced by the appearing substituent at the meta position (see Section 3.5 for details). The ligand structures in case of CDK2, TYK2, MCL1, PTP1B and thrombin were downloaded from the Supporting Information of an open access article[196]. The ligand structures for BRD4 and TRKA were provided by our experimental collaborators at the pharmaceutical companies GSK and Pfizer respectively.

All the protein-ligand complexes were simulated in an orthorhombic water box with a buffer width of 14 Å. The net charge of the system was neutralised by addition of counterions. The AMBER ff99SB-ILDN force field[223] was used for protein parameters and general AMBER force field (GAFF)[41] was employed for ligands. TIP3P model [224] was used for water molecules. Standard protonation states were assigned to all titratable residues at pH 7, with histidines protonated on the ϵ position (HIE). The partial atomic charges for ligand atoms were calculated using the restrained electrostatic potential (RESP) method after geometry optimisation by Gaussian03 package using the Hartree-Fock method and 6-31G** basis set. RESP calculations were performed using Antechamber (AmberTools 12). All simulations were performed using the package NAMD 2.9[45] with three-dimensional periodic boundary conditions. A cut-off of 12 Å was used for non-bonded interactions and long range Coulomb interactions were calculated using Particle Mesh Ewald (PME) method.

The simulations were performed in an isothermal-isobaric ensemble at temperature 300 K and pressure 1 bar. Langevin thermostat (with a damping coefficient of 5 ps^{-1}) and Berendsen barostat (compressibility of 4.57×10^{-5} bar^{-1} and a relaxation time of 100 fs) were used to maintain the temperature and the pressure at these values. Constrained dynamics with a time step of 2 fs were performed employing RATTLE algorithm. A soft core van der Waals potential was used to avoid the problem of end point catastrophes as described in

the previous chapter. The electrostatic interactions of the disappearing atoms were decoupled linearly between $\lambda = 0$ and 0.55, and do not interact at all beyond that; for appearing atoms they were linearly coupled between $\lambda = 0.45$ and 1, and do not interact otherwise.

3.3.2 Hybrid Ligand Structure and Parameters

In this study, alchemical transformations of ligands have been studied using dual topology scheme[225]. A hybrid ligand contains a common region to which both the disappearing part (belonging exclusively to the initial state) and the appearing part (belonging exclusively to the final state) are bonded. The latter two do not interact with each other at all. The initial structure of the hybrid ligand for an alchemical transformation from ligand L1 to ligand L2 is generated by simply appending the coordinates of the set of appearing atoms from L2 to the structure file of L1 after aligning the coordinates of all atoms in their common region. The last atom of the common region in the hybrid ligand is connected to the first atom of both the disappearing as well as the appearing regions. In order to ensure that the common region is chemically similar in both the ligands, it is chosen such that the overall charge of all the atoms as well as the charge on each atom in the common region do not vary by more than 0.1 e in individual ligands. However, this threshold limit of 0.1 e may need to be relaxed in the cases of highly charged or polar ligands. The partial atomic charges need to be recalculated for the hybrid ligand so as to have unique charges for the atoms in the common region. This is done by setting the latter's charges in the hybrid ligand to the average of their charges in the individual ligands. Thereafter, the charges on disappearing and appearing parts are adapted accordingly by reparametrising the individual ligands after constraining the charges on the common part to their newly derived values.

3.3.3 Protocol for Free Energy Calculation

Figure 3.3 shows a schematic of the protocol used to calculate all the free energies in this study. A total of 13 values for the alchemical coupling param-

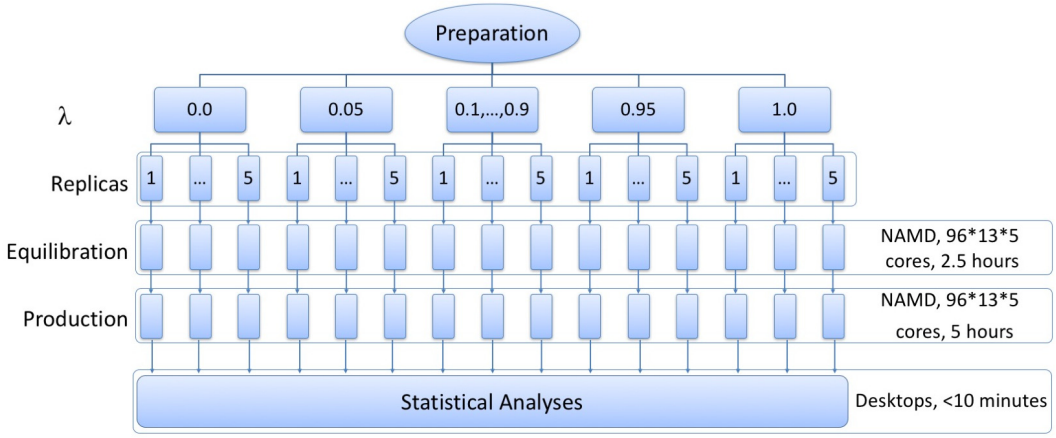

Figure 3.3: TIES protocol requiring 5 replica simulations at each λ window. For a single alchemical transmutation, 13 λ-windows are used amounting to 65 molecular dynamics simulations in total. The number of cores and wall-clock time employed on a Cray XC30 supercomputer are displayed on the right side of the figure.

eter λ were chosen between 0 and 1. The size of the ensemble simulation was taken to be 5, that is, 5 replicas were performed at each λ-window. Thus, a single TIES calculation involves running 65 replicas in total using this protocol. Each replica comprises of energy minimisation followed by 2 ns long equilibration and 4 ns long production run. The coordinates were written out every 10 ps and $\partial E/\partial\lambda$ recorded every 2 ps. In order to calculate the relative binding affinities of two ligands L1 and L2, the thermodynamic cycle approach as described in Chapter 2 is employed and Equation 2.31 is rewritten as:

$$\Delta\Delta G = \Delta G_1 - \Delta G_2 = \Delta G^{aq}_{alch} - \Delta G^{bound}_{alch} \tag{3.1}$$

where ΔG_1 and ΔG_2 are the binding free energies of ligands L1 and L2 respectively. ΔG^{aq}_{alch} and ΔG^{bound}_{alch} are the free energy differences associated with the alchemical transformation of ligand L1 into L2 in free and bound states respectively, each of which needs a separate TIES calculation.

The TIES protocol mentioned above has three adjustable parameters: the duration of an individual replica simulation, the number of replicas (the ensemble size) and the values of λ to be used. For all simulations in this thesis, the former two have been chosen to be 4 ns and 5 respectively. Figure 3.4

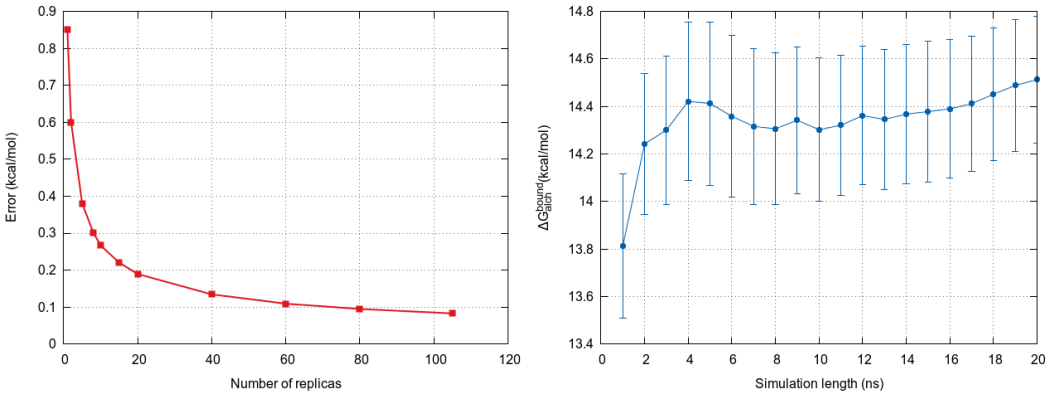

Figure 3.4: (a) Variation of error with ensemble size per λ window and (b) the variation of ΔG^{bound}_{alch} with simulation length for the transformation of ligand L1Q to ligand LI9 bound to CDK2. The above plots form a basis for our choice of simulation length as 4 ns and ensemble size as 5.

provides the justification for the same. These choices were based on the statistical analysis of the variation in results and the associated errors with the parameters under consideration. Figure 3.4a shows the variation of the uncertainty in TIES results with the number of replicas run at each λ-window, while the simulation length for each replica is fixed at 4 ns. An ensemble simulation with 105 replicas was performed at each λ-window for the ligand transformation L1Q to LI9 bound to CDK2. It is clear from this figure that the result converges around the number of replicas equal to 30 or so, when the uncertainty in results falls below 0.15 kcal/mol. However, the uncertainty is already below 0.4 kcal/mol at 5 replicas, reduces further to 0.3 kcal/mol at 10 replicas, and to about 0.2 kcal/mol at 20 replicas. This means that there is a marginal reduction in uncertainty from a 4-fold increase in computational cost. This leads us to choose 5 replicas as a trade-off between computational cost and precision of results. It should be noted here that very precise results can be obtained given a sufficient amount of compute resources. Figure 3.4b shows the variation of ΔG^{bound}_{alch} with the duration of simulation using 5 replicas at each λ-window (same duration was used for all 65 replicas); its value stabilises after 4 ns. The choice of 2 ns as the equilibration time is based on

the observation that the cumulative averages of $\partial E/\partial\lambda$ converge within this duration, as shown in Figure 3.5. Several previous studies from my group have reported a similar convergence behaviour for a large variety of ligand-protein systems[214, 226]. It should be noted that we used CDK2 as a representative system to establish a standard protocol for all systems in this study. This holds true in the current scenario as all systems investigated here have relatively rigid ligands and small globular protein. However, if the system being studied has a flexible ligand or larger protein, it may be necessary to increase the ensemble size and/or simulation duration to improve sampling and the precision of results.

Figure 3.3 indicates the number of cores and wall-clock time required for a typical TIES calculation. It is possible to finish the entire calculation using the protocol mentioned above in ∼6-8 hours given sufficient computational resources. This is of course dependent on the size of the system studied and the number of cores used (GPUs may further reduce the time). The important thing is that the TIES workflow is perfectly scalable and it is possible to perform multiple calculations concurrently by increasing the allocated cores keeping the wall clock time same as that for a single calculation.

3.3.4 Stochastic Integration and Error Propagation

As mentioned in Section 3.1, $\partial E/\partial\lambda$ has the characteristic of Gaussian random variable (Figure 3.1). Therefore, in TIES, the integral in Equation 2.26 is interpreted in terms of stochastic calculus. Each point of the integrand is the ensemble average of $\partial E/\partial\lambda$ at that λ-window, which is taken to be the average of its values from all five replicas such that the value from each replica is itself the average over the whole simulation length. The integral is then calculated numerically using the values of the integrand so obtained. The error in the value of integrand at window λ (σ_λ) is taken to be the bootstrapped standard error of the mean of potential derivatives from all replicas. In stochastic calculus, the integral of a Gaussian random process is itself a Gaussian random process and the variance on the resultant integral is the convolution of the

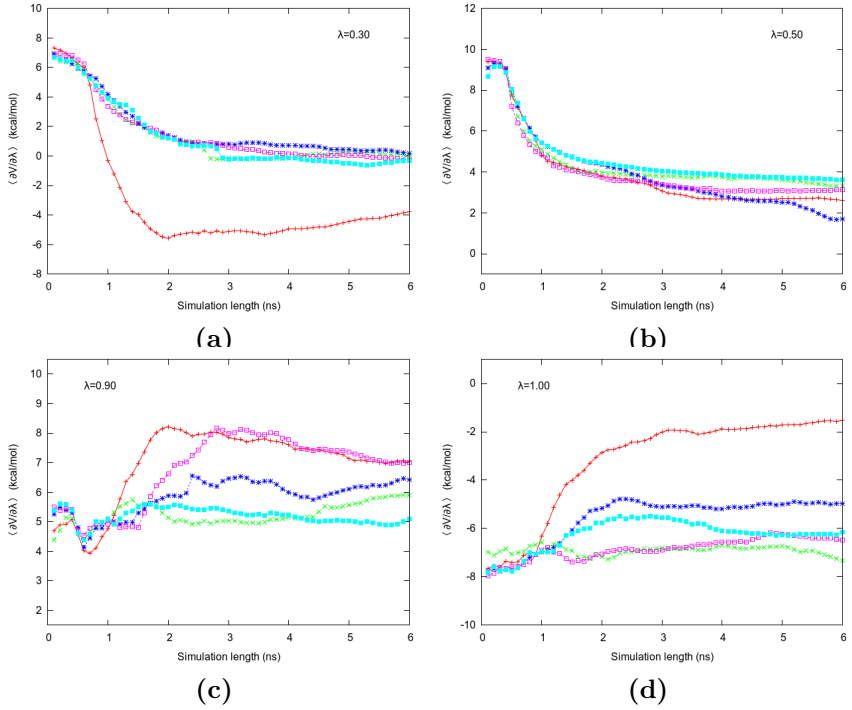

Figure 3.5: Variation of $\langle \partial E/\partial \lambda \rangle$ with the simulation length (including both equilibration and production phases) for all five replicas at four different λ windows in the case of the transformation from ligand L1 to L4 binding to thrombin. It is clearly visible that all replicas converge at about 2 ns which is the length of the equilibration run in our existing protocol. The variation in the final converged values of $\langle \partial E/\partial \lambda \rangle$ for different replicas at a given λ window as shown above emphasises the advantage of performing ensemble simulation.

variance of all the points of the integrand[227]. Thus, the variance of ΔG^{bound}_{alch} (σ_1^2) and ΔG^{aq}_{alch} (σ_2^2) and the variance of $\Delta\Delta G$ (σ^2) are calculated as below:

$$\sigma_{1/2}^2 = \sum \sigma_\lambda^2 (\Delta\lambda)^2 \tag{3.2a}$$

$$\sigma^2 = \sigma_1^2 + \sigma_2^2 \tag{3.2b}$$

3.4 Binding Affinity Predictions

In this section, all the binding affinity predictions made using the method described in the previous section are presented. A detailed analysis of the results showing the high level of accuracy and precision obtained is provided. The repeatability as well as reproducibility of the results based on ensemble

simulations has been discussed. A comparison of the TIES results with those obtained using another alchemical method called FEP/REST (described in Chapter 2) has been done. Finally some comments on the variation of the results with extension of the simulation duration and the size of alchemical transformations studied in this study are made.

It should be noted here that, in case of BRD4 and TRKA, blind predictions were made and the experimental data was only disclosed for comparison by our experimental collaborators at GlaxoSmithKline and Pfizer, respectively, after the TIES predictions were provided to them. Both of these studies have been published and the results presented here are taken from the respective publications[22, 23].

3.4.1 Comparison with Experimental Data

The relative binding affinity calculations using the TIES protocol were carried out for 81 alchemical transformations between ligands binding to seven different target proteins capturing different types of chemical interactions. A graphical display of all these ligand transformations have been included in Table A.7. Table 3.1 summarises the results along with the accuracy and precision of the predictions. There is excellent agreement with the experimental values (Figure 3.6). The mean absolute error (MAE) and the root-mean-square error (RMSE) for all predictions collectively are 0.7 kcal/mol and 0.9 kcal/mol, respectively (Figure 3.6a). The correlation of predicted binding affinities with those obtained experimentally is very good, with a Pearson's r of 0.86. The ranking of ligands based on their predicted relative binding affinities is excellent, with a Spearman's ρ of 0.87 as shown in Figure 3.6a. The results have a high level of precision with a range of uncertainty from 0.03 to 0.5 kcal/mol (Table 3.1).

The performance of the TIES protocol for individual target proteins is shown provided in Table 3.1. The level of accuracy and precision of the results is of the same level as that for the combined results. The MAE and RMSE values are below 0.7 and 0.8 kcal/mol, respectively, for all proteins except MCL1,

Table 3.1: Summary of TIES results for the seven different target proteins studied. The number of alchemical transformations, crystal structures used, original publications reporting the experimental binding affinities and the experimental method used to determine the binding affinities are provided. Isothermal titration calorimetry is abbreviated as ITC, IC_{50} stands for half maximal inhibitory concentration and K_i denotes inhibition constant. The range of uncertainty obtained is mentioned such that all the predictions have uncertainties lying within it. Values of several statistical parameters - root mean squared error (RMSE) and mean absolute error (MAE) for all TIES predictions as well as Pearson's r and Spearman's ρ correlation coefficients between $\Delta\Delta G_{TIES}$ and experimental results - are also reported in order to assess the quality of TIES results.

	CDK2	**Thrombin**	**TYK2**	**MCL1**	**PTP1B**	**BRD4**	**TRKA**
No. of ligands	7	11	9	20	16	16	16
No. of transformations	7	11	11	16	10	12	14
PDB	1H1Q	2ZFF	4GIH	4HW3	2QBS	4BJX	5JFV
Exp metrics (assay/source)	IC_{50}	ITC	K_i (cell-based)	K_i (FPA)	K_i (IC_{50})	IC_{50}	IC_{50}
Reference	[216]	[217]	[218, 219]	[220]	[221]	[22]	[23]
Range of uncertainty (kcal/mol)	0.2-0.3	0.2-0.4	0.1-0.2	0.2-0.5[†]	0.2-0.5	0.03-0.2	0.1-0.5
RMSE (kcal/mol)	0.8	0.8	0.5	1.4	0.5	0.8	0.8
MAE (kcal/mol)	0.7	0.7	0.4	1.2	0.4	0.7	0.7
Pearson's r	0.87	0.90	0.88	0.80	0.84	0.84	0.88
Spearman's ρ	0.86	0.91	0.88	0.80	0.82	0.94	0.70

[†] 5 of the 16 transformations have uncertainties between 0.7-0.8 kcal/mol due to the presence of a charged carboxylate group in the transforming part of the ligands. See details in Section 3.6.

for which these values are 1.2 and 1.4 kcal/mol, respectively. The value of the Pearson coefficient is above 0.80 for all targets and attains a value of 0.90

for thrombin. Similarly, the value of the Spearman coefficient is greater than 0.80 for all of them, attaining 0.91 for thrombin. The results are very precise for all proteins (their individual ranges of uncertainties are provided in Table 3.1). It is to be noted that 5 of the transformations of MCL1 ligands have higher uncertainties (in the range of 0.7-0.8 kcal/mol) than the remainder due to the presence of a charged carboxylate group in the transforming part of the ligands. Refer to Section 3.6 for details.

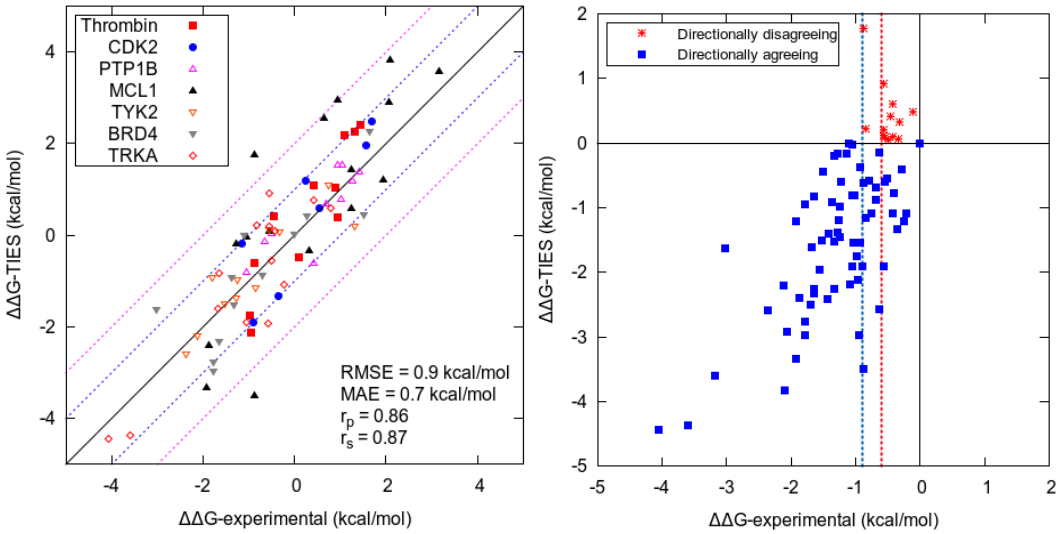

Figure 3.6: (a) Correlation between TIES-predicted relative binding affinities and experimental data for all seven protein targets studied. The black line is the perfect correlation line. Blue and pink dotted lines show the ±1 kcal/mol and ±2 kcal/mol ranges respectively. The majority of points lie within the ±1 kcal/mol band, a few points lie in the ±1 kcal/mol to ±2 kcal/mol band and only two points lie outside the ±2 kcal/mol range. (b) An alternative representation of the same data such that all the experimental values are negative. Blue squares are the directionally agreeing predictions while red stars are the directionally disagreeing ones. Red and blue dotted lines show the boundary of experimental values equal to -0.6 kcal/mol and -0.9 kcal/mol. All the predictions with $\Delta\Delta G <$ -0.9 kcal/mol are in directional agreement, while all directionally disagreeing predictions lie on the right side of the red dotted line except two.

Figure 3.6a is a correlation plot of the predicted binding affinities with the corresponding experimental values for all 81 transformations. The blue and pink dotted lines denote the ±1 kcal/mol and ±2 kcal/mol bands, respectively, from the perfect correlation denoted by a black line. All but two predictions lie

within the pink lines, while a few of them lie between the blue and pink lines. The high level of accuracy can be noted by the fact that the majority of points lie within the blue lines. 61 predictions (75.31%) deviate from the experimental binding affinities by less than 1.0 kcal/mol, while 79 predictions (97.53%) do so by less than 2 kcal/mol (Table 3.2 (left)). It is worth mentioning here that experimental binding affinities have significant uncertainties[228, 229]. The experimental error for relative binding affinities between two compounds has been reported to be in the range of 0.4-0.7 kcal/mol for high-quality binding affinity measurements[196]. However, for CDK2, TYK2, MCL1, PTP1B and thrombin, the error bars on experimental binding affinities are unavailable. Figure 3.7 shows the correlation for each protein separately along with the uncertainties in the results shown as error bars.

Table 3.2: A summary of the level of accuracy obtained for the total set of TIES predictions. The number of predictions found to be accurate for a specified absolute error range (left) and the number of predictions found to be in directional agreement with the increasing absolute values of experimental results (right). The lack of experimental errors means that the entire discrepancy is assigned to the theoretical predictions.

MAE <	**No. of predictions**
0.4	27
0.6	36
0.8	49
1.0	61
1.2	72
1.4	74

$\mathbf{\lvert\Delta\Delta G_{exp}\rvert >}$	**No. of directionally disagreeing predictions**
0.0	13
0.3	12
0.4	10
0.5	6
0.6	2
0.9	0

Figure 3.6b represents the results differently. When a prediction has the same sign as that of the corresponding experimental value it is said to be directionally agreeing with experiments, and otherwise it is taken to be directionally disagreeing. In Figure 3.6b the data-points from Figure 3.6a are rearranged such that all the experimental $\Delta\Delta G$ values are negative. This was done by flipping the signs of all the sets of $\Delta\Delta G_{TIES}$ and $\Delta\Delta G_{exp}$ for which the latter was positive originally. This representation of the results helps to see if the predictions follow the same trend as the experimental values. In Figure 3.6b,

all the points lying above the x-axis are directionally disagreeing (denoted by red stars) and those below the x-axis are directionally agreeing (denoted by blue squares). The red and blue dotted lines denote the experimental $\Delta\Delta G$ equal to -0.6 kcal/mol and -0.9 kcal/mol respectively. 13 points directionally disagree with experimental results. However, all but two of them lie to the right of the red line, while the remaining two lie between the blue and the red lines. This means that for experimental $|\Delta\Delta G|$ greater than or equal to 0.9 kcal/mol all the TIES predictions are in directional agreement. This is true given that the experimental values used in this study do not have error bars. Reports suggest that the uncertainties on the experimental $\Delta\Delta G$ are of the order of 0.4-0.7 kcal/mol[196]. Majority of the directionally disagreeing points lie within the range of experimental uncertainties. Therefore, a better agreement may be observed between TIES predictions and the experimental values when the errors bars on both of them are taken into account.

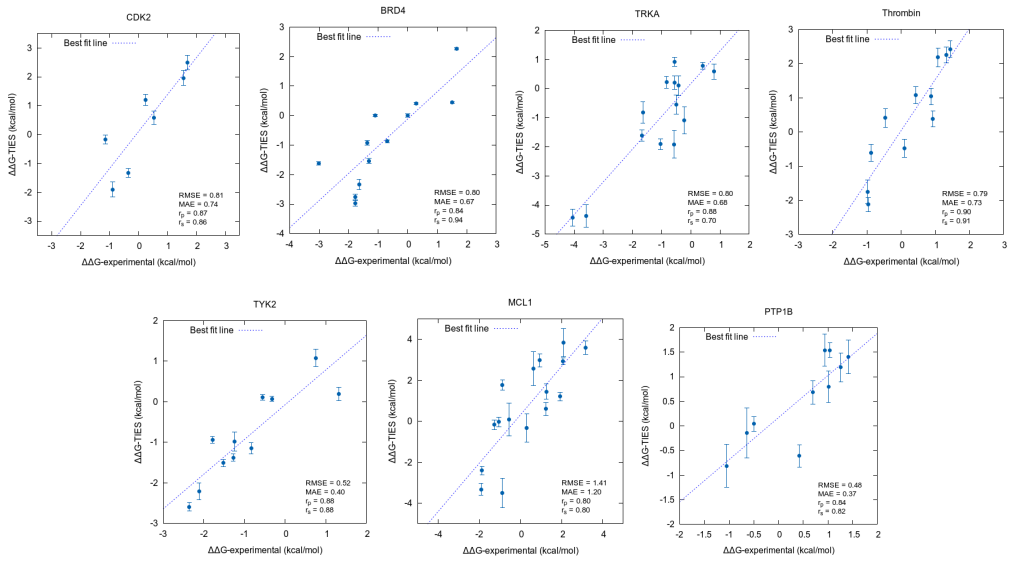

Figure 3.7: Correlation between TIES-predicted binding affinities and the experimental data for each biomolecular system shown separately. The uncertainties in the TIES predictions are included as error bars. The dashed line is the regression line in each case.

Theoretically, the $\Delta\Delta G$ predictions for a set of alchemical transformations which form a closed thermodynamic cycle should add up to zero. This value is

often referred to as the "hysteresis" and provides a way to assess the accuracy of predicted relative binding affinities. A zero hysteresis is a necessary but not sufficient condition for accurate and converged relative binding affinities along a closed thermodynamic cycle. Given the uncertainties associated with the $\Delta\Delta G$ predictions, the hysteresis value also has an associated uncertainty. This means that on repeating the calculations along the closed cycle, the value of hysteresis will be different. Table 3.3 lists the closed cycles formed by the ligand transformations studied here and the corresponding hysteresis values. Except one, all the values of hysteresis are zero within the error bars. It is interesting to note that one inaccurate prediction in the closed cycle may lead to large deviation of the hysteresis from zero. An example of this is the set of ligands L32,L42,L38 bound to MCL1 (Table 3.3) where the large value of hysteresis is just due to a large error in L38-L42 transformation. The predicted $\Delta\Delta G$ values for L32-L38, L38-L42 and L32-L42 are 3.59, -3.33 and 1.45 respectively and the corresponding experimental values are 3.17, -1.92 and 1.25.

Table 3.3: Hysteresis in the TIES predictions for the closed cycles formed by the ligand transformations studied.

Protein	Ligands forming closed cycles	Hysteresis (kcal/mol)
CDK2	L1Q,L20,L21	0.02
MCL1	L32,L42,L38	1.19
TYK2	L1,L6,L10,L15	0.01
	L1,L6,L10	0.32
	L1,L10,L15	0.31
	L1,L15,L6	0.06
	L6,L10,L15	0.07
Thrombin	L3,L5,L6,L7	0.06

3.4.2 Repeatability and Reproducibility of the TIES Protocol

Repeatability and reproducibility (as defined in Chapter 1) are the important features of TIES. This means that on repeating the TIES protocol for

any transformation (with or without any variation in its implementation, the software and/or the hardware employed), the new $\Delta\Delta G$ prediction would lie within $\pm\sigma$ and $\pm 2\sigma$ of the original $\Delta\Delta G$ with probabilities 0.68 and 0.95, respectively, as dictated by the central limit theorem. Figure 3.8 illustrates the repeatability of TIES results for a subset of ligand transformations binding to the CDK2 target protein. An ensemble simulation of size 20 was performed at each λ-window for all these transformations. Thereafter, the TIES analysis was performed on a large number of samples of 10 replicas out of the 20 at each λ-window to get a distribution of $\Delta\Delta G$ values. The mean of this distribution is denoted by open black circles along with their $\pm\sigma$ and $\pm 2\sigma$ ranges. The red and blue filled circles denote two independent TIES predictions using two randomly chosen nonoverlapping subsamples of 10 replicas at each λ-window. The red and blue circles lie within $\pm\sigma$ range for four transformations and within $\pm 2\sigma$ range for the remaining two transformations. This shows that the TIES protocol is indeed repeatable.

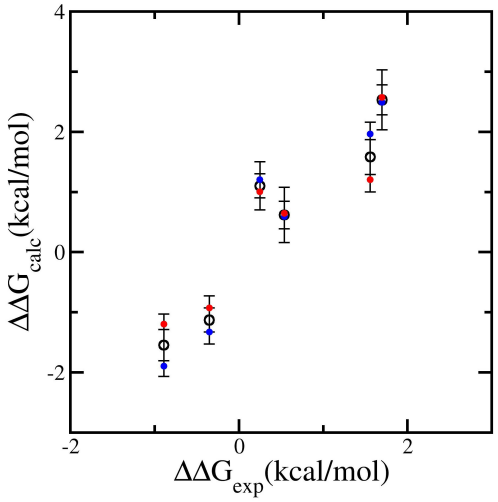

Figure 3.8: Repeatability of TIES: The relative binding affinities of the CDK2 ligands (black circles) were calculated using 10 values resampled from an ensemble of 20 replica simulations. Error bars are represented as standard deviations of σ and 2σ. For each calculated $\Delta\Delta G$ value, results are also shown for two randomly chosen non-overlapping 10-replica samples (blue and red dots). The data demonstrate that a 10-replica prediction will lie within $\pm\sigma$ and $\pm 2\sigma$ of the averaged relative binding affinities (open black circles) with confidence intervals of 0.68 and 0.95, respectively.

Table 3.4: Comparison of different parameters used in this study with those used in the study at Merck for the TIES calculations using the pmemdGTI software package.

Parameter	Original TIES	pmemdGTI
MD engine	NAMD	AMBER
Processor	CPU	GPU
Method	dual topology	single topology
Ensemble	NPT (300 K, 1 bar)	NVT (300 K)
Timestep	2fs	1fs
elec cut-off	12Å	9Å
elec decoupling/coupling	0-0.55/0.45-1	0-1
Softcore potential	vdW	vdW+elec
Buffer size	14Å	11Å
Number of λ-windows	13	11 (0,0.1,...0.9,1)
Initial structures	Min.*	Min.*, seq. eq.†(1.4 ns/λ)
Simulation run	2 ns equl., 4 ns prod.	1 ns equl., 4 ns prod.
Number of replicas	5	10

† seq. eq. stands for sequential equilibration, where the initial conformation for each λ-window is sequentially generated with 1.4 ns equilibration such that the equilibrated conformation of the current λ-window is used as the starting conformation for equilibration of next λ-window.
* Min. stands for minimization.

To illustrate the reproducibility of the TIES protocol, binding affinity predictions for all the BRD4 ligand transformations from this study (referred to as original TIES in this section) have been compared with the ones from an independent study by our collaborators at Merck. The binding affinity calculations at Merck were performed with GPUs (NVIDIA Tesla K80 and P100 nodes) using the pmemdGTI[230] software patch for the AMBER 16 package[33], which is an implementation of TI within the pmemd module of the AMBER 16 package (`http://lbsr.rutgers.edu/software-downloads`). The initial structures and the parameters for the protein and the ligands used for the Merck study were the same as used in this study. However, the two studies differ in the software, the hardware and the implementation of the free energy calculations. Table 3.4 details the differences in parameters used in the two studies. The key differences are those in the MD engines employed (NAMD vs AMBER), the hardware used (CPU vs GPU) and the topology schemes implemented (dual vs single). Figure 3.9 displays a comparison of the predicted relative binding affinities from the two studies with the correspond-

ing experimental data as well as with each other. Predictions from both the studies agree well with the experiments with Pearson correlation coefficients of 0.84 and 0.79 for the original TIES method and the pmemdGTI method respectively. When compared with each other, excellent agreement is achieved between the relative binding affinity predictions from the two studies with a correlation coefficient of 0.92. This provides an evidence of the reproducibility of the TIES protocol irrespective of the variations in the software, the hardware and the implementation of the free energy method employed.

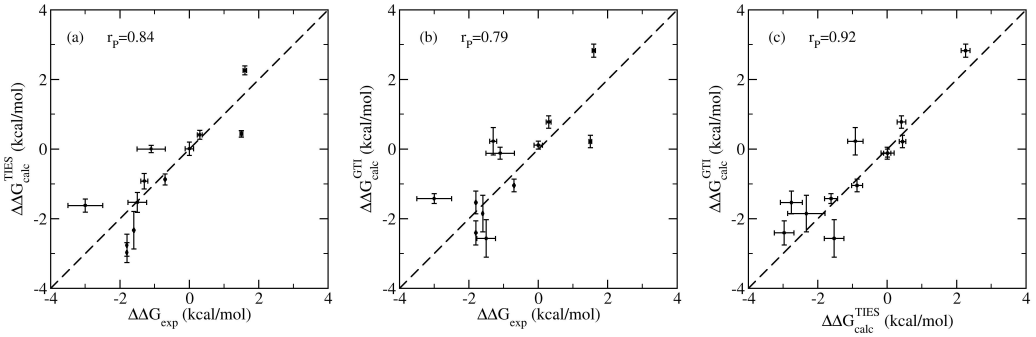

Figure 3.9: Correlation plots for the TIES results from two different sources when compared with the experimental data as well as with each other. Relative binding affinities: (a) from the original TIES study compared with the experimental data, (b) using pmemdGTI software employing GPUs compared with the experimental data, (c) from the two calculations compared with each other. Pearson's correlation coefficients (r_p) are shown for each plot to quantify the degree of agreement in each case.

3.4.3 Variation with Extended Simulation Duration

Here, the variation in results on extending the simulations is discussed and a comparison of the TIES result with those from the longer simulations is made. The transformation from ligand L1Q to LI9 bound to CDK2 is chosen and Figure 3.10 shows the variation of ΔG_{alch}^{bound} with simulation time up to 20 ns for all the five replicas of this system. In the inset, the variation of the absolute difference between the values corresponding to two farthest replicas is shown. The value of ΔG_{alch}^{bound} varies by as much as 0.8 kcal/mol between the 5 replicas after 20 ns. On the other hand, the $\pm\sigma$ range of the corresponding TIES prediction is 0.38 kcal/mol (the total simulation time for

TIES calculation is also 20 ns; 5 replicas for 4 ns each). Therefore, in this case, the results from the standard TIES protocol and those from the equivalent duration single TI calculation have similar variability. However, this is highly system dependent and larger variations between replicas can be seen in case of flexible systems[105, 199, 213, 214]. In such cases, TIES results will be more accurate and precise. It has been reported that the prediction from an ensemble of 50 short (4 ns) simulations is better than that from a single 1 μs simulation[212]. In addition, the TIES protocol allows a substantial reduction in the wall-clock time required to get results by running multiple replicas concurrently, which is not possible while performing a single "long" simulation.

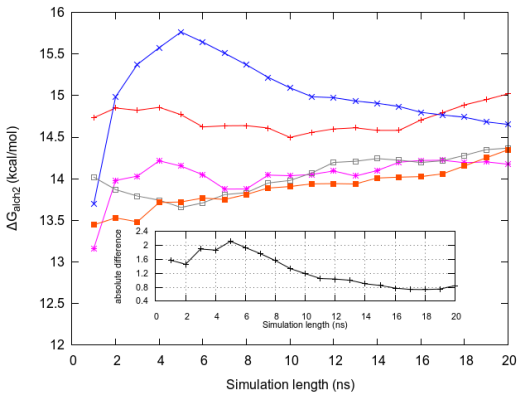

Figure 3.10: The replica-wise variation of ΔG^{bound}_{alch} with simulation length for the transformation L1Q-LI9 bound to CDK2. The variation of the absolute difference between the values corresponding to two farthest replicas is shown in the inset.

3.4.4 Size of the Alchemical Transformations

The size of the alchemical transformations studied using different free energy methods has been limited to one or two heavy atoms in most of the published studies. However, recently the FEP/REST method has been applied to ligand transformations up to 10 heavy atoms[196]. Here, the same level has been achieved by the successful application of TIES to a broad range of chemical modifications with the size of the alchemical transformations up to 10 heavy atoms included. The following is a list of a few chemical transformations with corresponding absolute errors (AE) studied here: benzyloxy to ethanamide

(AE = 0.5 kcal/mol), cyclohexyl to phenyl (AE = 0.5 kcal/mol), cyclopentyl to cycloheptyl (AE = 0.0 kcal/mol), indole to indane (AE = 2.1 kcal/mol), cyclohexyl methyl to 2,2,4,4-tetramethylcyclohexyl (AE = 0.2 kcal/mol), benzamide to p-fluorobenzenesulfonamide (AE = 0.6 kcal/mol) and hydrogen to methyl cyclohexane (AE = 0.1 kcal/mol).

3.4.5 Comparison with Another *In Silico* Method

FEP/REST (described in Chapter 2) has recently attracted a lot of attention by pharmaceutical companies as a reliable tool to be applicable in their virtual screening of ligands. It should be noted that FEP/REST, as published by Wang *et al.*[196], relies on a single MD simulation at each λ-window. In this study, five of the target proteins (CDK2, TYK2, MCL1, PTP1B and thrombin) and corresponding ligands used are the same as those used by Wang *et al.*, and hence a direct comparison of TIES predictions is made with theirs. The RMSE and MAE for each protein target using TIES (Table 3.1) are smaller than those reported by Wang *et al.*, except for MCL1, for which they are the same in both cases. The correlation coefficients obtained using TIES are better than those from FEP/REST in the case of CDK2 (0.87 versus 0.48) and thrombin (0.90 versus 0.71), while almost the same for the other proteins. 81.82% and 96.36% of TIES predictions are accurate within MAE range of 1.0 and 2.0 kcal/mol (these percentages are just considering the transformations corresponding to the five proteins which are in common with FEP/REST), respectively, while these values from Wang *et al.*'s report are 63.3% and 92.4%, respectively. Eighteen of the transformations studied here are in common with those studied by Wang *et al.* using their FEP/REST method[196]. Figure 3.11 shows a direct comparison of these 18 predictions from both the studies. The results from TIES are marginally better with slightly larger correlation coefficients and smaller RMSE and MAE. The number of transformations with MAE larger than 1 kcal/mol is only one in the case of TIES while three in the case of FEP/REST. The number of directionally disagreeing predictions in the case of TIES and FEP/REST are 1 and 2, respectively. It is important to

note that, unlike TIES, FEP/REST results are based on a single replica and there is no evidence of their repeatability. The comparable accuracies of the two methods gain further importance given the fact that TIES employs the open-source AMBER/GAFF force fields unlike the proprietary ones needed for FEP/REST. Moreover, the licence fee of the FEP+ package needed to run FEP/REST calculations is much higher than those of the standard MD engines.

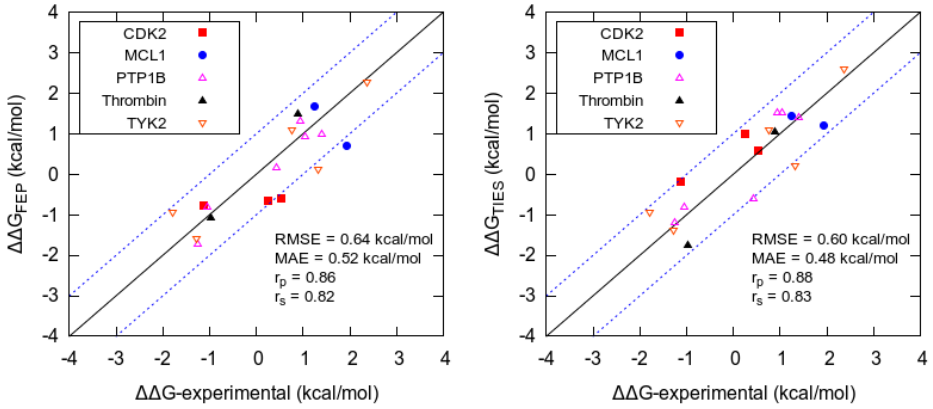

Figure 3.11: A comparison between the 18 ligand transformations which are common between the ones studied here and those studied by Wang *et al.* using FEP/REST[196]. Results from the FEP methodology are shown on the left, while those from TIES are shown on the right.

It is noteworthy here that the FEP/REST method always involves performing $\Delta\Delta G$ calculations in a closed thermodynamic cycle and artificially correcting the predictions by shifting their values in order to diminish the associated hysteresis. However, the reliability of this approach is debatable given the uncontrolled uncertainty associated with the value of hysteresis itself. In addition, it has the risk of distorting the correct predictions through the possible distribution of a large error in one prediction to all predictions along the thermodynamic cycle (as shown in Section 3.4.1) .

3.5 Dynamics of the Water Molecule in the Binding Pocket

Experimentally, it has been found that the S1 pocket of the active site of the human thrombin protein contains a water molecule when the ligand bound to

it has no substituent on the benzylamine ring[217]. This water molecule plays an important role in the ligand binding by mediating the hydrogen bonding between the amidino group of the ligand and the protein. However, if the benzylamide ring of the ligand has a substituent at the meta-position, the water molecule is absent. In this study, TIES methodology has been applied to study the transformation from meta-substituted benzylamide to benzylamine (denoted as A) and the reverse of this transformation (denoted as B); the predictions are in excellent agreement with those from experiments. TIES predicted $\Delta\Delta G$ values for the transformations A and B are 0.6 $\pm$ 0.2 kcal/mol and 1.0 $\pm$ 0.2 kcal/mol, respectively; the corresponding values from experiments are -0.9 and 0.9 kcal/mol, respectively. In addition, TIES successfully captures the dynamics of the water being pushed into the S1 pocket (in the case of transformation A) and pushed out from there (in the case of transformation B). The presence of water molecule in the S1 pocket has been quantified by calculating the probability of the occurrence of a water molecule in a cubic box (volume 1000 Å^3) centered around the S1 pocket over all conformations from the five replicas after aligning them to the initial structure. The probability goes from 0 at $\lambda = 0$ to 0.7 at $\lambda = 1$ for transformation A and from 0.6 at $\lambda = 0$ to 0.3 at $\lambda = 1$ for transformation B. The two end points ($\lambda = 0, 1$) of transformation A have been displayed in Figure 3.12 along with a representation of the occurrence of water molecule in the S1 pocket. The red frames represent the regions where the number density of water oxygen atoms is greater than or equal to that in bulk water. It is evident that the presence of water molecules is confined to channels C1 and C2 in the presence of a chlorine atom on the meta-position of the ligand ring but water molecules enter the pocket through C1 and C2 when the chlorine transforms into hydrogen.

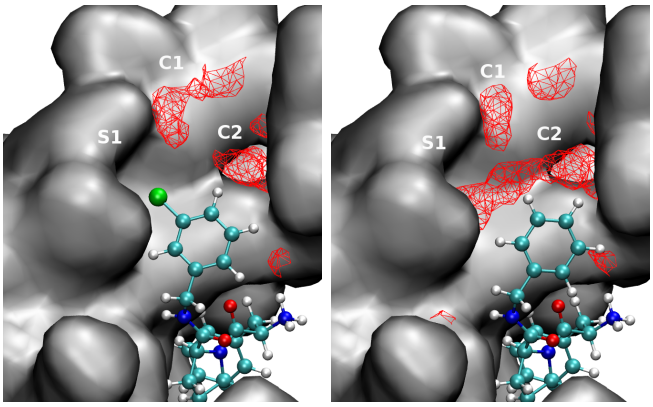

(a) (b)

Figure 3.12: Cross sections of the S1 pocket of thrombin for the two end λ-windows of an alchemical transformation involving mutation of *m*-chloro benzylamide to benzamidine. Red frames show the regions of water occupancy averaged over all the conformations from the 5 replica simulations aligned to the corresponding initial structures. (a) No water molecule bound in the S1 pocket in the presence of chlorine (green) at $\lambda = 0$; (b) Water molecule enters the S1 pocket through channels C1 and C2 on fully transforming Cl to H at $\lambda = 1$. The protein surface is shown in grey and ligand atoms are denoted according to the standard colour code.

3.6 Charged Groups in Alchemical Transformations

In the intermediate λ-windows, the electrostatic interactions are scaled down substantially and hence the charged group(s), if any, in the alchemically transforming part of the calculation are very weakly coupled to the remainder of the system. This results in largely fluctuating $\partial E/\partial\lambda$ value and, as a result, the TIES predictions in such cases are less precise. For instance, 5 out of the 16 transformations studied for MCL1 have larger uncertainties (0.7-0.8 kcal/-mol) as compared to the remaining 11 (uncertainties in the range of 0.2-0.4 kcal/mol). This is because all five of them have a charged carboxylate group in the mutating part of the ligand. To handle such cases, it may be necessary to modify the standard TIES protocol by increasing the number of replicas for the intermediate λ-windows and/or excluding the charged group from the mutating part of the ligands (an example provided in the next paragraph).

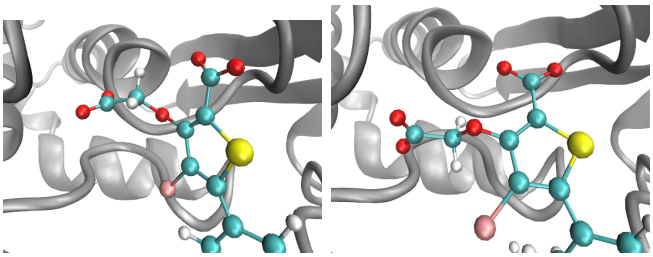

(a) (b)

Figure 3.13: Two different conformations of the flexible carboxylate group of ligand L14 inside the binding pocket of PTP1B taken from the same molecular dynamics simulation. Due to three adjacent rotatable bonds through which the carboxylate group is attached to the ligand, the corresponding dihedral angle changes substantially inside the binding pocket when the electrostatic interactions are scaled to small values. The protein is shown in grey ribbon and ligand atoms are colored by element; hydrogen in white, carbon in cyan, oxygen in red and nitrogen in blue.

One of the two carboxylate groups in all of the PTP1B ligands is attached to the thiophene ring of the ligand through three rotatable bonds. There is enough space in the binding pocket to allow this carboxylate group to move around making this group very flexible. Figure 3.13 shows two different conformations of this group captured from the same simulation at an intermediate λ-window of the transformation L6-L14 where it forms part of the alchemical region. It is evident that charged groups are quite flexible in the absence of strong electrostatic interactions. The $\Delta\Delta G$ prediction for this transformation using TIES is 0.6±1.7 kcal/mol, which is quite different from the experimental value of -1.0 kcal/mol. On repeating the calculation after excluding the charged carboxylate group from the alchemical transformation, the predicted $\Delta\Delta G$ value is -0.8±0.4 kcal/mol, which is both more accurate and precise.

3.7 Effect of Ligand Flexibility on Accuracy

From Table 3.1 and Figure 3.6, it can be seen that the predictions for MCL1 ligands have the largest deviation from their corresponding experimental values (largest RMSE and MAE). This can be attributed to their highly flexible structure. The structure of one of the MCL1 ligands has been shown in Figure 3.14 as a representative for all of them. Their generic structure includes a

4-membered linker connecting their two ends. One end of these ligands is a hydrophobic aromatic group buried deep into the lower pocket (LP) of the protein, while the other end is a fused heterocyclic carboxylic acid group bound to the upper pocket (UP) of the protein through an electrostatic interaction with the oppositely charged arginine residue (R263). Due to the presence of four adjacent rotatable bonds in the linker chain, the two ends of the ligands have flexible relative positions. The end buried inside the LP is relatively rigid compared to the other. Moreover, the latter is held by an electrostatic attraction which becomes very weak in the intermediate λ-windows further adding to its flexibility. This flexibility, which is a property of all the MCL1 ligands, can be held accountable for the least accurate predictions for MCL1 ligands.

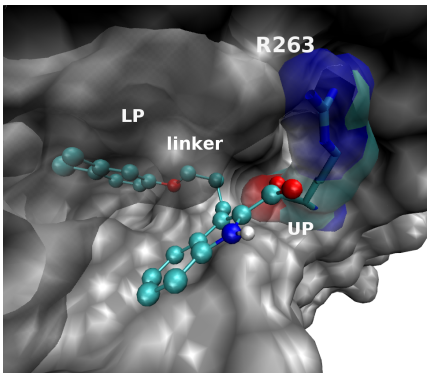

Figure 3.14: The generic structure of MCL1 ligands with the four membered linker joining the two ends of the ligand containing different functional groups. One end of the ligand is bound to the lower pocket (LP) of the protein and is relatively rigid, while the other end of the ligand is bound to the upper pocket (UP) of the protein and is quite flexible. The carboxylate group present at the second end of the ligand interacts with the side chain of the arginine residue of the protein (R263). The protein surface is shown in grey, the arginine residue (R263) is shown in colored electrostatic surface and ligand atoms are colored by element; hydrogen in white, carbon in cyan, oxygen in red and nitrogen in blue. All non-polar hydrogens have been excluded for clarity.

3.8 Conclusions

This chapter describes an ensemble-simulation approach based on thermodynamic integration to calculate relative binding affinities accurately and precisely. The accuracy in this context is defined as the closeness to the experi-

mental values and is achieved within the limitations of the force field employed. It has been shown to yield repeatable predictions with and without the variation in parameters like the MD code, the hardware and the topology scheme. Its excellent scalability allows one to perform multiple calculations concurrently. The protocol used is flexible and the parameters like ensemble size and simulation length can be adjusted to achieve the desired level of precision. The results provided in this chapter have very high accuracy for a diverse set of ligands bound to seven different protein targets showing the wide applicability of this approach. The alchemical transformations studied cover several types of chemical group modifications (up to 10 heavy atoms).

All MD simulations for this chapter were performed using the standard force fields which are known to be reliable for the systems studied. However, this may not always hold true and it is necessary to choose the potential parametrisations carefully as the accuracy of results is dependent on them. The version of TIES described here is unable to handle the situations where the alchemical transformation involves a change in the net charge. However, it can handle situations where the mutating part of the ligand is charged; although this may sometimes need a modification in the standard TIES protocol.

Given the features of rapidity, high accuracy, high precision, repeatability and reproducibility in the TIES predictions, this approach has the potential to be routinely applicable in drug design and personalised medicine. In fact, TIES calculations for BRD4 and TRKA included in this chapter were conducted as blind studies in collaboration with two major pharmaceutical companies, Glaxo Simth Kline and Pfizer, respectively. The experimental binding affinities in both these cases were only disclosed after the predictions using TIES were made available to the experimental collaborators. Both of these studies have been published and the results are in excellent agreement with the experimental data[22, 23]. This exhibits the suitability of ensemble simulation based approaches for their application as a virtual screening tool in the process of drug design.

Chapter 4

Hamiltonian-Replica Exchange Methods and Uncertainty Quantification

In the previous chapter, an ensemble simulation based approach (TIES) was described as a reliable way to predict relative binding affinities for ligand-protein complexes. It was shown that the free energy predictions from TIES are accurate and precise. TIES provides a control on the errors associated with the predictions made using the free energy methods based on classical MD simulations and its results are repeatable as well as reproducible. Thus, TIES can be useful in several important applications relying on the reliable prediction of ligand-protein binding affinities as mentioned in Chapter 1.

A large number of *in silico* methods based on one of the many accelerated sampling protocols are available to calculate free energy as described in Chapter 2. These methods seem to be useful in cases where the system studied has multiple local minima separated by large energy barriers. Among them, the Hamiltonian-replica exchange (H-REMD)[17] has proved to be very useful in the case of large solvated biomolecules. As discussed in Chapter 2, REST2[18] is an important variant of H-REMD, based on which, Wang *et al.* recently proposed a method called FEP/REST[19]. FEP/REST has been referred to as λ-REST2 in this thesis. In addition, free energy estimators like multistate

Bennett acceptance ratio (MBAR)[20] have been proposed which claim to get better estimates of free energy by utilising the maximum amount of information from the simulation data. It is sometimes claimed that the problem of the variability in results from independent short simulation based calculations as mentioned in Chapter 1 can be overcome by using such enhanced sampling methods and improved free energy estimators. However, a systematic investigation of their repeatability has not yet been done.

In this chapter, the idea of ensemble simulation from the previous chapter has been applied to the above mentioned accelerated sampling methods, REST2 and λ-REST2, and the free energy estimator, MBAR. An account of the variability in their free energy predictions, when performing a single short replica*, is provided. It has been found that the sensitivity of the classical MD simulations to their initial conditions and the resultant variation in the macroscopic properties calculated from short simulations (as discussed in Section 2.4) holds irrespective of the sampling protocol used or the free energy estimator employed. It is found necessary to perform ensemble simulation even when such improved sampling protocols and free energy estimators are employed in order to get a proper control on the statistical uncertainties associated with the free energy predictions. Extending the simulation duration (up to the cumulative duration of the ensemble simulation) does not help get over this variation and cannot be an alternative to ensemble simulation, an observation similar to the one made in Chapter 3 for non-biased MD simulations. In this chapter, REST2 and λ-REST2 are chosen as the representatives for all other accelerated sampling methods based on the replica-exchange technique. It should be noted that the work presented in this chapter has been published and some figures and tables have been reproduced from the published article[231]. Importantly, although this chapter focusses on a selected few free energy methods, the ob-

*The term "replica" means an independent MD simulation initiated from a random initial condition in the context of ensemble simulation. It should not be confused with the term "replica" within the context of replica-exchange simulation. To avoid such confusion in this chapter, the term "replica" has always been used to refer to the former, while the latter has been denoted as a "REST2 replica".

servations made are general and applicable to other free energy methods based on classical MD simulations.

4.1 Protein Targets and Ligands

Three different classes of proteins are chosen here to exhibit the wide applicability of the below described methods. Two of them, namely thrombin and bromodomain-containing protein 4 (BRD4), are the ones also used for the TIES study in Chapter 3. The third is fibroblast growth factor receptor 1 (FGFR1). The structure of all proteins and ligands studied are shown in Figure 4.1. It is known that the activation of FGFR1 is related to the pathogenesis of several human malignancies including various types of cancers[214]. Therefore, efforts are ongoing to develop FGFR1 inhibitors as anticancer treatment. Most inhibitors bind to the kinase domain (KD) of the FGFR1 protein.

It is well known that mutations in the FGFR1 KD can alter inhibitor binding rendering some drugs ineffective[214]. In this study, alchemical methods are applied to study the transformation of FGFR1 wildtype to V561M mutant when bound to two inhibitors, namely PD173074 and TKI258 (Dovitinib). V561M is the gatekeeper mutation. It occurs frequently and often leads to the development of resistance against several drugs.

4.2 Methods

In this section, the free energy schemes employed in the study have been described and the details about their implementation provided. The simulation protocol used and parameters employed for the same have been described. The parameters specific to REST2 and λ-REST2 have also been provided. The post simulation analysis method has been described and an estimate of the computational cost of the different free energy methods has been provided along with their comparison with that for TIES (as described in Chapter 3).

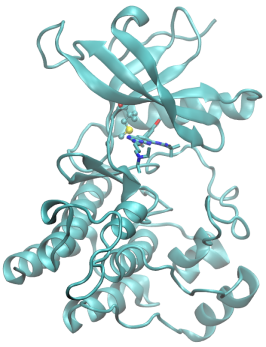

(a) FGFR1

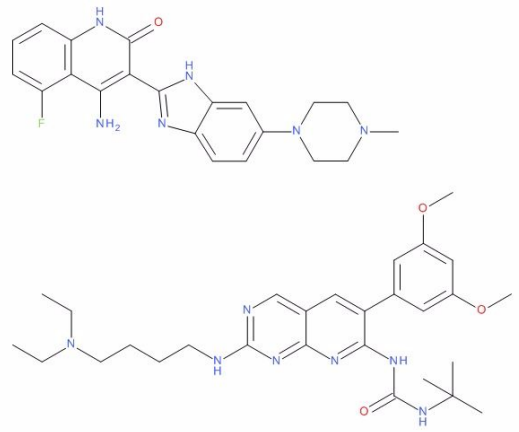

FGFR1 ligands: TKI258, PD173074 (top-down)

(b) Thrombin

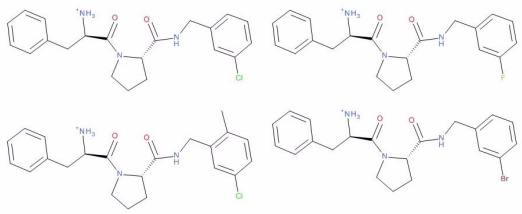

Thrombin ligands: L1, L4, L11, L9 (clockwise)

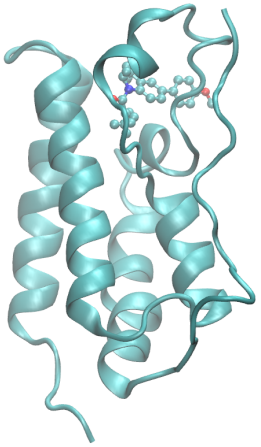

(c) BRD4

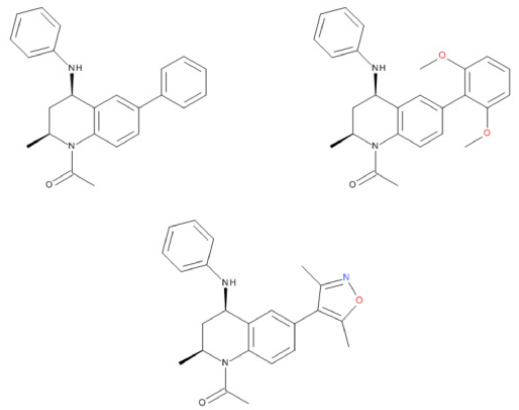

BRD4 ligands: L3, L6, L7 (clockwise)

Figure 4.1: Structures of all the target proteins (ribbon representation) studied, in each case shown bound to a ligand: (a) Fibroblast growth factor receptor 1 (FGFR1), (b) Serine protease thrombin and (c) Bromodomain-containing protein 4 (BRD4). The ligand is shown in stick representation while the hybrid side-chain is shown in ball-line representation for FGFR1, while the ligand is shown in ball-stick representation for others.

4.2.1 Free Energy Schemes

In this chapter, the method employed to calculate the relative free energy is identical to the TIES method as described in the previous chapter except the sampling protocol used to generate the ensemble of conformations which is different in the two. Unlike in the previous chapter, enhanced sampling protocols based on replica-exchange methods, REST2 and λ-REST2, have been used here. $\langle \partial E/\partial \lambda \rangle$ (Equation 2.26) is determined by performing an ensemble simulation at each λ window. Since the integrand in Equation 2.26 comprises points which are Gaussian random processes, stochastic calculus is employed to calculate ΔG_{alch} and the associated error as prescribed for TIES in the previous chapter. The following sampling schemes are used in this study to calculate the relative binding affinities:

I. **TIES-REST2:** In this scheme, the number of λ-windows and the corresponding values of λ are pre-defined and an ensemble of REST2 simulations is performed at each window. Each REST2 simulation amounts to running a set number of REST2 replicas in parallel which vary only in their solute potential scaling factors (or equivalently their effective temperatures, T_{eff}) and exchange of configurations are attempted regularly between the neighbouring REST2 replicas. TIES analysis is performed using $\partial E/\partial \lambda$ values of samples only from the REST2 replicas at $T_{eff} = 300$ K to get the ΔG_{alch} and associated uncertainty.

II. **TIES-REST2-M:** This scheme involves just re-analysing the simulation data from scheme I and does not require any additional simulations. It employs MBAR as a reweighing technique to calculate $\partial E/\partial \lambda$ using samples from REST2 replicas at all T_{eff} values from scheme I at each λ-window for each REST2 simulation followed by the standard TIES analysis. This scheme is expected to yield free energy predictions more precise than those from scheme I as the entire simulation data generated by the REST2 simulations is utilised unlike scheme I where a majority of it is discarded.

III. **TIES-λ-REST2:** This scheme involves running an ensemble of λ-REST2 simulations. A λ-REST2 simulation is performed by running a pre-defined number of REST2 replicas in parallel which vary in their T_{eff} and λ values and exchange of configurations are attempted regularly between neighbouring REST2 replicas (neighbouring REST2 replicas are the ones with adjacent values of λ). Among REST2 replicas, λ varies from 0 to 1 in a linear fashion, whereas T_{eff} attains its maximum value at the middle λ value and minima at the end-points (that is, $\lambda = 0, 1$). The $\partial E/\partial\lambda$ value is calculated for each REST2 replica (defined by the pair of λ and T_{eff}) using the samples only from itself. The standard TIES analysis follows to get ΔG_{alch} and associated uncertainty.

IV. **TIES-λ-REST2-M:** This scheme involves just re-analysing the simulation data from scheme III and no additional simulations are required. MBAR is used to calculate the $\partial E/\partial\lambda$ value for each REST2 replica using samples from multiple REST2 replicas followed by the standard TIES analysis. This allows maximum utilisation of the available samples and is expected to yield more precise results than those from scheme III.

In schemes I and II, 13 λ-windows (0.00, 0.05, 0.10, 0.20,....0.80, 0.90, 0.95, 1.00) are used. The ensemble size is taken to be 5 (same as that for TIES as described in Chapter 3), which means that 5 REST2 simulations are performed at each λ-window. For each REST2 simulation, 10 REST2 replicas are run with T_{eff} varying from 300 K to 600 K. Thus, a single TIES-REST2 run amounts to performing 650 MD simulations.

Schemes III and IV involve performing 5 λ-REST2 simulations (that is, the ensemble size is taken to be 5). For each λ-REST2 simulation, 13 REST2 replicas are run with their corresponding λ values linearly varying from 0 to 1. At $\lambda = 0.5$, T_{eff} is taken to be 600 K which symmetrically reduces to 300 K at both the end-points ($\lambda = 0, 1$). Thus, a single TIES-λ-REST2 run amounts to running 65 MD simulations.

4.2.2 Definition of the "Hot" Region

As described in Chapter 2, for all REST2 as well as λ-REST2 simulations, a small region of the system (usually a few atoms from the solute) is defined as the effectively "hot" region. This region is usually referred to as the REST2 region and is the one whose non-bonded interactions are scaled down by a potential scaling factor (see details in Chapter 2). In this study, the REST2 region for all ligand alchemical transformations has been defined as follows: for unbound ligand calculations - all the alchemically mutating atoms; for bound ligand calculations - all alchemically mutating atoms and all protein residues within 3Å distance of the former. For protein mutations, the REST2 region is defined as follows: for unbound protein calculations - the mutant residue and all protein residues within 3Å distance of the former; for bound protein calculations - the mutant residue, all protein residues within 3Å of the mutant residue and 4Å of the ligand, and all ligand atoms within 4Å of the mutant residue.

4.2.3 Initial Structures and Simulation Setup

All the initial structures and parameters for the systems studied here have been taken from the previous TIES studies[21, 22, 214], out of which thrombin and BRD4 have been described in the previous chapter. The force field used for all proteins is AMBER[223] and that for all ligands is GAFF[41], which are known to be reliable for the protein-ligand systems like those studied here. TIP3P model [224] was used for water molecules. Standard protonation states were assigned to all titratable residues at pH 7, with histidines protonated on the ϵ position (HIE). The customised version of NAMD 2.11 package[45, 232] has been used to perform all simulations for this chapter. Three-dimensional periodic boundary conditions were employed. Non-bonded interactions were turned beyond the cut-off distance of 12 Å. Long range electrostatic interactions were handled using Particle Mesh Ewald (PME) method. RATTLE algorithm was employed to constrain all the bonds with hydrogen atoms in order to obtain a timestep of 2 fs in the simulations. The system temper-

ature and pressure were maintained at 300 K and 1 bar, respectively, using Langevin thermostat (with a damping coefficient of 5 ps^{-1}) and Berendsen barostat (compressibility of 4.57 $\times$ 10^{-5} bar^{-1} and a relaxation time of 100 fs). The simulation length for all replicas (and REST2 replicas) has been taken to be 4 ns with the timestep of 2 fs. An exchange of configuration was attempted every 1 ps and the conformations were saved after every 10 ps. Van der Waals interactions were scaled linearly between $\lambda = 0$ and 1 with a soft core potential being used for the same to avoid the problem of "end-point catastrophes" as described in Chapter 2. In the case of electrostatic interactions, they are decoupled linearly for the disappearing atoms from $\lambda = 0$ to 0.55 and fully decoupled beyond that, while coupled linearly for the appearing atoms from $\lambda = 0.45$ to 1 and are fully decoupled otherwise.

4.2.4 Computational Cost

As pointed out earlier, each of the four free energy schemes described above require a large number of MD simulations to be performed. However, it is possible to run all simulations in parallel and complete them in the wall clock needed to complete one simulation given that sufficient computational resources are available, which is another important advantage of the methods described in this chapter. The time to solution is about 6-8 hours (which may be further reduced by the use of GPUs). Scheme I/II cost an order of magnitude more than schemes III/IV, which are slightly more expensive than the standard TIES calculation. Table 4.1 contains the data on the computational costs of all these schemes and their comparison with TIES.

Table 4.1: A comparison of computational costs for different free energy calculations using L1-L9 ligand alchemical transformation bound to thrombin (∼60k atoms). All the data is taken from 4 ns long MD simulations performed on SuperMUC, a machine at the Leibniz Supercomputing Center (LRZ).

Calculation	No. of cores	Wall clock time (hrs)	Core hours
TIES	8320	5.75	47840
Scheme I/II	83200	6.82	567424
Scheme III/IV	8320	6.82	56742

4.2.5 Uncertainty Quantification

As mentioned earlier, the simulation output of all the methods described in this chapter has been analysed using the TIES methodology to yield the free energy predictions and associated uncertainties. It is worth mentioning here that TIES analysis is different from merely running the conventional TI calculation five times followed by computing five integrals and assessing the error. TIES involves performing stochastic integration recognising that each point of the integrand is a Gaussian random process and the uncertainty in the final integral is given by the convolution of the uncertainties in individual points of the integrand. The error bars so obtained furnish an estimate of the repeatability of the results and hence this approach provides a reliable way of uncertainty quantification.

4.3 Binding Affinity Predictions

In this section, the results obtained from all four free energy schemes have been described. The replica-wise variation of results has been provided and discussed. A comparison of the results from all four schemes with each other as well as with the experimental data has been done. The effect of the duration of simulations on the accuracy and precision of the results for each scheme has been provided.

4.3.1 Variability in Different Free Energy Schemes

The relative binding affinity predictions for all protein-ligand complexes using all 4 schemes have been provided in Table 4.2. The notation of "forward" and "reverse" transformations have been borrowed from the previous FGFR1 TIES study[214]. Here, "forward" means V $\rightarrow$ M transformation while "reverse" means M $\rightarrow$ V transformation; their initial structures were prepared from different PDB files. The hysteresis, which is the residual $\Delta\Delta G$ over a closed thermodynamic cycle, can be eliminated here by calculating $\Delta\Delta G$ in both directions. An account of the replica-wise variation of results for all schemes is provided in Table 4.2. This variation is 0.8-1.3 kcal/mol for FGFR1 and

Table 4.2: Relative binding affinity predictions for all complexes using the four schemes (I to IV†). The range of $\Delta\Delta G$ values is derived from the differences between the largest $\Delta G_{alch}^{protein/lig}$ and the smallest $\Delta G_{alch}^{complex}$ and *vice versa*, whose values are provided in Table A.8 of the Appendix. All values are in kcal/mol.

System	Scheme	Range using 5 replicas	$\Delta\Delta G_{TIES}$	$\Delta\Delta G_{exp}$‡
V561M mutant (forward) with PD173074	I	2.86 to 3.95 (1.09)	3.56(0.18)	2.73(0.13)
	II	2.80 to 4.08 (1.28)	3.54(0.17)	
	III	2.84 to 3.70 (0.86)	3.23(0.08)	
	IV	2.82 to 3.61 (0.79)	3.19(0.06)	
V561M mutant (reverse) with PD173074	I	2.20 to 2.97 (0.70)	2.65(0.13)	
	II	2.14 to 3.17 (1.03)	2.65(0.12)	
	III	2.91 to 3.87 (0.96)	3.42(0.10)	
	IV	3.00 to 3.82 (0.82)	3.42(0.09)	
V561M mutant (forward) with TKI258	III	-0.67 to 0.25 (0.92)	-0.15(0.09)	-0.60(0.82)
	IV	-0.73 to 0.31 (1.04)	-0.19(0.08)	
L1-L9 with thrombin	III	0.29 to 1.14 (0.85)	0.67(0.10)	0.43
	IV	0.38 to 1.14 (0.76)	0.67(0.08)	
L4-L11 with thrombin	III	0.29 to 1.82 (1.53)	1.06(0.14)	1.08
	IV	0.24 to 1.82 (1.58)	1.05(0.12)	
L3-L6 with BRD4	III	-1.60 to -0.45 (1.15)	-1.14(0.10)	-1.65(0.05)
	IV	-1.61 to -0.38 (1.23)	-1.14(0.08)	
L3-L7 with BRD4	III	-0.07 to 0.61 (0.68)	0.27(0.10)	-1.37(0.10)
	IV	-0.18 to 0.67 (0.85)	0.27(0.09)	

† In scheme IV, the samples from states which are electrostatically fully decoupled from the state of interest are excluded from MBAR analysis. This is because the energies of such samples at the state of interest may approach infinitely high values due to overlapping atoms by virtue of the non-softcore electrostatic potential used in these simulations.

‡ The experimental error bar is the standard error of repeated measurements. It is unavailable for thrombin complexes.

goes up to as high as 1.6 kcal/mol and 1.2 kcal/mol for thrombin and BRD4, respectively. These ranges are calculated by taking the differences between the largest $\Delta G_{alch}^{complex}$ and the smallest $\Delta G_{alch}^{protein/lig}$ and *vice-versa* (all these values are provided in Table A.8 of the Appendix). Such a variation in results can be attributed to the sensitivity of classical MD simulations to the initial conditions as discussed in Section 2.4. It is important to note that such variation is observed even on using enhanced sampling protocols and improved free energy estimator. It is worth mentioning that this variation is system-dependent and may be larger for more flexible complexes and larger transformations.

4.3.2 Comparison of Different Free Energy Schemes

Interestingly, the $\Delta\Delta G$ predictions from scheme II and IV are very close to those from schemes I and III respectively (Table 4.2). However, the former

have marginally smaller error bars than the latter. This clearly implies that performing the MBAR anlaysis on the simulation data does not affect the accuracy of the results and only very slightly improves their precision for the systems studied here. However, this may not be true for larger proteins which may benefit from MBAR unlike the ones used here which are all small and compact. An additional comparison between the results from scheme I/II with those from scheme III/IV suggests that both the accelerated sampling protocols, REST2 and λ-REST2, have comparable accuracy within error bars. However, as noted earlier, the latter is computationally an order of magnitude cheaper than the former. Thus, the preference of scheme III over scheme I logically follows. Therefore, in the light of these observations, it can be concluded that scheme IV is the most cost-effective method of obtaining reliable binding affinity predictions.

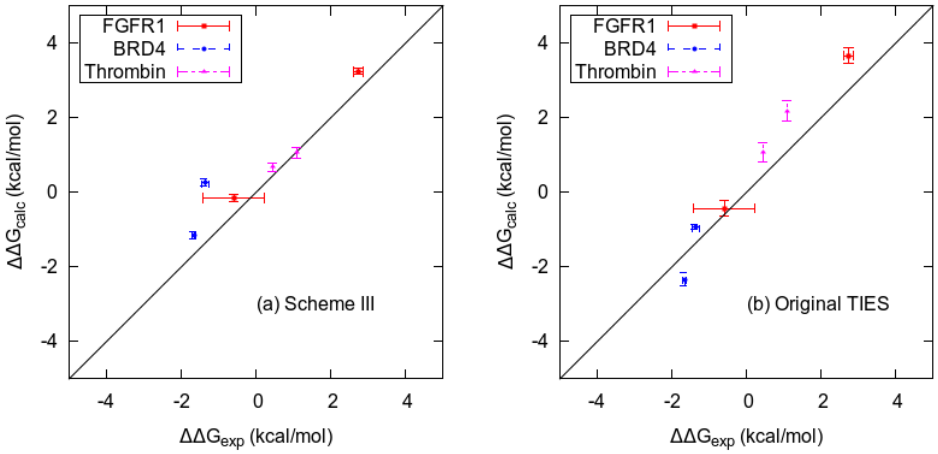

Figure 4.2: Comparison of the relative binding affinities for all complexes using (a) scheme III and (b) the original TIES scheme with normal MD simulations without REST2. The correlation coefficients for both the schemes are good (> 0.9). The RMSE and MAE for both schemes are $\sim$0.7 and 0.6 kcal/mol respectively.

It should be noted that the binding affinities predicted by scheme I/II and scheme III/IV for V561M mutant (reverse) bound with PD173074 are statistically different at the 95% level (Table 4.2). This suggests that the errors bars reported here underestimate the true uncertainty in the binding affinity as expected from any bootstrap approach. However, an ensemble simulation is expected to provide a better estimate of uncertainty than a single simulation

as the latter may suffer from the presence of correlated samples unlike the former.

4.3.3 Comparison with Experimental Data

As noted above, scheme IV appears to be the best of all the schemes used in this study. However, its results are almost identical to those from scheme III. Therefore, the results from the latter have been compared with the experimental values. They are very accurate with their differences from the corresponding experimental values lying in the range of 0.02-0.69 kcal/mol for all but one transformation. The excellent agreement of the $\Delta\Delta G$ predictions from scheme III with those reported from experiments is shown in Figure 4.2(a). It is noteworthy that the hysteresis in the predicted $\Delta\Delta G$ for FGFR1 V561M bound to PD173074 has diminished to zero in this study (0.19 kcal/mol for scheme III which can be considered zero within the reported error bars) from 0.83 kcal/mol as reported in the previous TIES study (reference [214] using 5 replicas; may reduce further on increasing the number of replicas). In case of the ligand transformation L4-L11 bound to thrombin, the difference between the predicted $\Delta\Delta G$ with that from experiment has come down to 0.02 kcal/-mol (in case of scheme III) from 1.10 kcal/mol as reported in the previous TIES study (reference [21]). This suggests that Hamiltonian replica-exchange, in combination with the TIES protocol, improves the accuracy of predictions by accelerating the convergence of results from different initial structures.

A comparison of the $\Delta\Delta G$ predictions for all ligand-protein complexes from scheme III and from the original TIES (without REST2) is made in Figure 4.2. Both of them are quite accurate with correlation coefficients greater than 0.9 and root mean square error (RMSE) and mean absolute error (MAE) of around 0.7 and 0.6 kcal/mol, respectively. Not surprisingly, Scheme III predictions have smaller uncertainties. It is clear from Figure 4.2 that λ-REST2 improves the accuracy of relative binding affinity predictions for thrombin over the straightforward TIES scheme. For other proteins, there is no observable change except the L3-L7 transformation bound with BRD4 where the results

from scheme III are less accurate. This suggests that thrombin, unlike the other two, has multiple local minima separated by energy barriers.

It should be noted that, although the methods used in this study are based on thermodynamic integration, the conclusions made here are general and applicable to other alchemical free energy methods like the recently published FEP/REST[196].

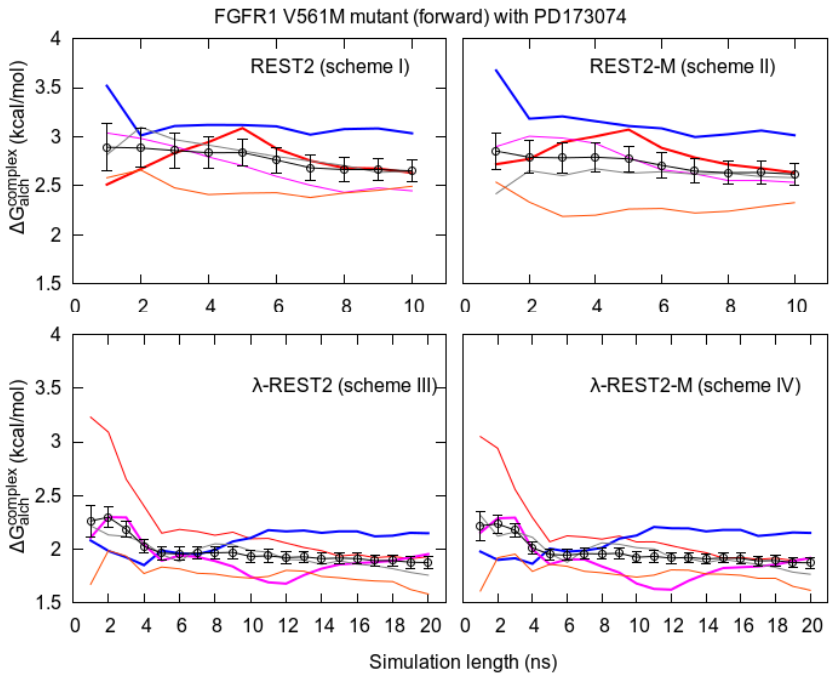

Figure 4.3: Variation of cumulative $\Delta G_{alch}^{complex}$ with simulation length for five replicas of relative free energy calculations (shown in different colours) and their combined TIES analysis result (shown in black with error bars) for all 4 schemes. The simulations were extended up to 10 ns for schemes I and II and up to 20 ns for schemes III and IV. Some of the replicas are highlighted (thick lines) to show how a single replica may fluctuate substantially or become trapped in a local potential minimum while the ensemble average overcomes such problems.

4.3.4 Dependence on the Duration of Simulation

The variation of the predicted free energies with the duration of simulation is shown in Figure 4.3. The top panel displays results from schemes I and II up to 10 ns while the bottom panel displays those from scheme III and IV up to 20 ns. The cumulative $\Delta G_{alch}^{complex}$ from individual replicas (coloured plots) and their ensemble averages calculated using TIES protocol (black plots with error bars)

are both included. There is negligible variation in results beyond 4 ns. It can be seen from Figure 4.3 that the differences between the values corresponding to the black line at 4 ns and 10 ns is less than 0.2 kcal/mol for schemes I and II and less than 0.1 kcal/mol for schemes III and IV. The contraction of error bars is also marginal beyond 4 ns for all schemes. It is worth mentioning here that such a behaviour is system-dependent; it may be necessary to increase the ensemble size and/or simulation duration to achieve a similar precision for larger alchemical transformations or more flexible proteins.

The variation of the results from individual replicas with the duration of simulation should be noted in Figure 4.3 (coloured plots fluctuate much more than the black plots). This indicates that a single replica consistently generates larger variation in predictions. Some of the coloured lines are highlighted in Figure 4.3 which correspond to the replicas which either fluctuate considerably or get trapped within a region of conformation space. For instance, in the top panel of Figure 4.3, the blue lines never get closer to the black ones. The ensemble average gets over such issues. Although the variation in results from a single replica is small for the complex shown in Figure 4.3, it may be larger for other protein-ligand complexes and hence performing a single replica is not reliable.

4.4 Conclusions

This chapter describes four different relative binding affinity calculation methods, namely TIES-REST2, TIES-REST2-M, TIES-λ-REST2, and TIES-λ-REST2-M, based on thermodynamic integration. They all employ the concept of ensemble simulation (that used for TIES as described in Chapter 3) in combination with the different versions of the Hamiltonian replica exchange method. The results are found to be accurate and precise for a range of ligand-protein complexes and the schemes have a built-in mechanism to control errors. An account of the replica-wise variation in results has been provided to emphasise the importance of ensemble simulation and the inability of a single replica to

properly assess statistical uncertainties. TIES-λ-REST2 is found to be equally accurate as TIES-REST2 for an order of magnitude less computational cost. MBAR[20] is shown to have to no effect on the accuracy and only marginally improve the precision of the results and hence is found to be not necessary for the biomolecular systems studied. In the case of thrombin complexes, the Hamiltonian replica-exchange methods are shown to yield more accurate results as compared to the ones from non-biased MD simulations. It is established that ensemble simulations provide a systematic means of uncertainty quantification for all methods based on classical MD simulations and hence are required irrespective of the sampling protocol, the free energy estimator and the duration of the simulation.

Chapter 5

Enhanced Sampling of Molecular Dynamics with Approximation of Continuum Solvent

Chapter 2 provides an overview of the *in silico* free energy methods available, categorised into alchemical and end-point methods. Two further points were also made. Firstly, that all the methods based on classical MD simulations are sensitive to the initial conditions. Secondly, that ensemble averages should not be replaced with time averages given that both are equal only in the limit of the Poincaré recurrence time, which is inaccessible. In Chapters 3 and 4, ensemble simulation based approaches based on an alchemical free energy method, thermodynamic integration, have been described and successfully applied to calculate accurate, precise and repeatable relative binding affinities for a large number of target proteins and ligands.

Most of the alchemical methods yield relative binding affinities and hence are of restricted validity as the relative change must be "small". However, this problem does not persist on calculating absolute binding affinities. As discussed in Section 2.3.3, a few alchemical methods can be used to calculate the absolute binding affinity. However, running a single (insufficiently long)

replica version of these methods has the similar issue of variability in results, as discussed in the previous chapters for other methods. The TIES approach (as described in Chapter 3) has led one of my colleagues to develop an ensemble simulation based approach to calculate the absolute binding affinity based on an alchemical method[231]. The variation in charge between the two end-points in alchemical methods also causes problems. However, corrections for electrostatic finite-size effects[233, 234] were used to tackle this issue in the case of charged ligands in our recently published work on absolute binding affinity calculations[231].

In some situations, it is preferred to compromise on the accuracy of the predictions in order to reduce the cost of the calculations. In such situations the end-point methods are employed to predict the absolute binding affinities. They do not have the problem of restricted validity and do not require additional correction terms for charged ligands, which are their additional advantages over alchemical methods. One of the most popular end-point method is MMPB(GB)SA as described in Chapter 2. In this chapter, a new approach called enhanced sampling of molecular dynamics with approximation of continuum solvent (ESMACS) to calculate absolute binding affinities based on the MMPBSA method has been described. It utilises ensemble simulation to yield precise and repeatable predictions with a proper control on statistical uncertainties.

The term "MMPBSA" has many different meanings in literature. Some authors use it to refer to the free energy calculation based on docked structures[196]. Generally, it refers to free energy calculation based on a single MD simulation, which may or may not include the configuration entropies. On the other hand, the ESMACS approach always involves an ensemble simulation to calculate converged binding affinities including the configuration entropy and the free energy of association. It may be performed using single or multiple trajectory approaches. The size of the ensemble simulations is determined systematically to obtain a desired level of precision. The time

required to get the results using ESMACS is short (typically ∼8 hours) which makes it directly applicable in drug design and personalised medicine.

The sensitivity to the initial conditions in the case of end-point methods has been acknowledged in the literature[105, 199, 201–203, 210]. Wan *et al.* have shown that the results from 50 4 ns long simulations are more accurate than those from a single 1 μs long simulation[212]. Furthermore, ESMACS exploits the concept of ensemble simulation to evaluate statistical uncertainties and obtain repeatable results.

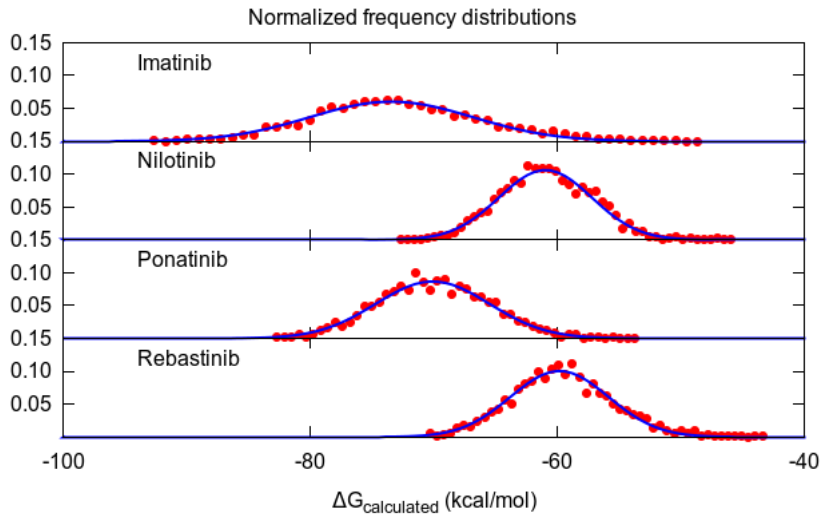

Figure 5.1: Normalized frequency distributions of ΔG values for a set of ligands bound to Abl T315I mutant kinase fitted to Gaussian distributions.

5.1 Ensemble Simulation Based Approach

Traditionally, MMPBSA method has been based on time averaging of a single MD simulation. However, it has been reported that the variation between two short replicas (where replicas have identical initial conditions with the exception of the intial velocities used which are randomly drawn from a Maxwell-Boltzmann distribution) can be as much as 12 kcal/mol[105]. A similar observation is made in Figure 5.1 where a normalised frequency distribution of ΔG values from 50 replicas is shown for a set of four ligands bound to Abl T351I kinase. All of them have a characteristic Gaussian distribution. Given such replica-wise variability in results, ESMACS follows the ensemble simu-

lation approach, where multiple replicas are run, with MMPBSA and normal mode analysis performed on each, yielding an ensemble of ΔG values which is used to calculate the final binding affinity and associated uncertainty to be reported (discussed in Section 5.3). Thus, ESMACS yields reliable free energy predictions.

5.2 Protein Targets and Ligands Studied

In this study, four important therapeutic target proteins have been chosen, namely Bcr-Abl kinase, HIV-1 protease, bromodomain-containing protein (BRD4) and tropomyosin receptor kinase A (TRKA). The latter two were also studied using TIES and have already been described along with their structures in Chapter 3. The fusion of Abelson (Abl) tyrosine kinase gene at chromosome 9 and the break point cluster (Bcr) gene at chromosome 22 results into chimeric oncogene Bcr-Abl. This oncogene causes chronic myelogenous leukemia (CML)[235]. Bcr-Abl tyrosine kinase has been implicated in the pathogenesis of CML and hence tyrosine kinase inhibitors (TKIs) are the first-line therapy for most CML patients[236]. Mutations in the Abl kinase domain are known to cause drug resistance[237]. In this study, the wildtype (WT) Bcr-Abl kinase and four of its commonly occurring mutants, E255K, T315I, Y253F, and F317R, are chosen for study in combination with a set of four TKIs, namely Imatinib, Nilotinib, Ponatinib and Rebastinib (or DCC-2036). Figure 5.2 shows the structures of the WT Bcr-Abl kinase and all four TKIs studied.

With the increasing understanding of the life cycle of the human immunodeficiency virus (HIV), a variety of drugs targeted to specific steps in the viral reproductive process are being developed. Protease inhibitors (PIs) are one class of such antiretroviral drug; they check virus replication by inhibiting the HIV-1 protease, an important component in the viral reproductive cycle[238]. Nine HIV-1 protease inhibitors have been approved by the US food and drug administrator. In this study, the binding of 3 HIV-1 PIs are investigated.

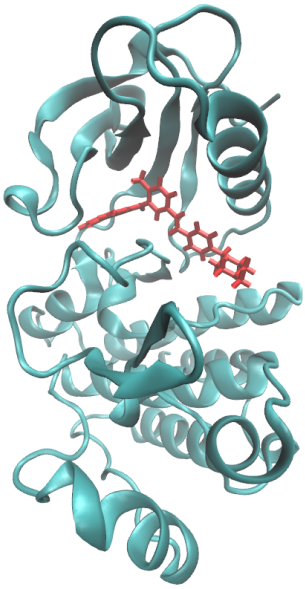

WT Abl kinase with Imatinib (red)

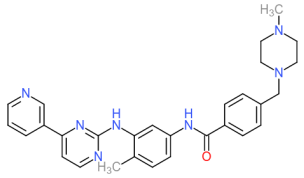

Imatinib

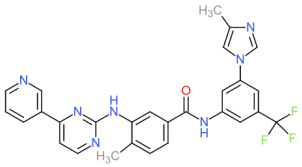

Nilotinib

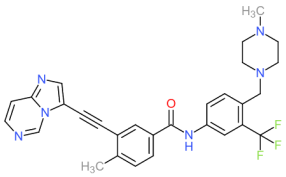

Ponatinib

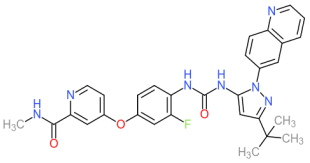

Rebastinib

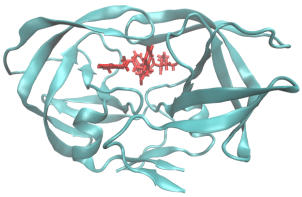

WT HIV-1 protease with LPV (red)

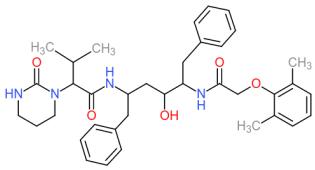

Liponavir (LPV)

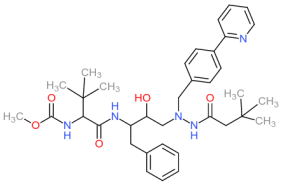

Atazanavir (AZV)

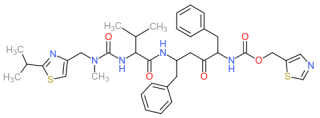

Ritonavir (RTV)

Figure 5.2: Chemical structures of the proteins and inhibitors studied. Proteins are shown in ribbon representation while the ligands binding to them are shown using stick model in red.

Figure 5.2 shows their structures.

5.3 Method

This section details the simulation setup and the ESMACS free energy workflow employed to calculate all the binding affinities reported in this chapter. A description of the evaluation of uncertainties in ESMACS results is also provided. In addition, the repeatability of ESMACS results is discussed.

5.3.1 Initial Structures and Simulation Setup

The starting structures for Abl kinase complexes were taken from 4 different PDBs: 1IEP for Imatinib complexes, 3CS9 for Nilotinib complexes, 3IK3 for Ponatinib complexes and 3QRI for Rebastinib complexes. Each PDB was bound to one of the 5 mutants of the protein. The other mutants were prepared by introducing the appropriate mutation into the original sequence using the binding affinity calculator (BAC)[239]. In the case of HIV-1 protease, the starting structures of the protein as well as all drugs were taken from a previous ESMACS study[105]. For BRD4 and TRKA, the initial structures were prepared as described in Chapter 3.

All the protein-ligand complexes were simulated in an orthorhombic water box with buffer width of 14 Å. The net charge of the system was neutralised by addition of counterions. The AMBER ff99SB-ILDN force field[223] was used for protein parameters and general AMBER force field (GAFF)[41] was employed for ligands. TIP3P model [224] was used for water molecules. Standard protonation states were assigned to all titratable residues at pH 7, with histidines protonated on the ϵ position (HIE). The partial atomic charges for ligand atoms were calculated using restrained electrostatic potential (RESP) method after geometry optimisation by Gaussian03 package using Hartree Fock method and 6-31G** basis set. RESP calculations were performed using Antechamber (available within AmberTools 12). All simulations were performed using the package NAMD 2.9[45] with three-dimensional periodic boundary conditions. A cut-off of 12 Å was used for Lennard-Jones interactions and Particle Mesh Ewald (PME) method employed for long range electrostatic interactions. The simulations were performed in an isothermal-isobaric ensemble at temperature

300 K and pressure 1 bar. Langevin thermostat (with a damping coefficient of 5 ps^{-1}) and Berendsen barostat (compressibility of 4.57 $\times$ 10^{-5} bar^{-1} and a relaxation time of 100 fs) were used to maintain the constant temperature and pressure. Constrained dynamics with a time step of 2 fs was performed using RATTLE algorithm. The MMPBSA calculations and normal mode analysis are performed using modules from AmberTools 12. For the polar solvation free energy, a cubic lattice grid with spacing of 0.5 Å was used for solving the linear Poisson-Boltzmann equation using 1000 iterations. The dielectric constants of solute and solvent were taken to be 1 and 80 respectively. The non-polar solvation free energy was calculated with equation 2.19 from the solvent accessible surface area determined using a 1.4 Å radius probe. The parameters γ and b were set to the standard values of 0.0052 kcal mol^{-1} $Å^{-2}$ and 0.92 kcal/mol respectively.

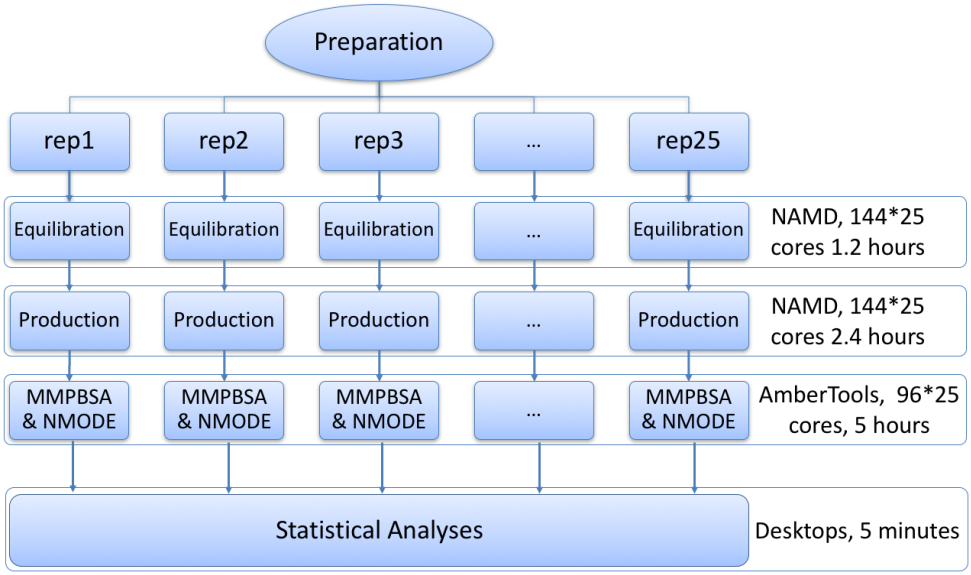

Figure 5.3: ESMACS protocol requiring 25 replica MD simulations followed by MMPBSA+NMODE calculation. The number of cores and wall clock time required are displayed on the right side of the figure, which are the estimates for a system of size ~60,000 atoms using UK's national high performance computer, ARCHER.

5.3.2 Free Energy Workflow

Figure 5.3 displays the ESMACS workflow which has been used to calculate all the absolute binding affinities reported in this chapter. It consists of performing an ensemble simulation of size 25, followed by the MMPBSA and the normal mode calculations on the conformations from each replica to yield a ΔG for each conformation. The ΔG values corresponding to all the conformations sampled in a particular trajectory are averaged to obtain a single ΔG value for each replica. This generates an ensemble of ΔG values of size 25 whose mean is the reported ESMACS binding affinity. The associated uncertainty is calculated as described in Section 5.3.3. It should be noted that ESMACS can be performed using the 1-trajectory or the 3-trajectory approach (refer to Section 2.3.1.D for details on these approaches). The ensemble size of 25 in this study has been chosen based on a systematic analysis of errors as described in Section 5.3.3. A similar error analysis was done in a previous study to arrive at the choices of 2 ns equilibration and 4 ns production simulation lengths[105]. It is worth mentioning here that these values may need to be adjusted for other biomolecular systems.

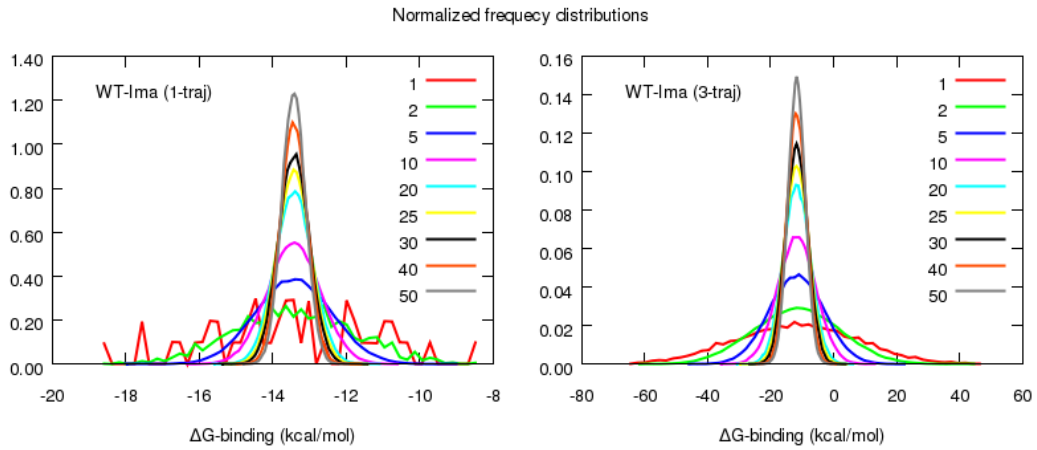

Figure 5.4: The normalized frequency distributions of the bootstrap distributions of mean ΔG values, resampling (with replacement) different number of replicas (1 through 50) from the original sample of 50 ΔG values. A comparison of 1-trajectory and 3-trajectory methods are shown for the wildtype Bcr-Abl kinase bound with Imatinib.

5.3.3 Uncertainty Quantification

As discussed above, ESMACS generates an ensemble of ΔG values (one ΔG value corresponding to each replica) and its mean is the predicted binding affinity. In order to get an estimate of the associated statistical uncertainty in this prediction, a bootstrap distribution of mean ΔG values is generated. This is done by resampling (with replacement) 25 (or the ensemble size in a general case) ΔG values from the original ensemble of 25 ΔG values to obtain a bootstrap resample. On repeating this step a large number of times (100,000 times in this study), many bootstrap resamples are generated. A frequency distribution of their means gives the bootstrap distribution of mean ΔG values. The standard deviation of this distribution provides an estimate of the uncertainty in the predicted value and is reported as an error bar on the predicted ΔG. In the case of the 3-trajectory approach, the bootstrap distribution of mean ΔG values is given by the differences of the bootstrap distributions of mean G values (for complex, receptor and ligand).

Figure 5.4 shows the plots of bootstrap distribution of mean ΔG values generated by bootstrap resamples of different sizes drawn from the original ensemble of 50 ΔG values (or 50 G values for complex, receptor and ligand each, in case of 3-trajectory approach). It can be seen that, on increasing the size of the bootstrap resamples, the distribution becomes narrower; however, beyond 25 the decrease in the distribution width is marginal. This suggests that an ensemble size of 25 is a good balance between the precision of results and computational costs. Thus, an ensemble size of 25 has been chosen for all calculations in this chapter.

5.3.4 Repeatability of Predicted Binding Affinities

The bootstrap distribution of mean ΔG values as discussed above provides an estimate of the repeatability of the predicted binding affinity from ESMACS. The broader the distribution is, the different any two estimates of ΔG can be. As can be seen in Figure 5.4, the width of the bootstrap distribution of mean ΔG values is much larger for ensemble size 1 as compared to that of 25. This

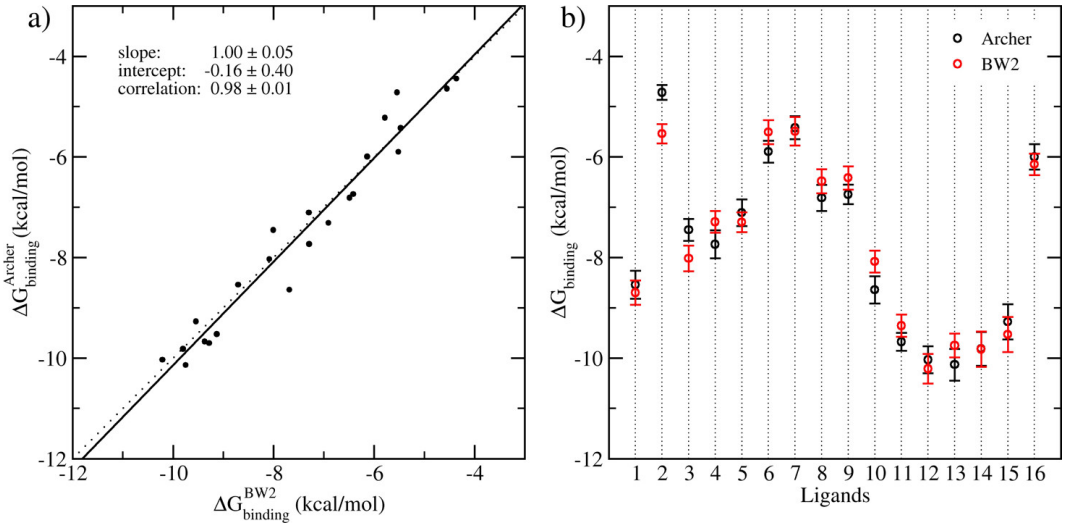

Figure 5.5: Correlation and repeatability of the calculated binding affinities from two independent studies of the BRD4 system performed on BlueWonder2 and ARCHER. (a) Correlation of the predictions from 1-traj calculations performed on BlueWonder2 (BW2, horizontal axis) and ARCHER (vertical axis). Solid line, regression of the data using the calculated free energies; dotted line, 1:1 ideal regression. (b) the ESMACS predictions along with error bars from the two separate calculations.

suggests that an estimate of binding affinity from a single replica would have large variation; however, that from an ensemble of 25 would be repeatable within a small error bar. The ESMACS error bars using ensemble size 25 are typically 0.5 kcal/mol for 1-trajectory approach, and about 2.5 kcal/mol for 3-trajectory approach. Figure 5.5 shows a comparison of the two sets of ESMACS predictions for BRD4 based on simulations performed independently on two different supercomputers, namely BlueWonder2 and ARCHER; the former is an IBM NextScale Cluster (8640 cores) located at the Science and Technology Facilities Council's (STFC's) Hartree Centre and the latter is a Cray XC30 supercomputer (equipped with $\sim$ 118000 cores), the UKs National High Performance Computing Service located in Edinburgh. The results are compared by linear regression. Results exhibit excellent repeatability with a correlation coefficient of 0.98$\pm$0.01. The calculated regression line has a slope of 1 and an intercept of 0 within the limits of error bars. Only 3 out of 16 predictions do not overlap within the error bars. Only the results from BlueWonder2 are reported in the following section. Figure 5.6 displays the

excellent repeatability of ESMACS predictions for Abl kinase complexes as discussed later in the chapter.

5.4 Case Studies

In this section, case studies employing the ESMACS methodology on four different target proteins are described. The binding affinity predictions using both single and multiple trajectory approaches have been provided and compared.

5.4.1 Bcr-Abl Kinase

As described earlier, 5 mutants of the Abl kinase and 4 of their tyrosine kinase inhibitors (TKIs) are chosen for this study amounting to a total of 20 complexes. Table 5.1 contains the ESMACS predictions and the corresponding experimental binding affinities for all 20 complexes. The experimental binding affinities are derived from the IC_{50} values[240] using Equation 2.7. Typical experimental noise for high quality binding affinity measurements is of the order of 0.5 kcal/mol[196]. However, experimental uncertainties are not available in this case. Spearman rank coefficient (r_s) and Pearson correlation coefficient (r) are provided as statistical measures of the rank ordering and the level of linear correlation, respectively, between the ESMACS predictions and the corresponding experimental values. The high values of correlation coefficients mean that the ESMACS predictions are in good agreement with the experimental data. It should be noted in Table 5.1 that ESMACS does not yield the actual binding affinities. This is because it is based on the MMPBSA method which involves several approximations (refer to Chapter 2). However, ESMACS does a good job at ranking the ligands based on their binding affinities with a given target protein, which is of greater interest than the actual values of binding affinities in most cases.

Figures 5.6 (a) to (e) display the correlation plots of the predicted and experimental ΔG values for all ligands bound to each variant of the Abl kinase for better visual comparison of the two. The error bars on the predicted values

Table 5.1: Binding affinities of all 20 complexes of Abl kinase calculated using the 1-trajectory approach of ESMACS (ΔG_{calc}) and their comparison with the experimental values (ΔG_{exp}; derived from IC_{50} values). All ΔG values are in kcal/mol. Spearman and Pearson rank coefficients (r_s and r respectively) are provided as measures of accuracy.

Mutant	**Inhibitor**	$\boldsymbol{\Delta G_{calc}}$	$\boldsymbol{\Delta G_{exp}}$	$\boldsymbol{r}$	$\boldsymbol{r_s}$
WT	Imatinib	-13.42(0.32)	-8.62	0.97	1
	Nilotinib	-19.38(0.28)	-10.64		
	Ponatinib	-20.59(0.32)	-11.91		
	Rebastinib	-17.37(0.44)	-10.49		
E255K	Imatinib	-14.95(0.34)	-7.55	0.95	0.8
	Nilotinib	-19.72(0.26)	-9.51		
	Ponatinib	-21.60(0.33)	-10.64		
	Rebastinib	-18.15(0.46)	-9.73		
T315I	Imatinib	-19.85(0.65)	-6.91	0.47	0.4
	Nilotinib	-19.92(0.21)	-8.45		
	Ponatinib	-25.71(0.26)	-11.26		
	Rebastinib	-18.41(0.34)	-10.73		
Y253F	Imatinib	-14.53(0.38)	-7.86	0.98	1
	Nilotinib	-17.83(0.26)	-9.94		
	Ponatinib	-20.57(0.34)	-11.13		
	Rebastinib	-19.18(0.51)	-10.00		
F317R	Imatinib	-14.48(0.33)	-8.12	0.99	1
	Nilotinib	-18.70(0.33)	-10.15		
	Ponatinib	-21.00(0.38)	-10.96		
	Rebastinib	-16.42(0.52)	-8.67		

are of the order of ± 0.5 kcal/mol which may be reduced by increasing the ensemble size. These plots contain two sets of results for each complex (shown in red and blue) which are obtained from independent ESMACS calculations. These two sets of predictions overlap nicely in all cases, indicating the excellent repeatability offered by the ESMACS protocol.

As discussed in Section 2.3.1.D, unlike the 1-trajectory approach, the 3-trajectory approach has an advantage of being able to capture the adaptation of receptor or ligand geometries induced by the event of their binding. However, if there are no such induced adaptations during binding, then the results from the 3-trajectory approach have no advantage over those from the 1-trajectory approach. In such cases, it is preferable to use the 1-trajectory approach as the results from the 3-trajectory approach would fluctuate widely

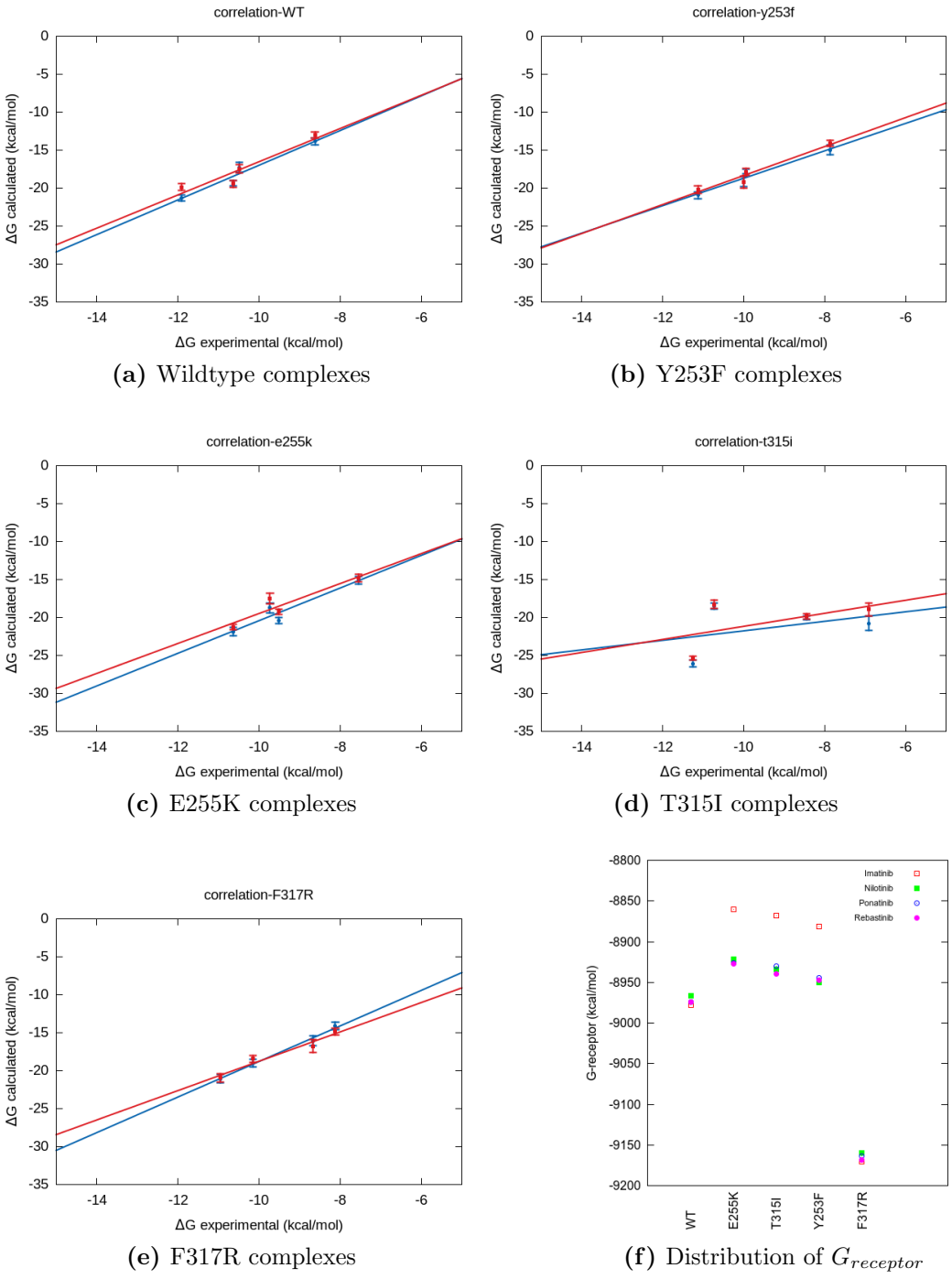

(a) Wildtype complexes

(b) Y253F complexes

(c) E255K complexes

(d) T315I complexes

(e) F317R complexes

(f) Distribution of $G_{receptor}$

Figure 5.6: (a) to (e):Correlation plots (along with the best fit lines) of all ligands bound to each variant of the Abl kinase. Each plot contains two sets of results (in blue and red) which are calculated from two independent ESMACS calculations. (f): Distribution of the absolute free energies of receptor ($G_{receptor}$) from 1-trajectory calculations for all mutants of Abl kinase bound to different inhibitors. All values are in kcal/mol.

and converge slowly. Figure 5.6(f) shows the distribution of $G_{receptor}$ from 1-trajectory calculations for all mutants of Abl kinase bound to different inhibitors. This distribution gives us a sense of the adaptation of receptor geometry when bound to different inhibitors. 3 out of the 5 mutants (E255K, T315I and Y253F) have an outlier which is different by more than 60 kcal/mol which suggests that in these cases receptor alters its conformation on binding with one of the inhibitors. Table 5.2 provides a comparison of the results from the 1-trajectory and the 3-trajectory approaches for all complexes. It is found that, in case of WT and F317R, where $G_{receptor}$ does not vary on binding with different inhibitors, the values of r degrade for the 3-trajectory results. However, in case of the other three mutants, where $G_{receptor}$ varies on binding to one of the inhibitors, the values of r either improve or remain approximately the same for the 3-trajectory results. These observations are in line with what was said above and suggest that the 3-trajectory calculations should not be performed when $G_{receptor}$ from 1-trajectory calculations do not vary. This could be a way to predict if there is a need to care about performing multiple trajectory approaches of ESMACS in specific cases, although more data is needed to make any firm conclusions. Further discussion on this is provided in the next section containing the results for BRD4 and TRKA systems.

Table 5.2: Comparison of the Pearson correlation coefficient from 1-trajectory and 3-trajectory results for all ligands bound to each mutant of Abl kinase.

Mutant	***r***	
	1-traj	**3-traj**
WT	0.97	0.26
E255K	0.95	0.94
T315I	0.47	0.80
Y253F	0.98	0.89
F317R	0.99	-0.52

5.4.2 BRD4 and TRKA

ESMACS approach was employed to perform blind predictions of the binding affinities for the ligands binding with BRD4 and TRKA in collaboration with pharmaceutical companies GlaxoSmithKline and Pfizer, respectively. The

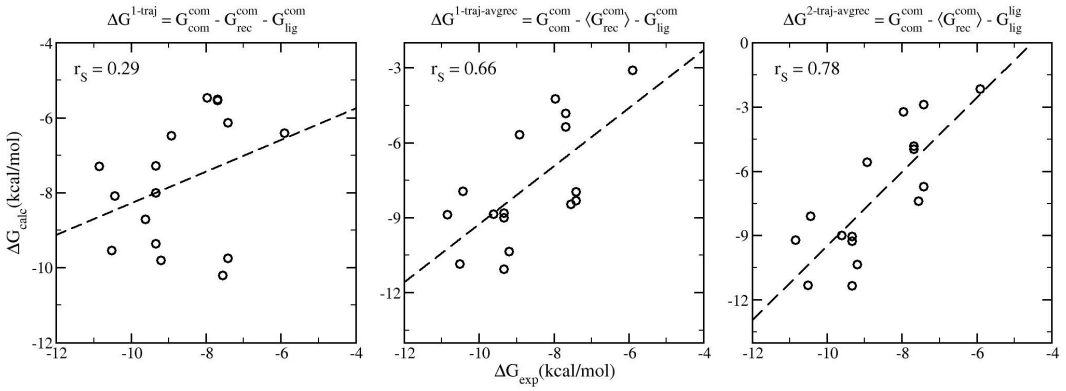

Figure 5.7: Spearman ranking correlations of the calculated binding free energies and the experimental data for BRD4 complexes from 1-traj (left panel), 1-traj-avgrec (center), and 2-traj-avgrec (right panel) ESMACS approaches. The equations on the subfigures indicate the calculations used in each case. The subscripts (com/rec/lig) and the superscripts (com/lig) in the equations indicate the components (complexes, receptor, and ligands) and the simulations (complexes and free ligands), respectively. The error bars, which are 0.19-0.34 kcal/mol for the 1-traj and 1.02-1.71 kcal/mol for the 1- and 2-traj-avgrec approaches, are not shown for reasons of clarity.

experimental data was only disclosed for comparison by our experimental collaborators after the ESMACS predictions were provided to them. Both of these studies have been published and the results presented here are taken from the respective publications[22, 23]. Figures 5.7 and 5.8 display the correlation plots of the ESMACS predictions with the corresponding experimental data for BRD4 and TRKA respectively. In these cases, the ESMACS results were obtained using three different approaches, namely 1-traj, 1-traj-avgrec and 2-traj-avgrec. 1-traj is the usual 1-trajectory approach where simulations are performed only for the ligand-protein complexes; the values of G_{com}, G_{rec} and G_{lig} for each complex are all calculated from the same trajectories. 1-traj-avgrec is a variant of the 1-trajectory approach where simulations are performed only for the ligand-protein complexes; the values of G_{com} and G_{lig} for each complex are calculated from the same trajectories (as in the case of 1-traj approach). However, unlike 1-traj, G_{rec} is assumed to be a constant across all complexes, whose value is taken as the average of G_{rec} values from individual complexes as calculated in the 1-traj approach. 2-traj-avgrec is the 2-trajectory approach where simulations are performed for ligand-protein

complexes as well as free ligands; the values of G_{com} and G_{lig} for each complex are calculated from respective simulations. In addition, G_{rec} is assumed to be a constant across all complexes with the same value as in the case of 1-traj-avgrec.

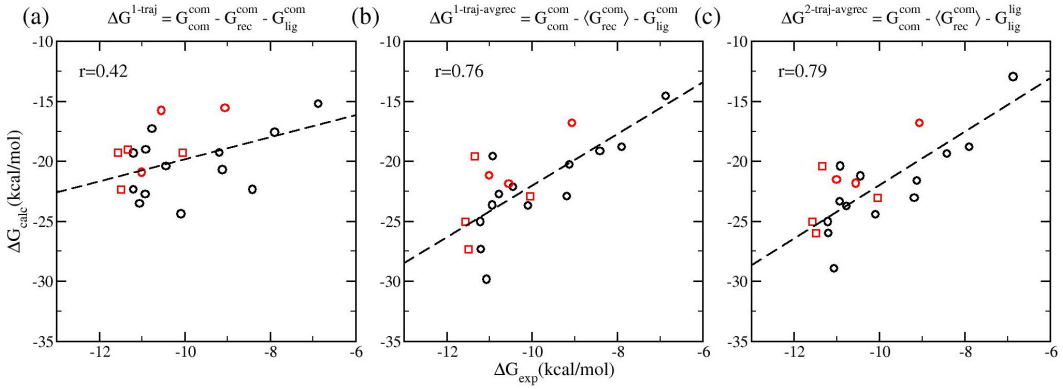

Figure 5.8: Spearman ranking correlations of the calculated binding free energies and the experimental data for TRKA complexes from 1-traj (left panel), 1-traj-avgrec (center), and 2-traj-avgrec (right panel) ESMACS approaches. The equations on the subfigures indicate the calculations used in each case. The subscripts (com/rec/lig) and the superscripts (com/lig) in the equations indicate the components (complexes, receptor, and ligands) and the simulations (complexes and free ligands), respectively. The error bars, which are ∼0.6 kcal/mol for the 1-traj and ∼3 kcal/mol for the 1- and 2-traj-avgrec approaches, are not shown for reasons of clarity. The experimental data from two sites (Pfizer, Sandwich and TCG Lifescience) are displayed in black and red, respectively. In cases where the experimental data is available from both the sites (shown as red squares and corresponding black circles), the data from the former has been used for calculating the correlation coefficients.

A comparison of results from the three ESMACS approaches has been provided in Figures 5.7 and 5.8. It is clear that the 1-traj approach yields moderately accurate binding affinity predictions, while the 1-traj-avgrec approach improves the accuracy of results substantially (Spearman coefficients improve from 0.29 and 0.42 to 0.66 and 0.76 for BRD4 and TRKA respectively). This is because the latter accounts for the adaptation of the protein conformation when bound to different ligands unlike the former. G_{rec} is the free energy of unbound protein, which is a constant for a given protein. However, the calculated G_{rec} in the case of 1-traj approach corresponds to the altered conformation of the protein in the given complex, which can be different from the constant G_{rec} for the unbound protein. The difference between these two values of G_{rec} is

sometimes referred to as the "adaptation energy"[22, 23]. The inclusion of adaptation energies leads to the improved accuracy of results in the case of 1-traj-avgrec approach. The 2-traj-avgrec approach further improves the accuracy of predictions (Spearman coefficients are 0.78 and 0.79 for BRD4 and TRKA respectively). This is because it includes the energetic penalties associated with the adaptation of both protein and ligand conformations in their bound form. It should be noted that the adaptation energies for receptors as well as ligands in the case of BRD4 and TRKA systems are of the order of ± 5 kcal/mol (see Figure 5 of references [22] and [23]).

It should be noted in Figure 5.8 that the experimental binding affinities for four ligands were determined from the IC_{50} values measured at two different laboratories and their values vary by as much as 1 kcal/mol (shown in red squares and corresponding black circles). Such a variation in experimental values can also affect the correlation between the predicted and experimental binding affinities.

5.4.3 HIV-1 Protease

The nine approved HIV-1 protease inhibitors (PIs) have been studied using ESMACS 1-trajectory approach; however, two of them, namely Ritonavir (RTV) and Atazanavir (AZV), were found to be outliers with overwhelmingly negative binding affinities[105]. It was suggested that this may be because of their large sizes due to which they distort protein conformation more than the other inhibitors and hence have large adaptation energies. It was shown in the previous section that the multiple trajectory approaches may be useful in such cases. In this study, three PIs from the previous study have been chosen to study with the ESMACS 3-trajectory approach (two large PIs, RTV and AZV, and one well-behaved PI, Liponavir, LPV). The motivation is to see if the binding affinities of the large ligands can be corrected by accounting for their adaptation energies.

Table 5.3 provides a comparison of the predicted and experimental binding affinities using both 1-trajectory and 3-trajectory approaches (data for

Table 5.3: Binding Affinities of the wildtype HIV-1 protease bound to three different inhibitors using ESMACS 1-trajectory and 3-trajectory approaches along with corresponding experimental binding affinities. All values are in kcal/mol

Inhibitor	ΔG_{1-traj}	ΔG_{3-traj}	ΔG_{exp}
LPV	-14.19(0.25)	-21.87(1.72)	-14.1(0.15)
RTV (outlier1)	-25.90(0.41)	-19.16(1.89)	-12.7(0.15)
AZV (outlier2)	-20.51(0.50)	5.09(2.23)	-13.4(0.14)

Table 5.4: Binding Affinities (relative to LPV) of the wildtype HIV-1 protease bound to three different inhibitors using ESMACS 1-trajectory and 3-trajectory approaches along with corresponding experimental binding affinities. All values are in kcal/mol

Inhibitor/Method	$\Delta\Delta G_{1-traj}$	$\Delta\Delta G_{3-traj}$	$\Delta\Delta G_{exp}$
LPV/1-traj	0.00	0.00	0.00
RTV (outlier1)	-11.71	2.71	1.4
AZV (outlier2)	-6.32	26.96	0.7

1-trajectory and experimental ΔG values has been taken from reference [105]). Table 5.4 contains all values relative to those of LPV (LPV is chosen as reference because it was in good agreement with the experimental values in the previous study). It can be seen from Table 5.4 that both RTV and AZV are outliers in the case of 1-trajectory approach as their predicted relative binding affinities are negative whereas they are positive in experiment; however, in the case of 3-trajectory approach, only AZV is an outlier with large relative binding affinity (although with the same sign as that of the corresponding experimental value). Therefore, based on this small data set, it appears that the 3-trajectory approach is able to improve the results of at least one of the two outliers.

Table 5.5: Comparison of $G_{receptor}$ and G_{ligand} in 1-trajectory and 3-trajectory studies of the HIV-1 protease. All values in kcal/mol. Error bars reported are the standard deviations.

Inhibitor	G_{ligand}		$G_{receptor}$	
	1-traj	3-traj	1-traj	3-traj
AZV	-308.08(1.55)	-319.93(1.40)	-5186.92(10.78)	-5200.64(10.08)
LPV	-313.10(1.30)	-315.21(1.18)	-5192.99(7.89)	-5183.20(9.24)
RTV	-277.75(1.07)	-282.22(1.37)	-5201.53(9.13)	-5203.81(9.11)

In order to further understand the behaviour of AZV whose predicted binding affinity changes from overwhelmingly negative in the case of 1-trajectory approach to overwhelmingly positive in the case of 3-trajectory approach, a comparison of $G_{receptor}$ and G_{ligand} for all inhibitors in both the cases has been reported in Table 5.5. It should be noted that the G_{ligand} changes by almost 12 kcal/mol between 1 and 3 trajectory results in the case of AZV. However, the data presented is insufficient to draw any firm conclusion and further investigations are needed.

5.5 Conclusions

This chapter describes a new approach, called ESMACS, based on MMPBSA to calculate precise and repeatable absolute binding affinities. It is not as accurate as TIES (described in Chapter 3). However, ESMACS is computationally cheaper than the absolute binding affinity approach based on alchemical methods as described earlier[231]. The ESMACS protocol is flexible, with parameters like simulation duration and ensemble size adjusted to obtain the desired level of precision. Another important feature of ESMACS is its scalability, which reduces the wall-clock time required to make predictions by running multiple replicas concurrently on a supercomputer. ESMACS has been shown to rank the inhibitors bound to 5 different variants of Abl kinase, BRD4 and TRKA well.

It should be noted that the accuracy of potential parametrisation has a great influence on the predicted binding affinities and care must be taken while choosing the parameters. In the HIV-1 protease case study, there is a need of further investigation to understand the behaviour of the inhibitors, Ritonavir and Atazanavir.

The discussion on the single and multiple trajectory versions of ESMACS and their applicability in different scenarios highlights the strength of the method and its potential applicability in real life context. Both TIES and ESMACS approaches were employed in two recent collaborative studies with pharmaceu-

tical companies, GlaxoSmithKline and Pfizer, where the blind binding affinity predictions were found to rank a large set of ligands bound to the target protein correctly when later compared with the corresponding experimental values[22, 23]. This exhibits the immense potential of ensemble simulation based approaches in the drug design process.

Chapter 6

Automation toolkit

In the previous chapters, several different approaches based on ensemble simulation are described to calculate accurate, precise and repeatable binding free energies. It has been shown that these approaches yield binding free energy predictions in good agreement with the experimental values and hence have the potential to be applicable in drug design and patient specific medicine. However, in order to have a positive impact in industrial or clinical settings, the predictions need to be made at the time scales which can compete with the experimental determination of binding affinities. The important feature of scalability of both TIES and ESMACS workflows (described in the previous chapters) allows us to reduce the time required to make predictions by running multiple replicas concurrently. However, these complex computational workflows are very tedious to perform manually and very error-prone. Automating the execution of these workflows further reduces the time to solution. In this chapter, the software tools developed in my group, namely the Binding Affinity Calculator (BAC)[239] and FabSim[241, 242], are described. I extended both of them to automate the implementation of the workflows described in previous chapters.

6.1 Binding Affinity Calculator

BAC is a tool which automates the end-to-end execution of the TIES and the ESMACS workflows (refer to Figures 3.3 and 5.3). It helps in managing the

large volume of simulation and free energy calculation data from all replicas, which have identical input but different output, in an error-proof manner. Broadly, both these workflows can be divided into three phases: preparation phase, production phase and analysis phase. Different components of BAC have been developed to handle different phases.

BAC-Builder is the component of BAC which executes the preparation phase. This phase involves preparing the simulation-ready solvated initial structure of the biomolecular system to be studied from its raw starting structure (usually in the form of a crystal structure in PDB format) and the appropriate potential parameters. BAC-Builder is a set of modules implemented in the Perl language. It takes the raw PDB file and ligand parameter files as input along with the specification of the desired force field as well as MD engine and generates the structure and parameter files to be used for simulations in the production phase. It also generates the input configuration files compatible with the specified MD engine for the execution of the stepwise equilibration and production simulations as described in detail in reference [239].

I extended the original BAC-builder by developing a new module to handle the preparation phase of the TIES method. As described in Chapter 3, unlike ESMACS, TIES requires hybrid structure and parameter files as raw input, which need to be prepared using a tedious protocol. The automation of this protocol substantially reduced the time and effort required in their preparation and was a major advancement towards the implementation of TIES on a large number of biomolecular systems.

In the production phase, before the simulations are performed, all the input data generated during the preparation phase need to be rearranged in a directory structure appropriate to perform ensemble simulations such that the common input is centrally accessible by all replicas and the distinct output is saved in different sub-directories. Such an arrangement is essential for handling the large amounts of data associated with ensemble simulations and makes it convenient to perform the post-production statistical analysis. This step has

been automated using the BAC-Builder and FabSim. After this rearrangement, FabSim automates the tasks of staging the data and submitting the job to run the ensemble simulation on a remote supercomputer. FabSim is described in the next section.

After the successful execution of the production phase, the final step is to perform the statistical analysis on the output generated (the analysis phase). I developed the BAC-Analysis tool to automate this phase for both the ESMACS and the TIES workflows. In the case of TIES, this can be performed on the local computer within a few minutes with a combination of bash, awk and R scripts. In the case of ESMACS, the post-production analysis consists of two parts: MMPBSA+NMODE calculations and the ESMACS binding affinity calculation (see Chapter 5). The former need to be performed on a supercomputer with the help of modules of AmberTools 12, while the latter can be performed on a local computer within a few minutes using the BAC-Analysis tool.

Cloud computing is increasingly becoming popular. The users are allowed to purchase access to appropriate number of CPUs on cloud resources for desired duration of time as and when needed. Given the growing popularity of cloud computing, BAC is now being deployed by my colleagues on commercial clouds like Amazon web services, Microsoft Azure and DNANexus. A user friendly interface of BAC, called UF-BAC, has been developed in order to make it available to widest range of users possible.

6.2 FabSim

FabSim is a toolkit scripted in the Python language to simplify a broad range of computational tasks for researchers in diverse disciplines[241, 242]. Its strength lies in the fact that it is highly customisable and hence can be adapted to a wide range of tasks. In addition, it provides a systematic route to automate the utilisation of HPC and distributed resources. FabSim has been employed in several diverse research domains including simulating cerebrovascular

bloodflow, modelling multiscale clay-polymer nanocomposites, and predicting ligand-protein binding affinities. Three application-specific modules of FabSim, namely FabHemeLB, FabMD and FabBioMD, have been developed for the three applications mentioned above respectively[241]. A fourth module, FabFlee, aimed towards migration modelling, is under development.

I developed the entire FabBioMD module of FabSim, which is relevant in the production phases of both the TIES and the ESMACS workflows. In order to effectively handle the large volume of data from these workflows, it is desirable to have a well-defined method of data curation, which also enhances data transferability between users. FabBioMD is configured to arrange all the data in a comprehensible directory structure, to automatically stage the data and submit the job to perform equilibration, simulation (for both ESMACS and TIES) and MMPBSA calculations (for ESMACS) on the desired remote supercomputer using one-line command. The command syntax is as follows:

```
fab <hostname> <command>:<configuration_name>,
<parameter1=x1>,(...),<parameterN=xn>
```

where, hostname is the remote machine to be used for the job, command is the pre-defined function to be executed, configuration_name is the location of the input configuration, and the user has the option to specify values of the parameters. In case no parameters are defined in the command, their pre-defined default values are taken. An example function of FabBioMD module with its usage is as follows:

```
fab archer bac_ties_archerlike:myhomedirectory,
cores=1000,wall_time=06:00:00,replicas=5
```

The above command when executed on the command line of my desktop calls the FabBioMD function "bac_ties_archerlike". It copies all the data from the directory named "myhomedirectory" to a pre-configured remote location on the supercomputer ARCHER, creates a submission script for a TIES job (using 1000 cores, 6 hours wall-clock time and 5 replicas per λ-window; the pre-defined

default values of λ are used) and submits the job to the queue on ARCHER; all with a single command. There is a long list of functions in FabBioMD module of FabSim, which I developed to perform different steps of both ESMACS and TIES workflows and to execute these workflows on a variety of supercomputers with different architectures[241, 242].

One of the major advantages of FabSim is that it subsumes the underlying complexities related to the submission of jobs on different HPC architectures by allowing the user to easily submit jobs on different supercomputers. All that needs to be done is a one-time configuration of each HPC resource and creation of templates for job submission scripts which can be accessed while executing the relevant function of the FabBioMD module. I have configured several major supercomputers of different HPC centres including the UKs National High Performance Computing Service (ARCHER; `www.archer.ac.uk`), the Science and Technology Facilities Council's (STFC's) Hartree Centre (BlueJoule and BlueWonder; `www.hartree.stfc.ac.uk`) and Leibniz Supercomputing Centre (SuperMUC; `www.lrz.de`). These supercomputers were used to perform almost all of the simulations related to this thesis.

It is possible for the users to define customised functions to suit their needs if the available functions are not sufficient for their purpose. Any new remote HPC resource can easily be configured and added to the known resources of the FabSim database by the user.

It is worth mentioning here that the level of automation achieved using BAC and FabSim made it possible for us to successfully perform hundreds of TIES and ESMACS calculations for a large number of ligand-protein complexes in a short period of 37 hours by occupying the whole SuperMUC ($\sim$250,000 cores)[243]. It was achieved by the swift execution of the different phases of these workflows through our automation toolkit. The successful execution of this unprecedented "giant workflow" has realised that these workflows have the ability to make useful binding affinity predictions within the span of a few hours, which can be exploited for clinical decision making to personalise

medicines for patients.

Chapter 7

Conclusions

This thesis addresses the issue of variability in results of the free energy methods based on classical molecular dynamics simulations when based on a single short simulation and establishes a route to reliable binding affinity predictions. It discusses the important property of sensitivity of classical MD simulations to their initial conditions[10], which leads to the large variation in the free energies predicted using a single short trajectory on repeating the calculation. In addition, it has been noted that the ensemble average can be considered equal to the time average via the ergodic theorem only in the limit of Poincaré recurrence time, which is usually extremely long for ligand binding and typically unapproachable on compute resources available today[10]. Moreover, for a non-equilibrium system, time averaging is meaningless, since the observables in that case are time dependent. With this in mind, ensemble simulations have been proposed as a way to calculate macroscopic thermodynamic properties like the Gibbs free energy through ensemble averaging over microstates instead of performing time averages over a single insufficiently long simulation. It has been shown that the employment of ensemble simulation based approaches yields precise and repeatable free energy predictions within a short span of time (∼6-8 hours, which can be further reduced using GPUs). The results are found to be accurate within the limitations of the force fields used. Given the reliability of predictions from the ensemble simulation based approaches, they promise to make a positive impact in the fields of drug design and personalised

medicine.

Thermodynamic integration with enhanced sampling (TIES) is a free energy prediction method based on one of the alchemical methods, thermodynamic integration, and employs the concept of ensemble simulation. The associated parameters like ensemble size and simulation length were chosen based on a proper assessment of statistical uncertainties. TIES has been shown to yield relative binding affinity predictions with high accuracy and precision for a large number of ligands bound to a variety of target proteins. TIES results are shown to be repeatable with and without the variation in the software, the hardware and the implementation of the free energy calculation. It has been shown that an ensemble of short simulations does a better job than a single simulation when the total simulation duration in both cases is the same. TIES is able to capture important dynamical properties of the system correctly.

TIES methodology has also been employed to several accelerated sampling protocols based on Hamiltonian replica-exchange technique and an improved free energy estimator. It has been shown that the variability in results from independent short MD simulations exists even when employing better sampling protocols and/or free energy estimators, and that ensemble simulation is necessary in order to properly handle the statistical uncertainties associated with the predicted free energies irrespective of such advancements in the free energy method used. In addition, such variability in results from these advanced free energy methods persists even on extending the simulations to durations up to the cumulative duration of the ensemble simulation.

The ensemble simulation approach has been applied to the end-point free energy method, MMPBSA, leading to a method called enhanced sampling of molecular dynamics with approximation of continuum solvent (ESMACS). The ensemble size was chosen based on the statistical assessment of errors with the note that it is system-dependent. The single and multiple trajectory approaches of ESMACS have been applied on several different protein systems and their results compared. ESMACS is highly precise but inaccurate in the

sense that it is unable to predict the actual values of binding affinities but it has been shown to rank the ligands well based on their binding affinities with a given target protein.

TIES and ESMACS have complementary domain of applicabilities. TIES is very accurate but its application is restricted to structurally similar compounds when calculating the relative binding affinities. On the other hand, ESMACS is not accurate given its underlying approximations but can be used to calculate binding affinities of a diverse set of molecules. It is important to note that, for these methods to yield reliable binding affinity predictions, it is necessary to employ reliable force fields and potential parametrisations during the simulations as the accuracy of predictions is dependent on them. It should also be noted that an ensemble of short non-biased MD simulations is suitable for determining free energy when the initial structure of the system studied is at equilibrium. However, it is unable to capture the dynamics of rare events such as, protein folding or DFG flip, which would require long simulation duration and/or biased potential employed for each replica of the ensemble[244].

The different free energy schemes described in this thesis comprise of complex workflows. Therefore, a fair amount of effort was put into the development of an automation toolkit, which made the execution of all workflows easier, quicker and error-free. The automation of workflow execution also helps in better management of the large volume of data generated by the free energy calculations based on ensemble simulations. Binding Affinity Calculator (BAC) and FabSim are the tools developed for this purpose and have been briefly described in Chapter 6.

All the methods described in this thesis along with the automation toolkit provide a solution to the issue of variability of results from independent short simulations in the field of *in silico* binding affinity calculations and provide a route to their reliable predictions. The ability to make accurate, precise and repeatable predictions using computational methods increases their scientific value as well as reliability in industrial and clinical context. This along with the

short time to solution makes it possible to apply these methods directly as tools in the process of drug design and clinical decision making. The applicability of TIES and ESMACS in pharmaceutical industry is evident from the published works co-authored by myself in collaboration with GlaxoSmithKline[22] and Pfizer[23] which were conducted as blind studies.

The work presented in this thesis has led to the development of another alchemical free energy method developed by one of my colleagues[231]. It applies the TIES methodology to an alchemical method based on double annihilation technique[245, 246] to reliably predict absolute binding affinities for a range of biomolecular systems.

The future directions of research based upon this thesis include applying the ensemble simulation based methods to study point mutations in proteins as well as the estimation of reaction rate parameters. Protein side-chain mutations occur naturally and sometimes may alter the ability of drug/ligand to bind with the protein. This is the most common way in which the target proteins develop drug resistance. Therefore, studying the effect of protein mutations on the binding affinity is important. I am currently working on the development of an alchemical method called TIES-PM which would employ the TIES methodology to yield rapid, accurate, precise and repeatable relative binding affinity corresponding to the mutation in a protein when bound with a ligand. In future, the ensemble simulation based methods described here could be used to develop reliable methods for the estimation of kinetic parameters involved in binding process, which are quite challenging given the long time scale of their occurrence.

Appendix: Ligand Structures and Additional Results

Table A.1: Chemical structures and experimental binding affinities of CDK2 ligands. No error bars are available on the values used in this study.

Common scaffold	Ligand	R1	R2	ΔG_{exp} (kcal/mol)
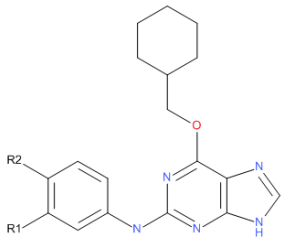	1Q	H	H	-8.18
	I9	H	OH	-9.74
	17	Br	H	-7.04
	20	CH_3OH	H	-8.72
	21	OCH_3	H	-7.83
	26	H	OCH_3	-8.43
	29	H	$SO_2N(CH_3)_2$	-9.88

Table A.2: Chemical structures and experimental binding affinities of TYK2 ligands. No error bars are available on the values used in this study.

Common scaffold	Ligand	R1	ΔG_{exp} (kcal/mol)
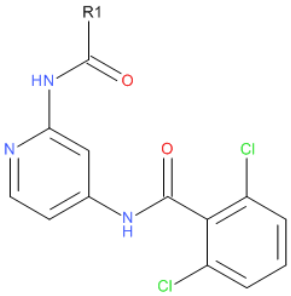	1	CH_3	-9.54
	3	CH_2OH	-8.98
	5	OCH_3	-9.21
	6	$CH(CH_3)_2$	-8.26
	8	Ph	-7.75
	10	$C(CH_3)_3$	-7.42
	11	2-chlorocyclopropyl	-11.28
	15	CH_2CH_3	-9.78
	16	$NHCH_2CH_3$	-10.53

Table A.3: Chemical structures and experimental binding affinities of thrombin ligands. No error bars are available on the values used in this study.

Common scaffold	Ligand	R1	ΔG_{exp} (kcal/mol)
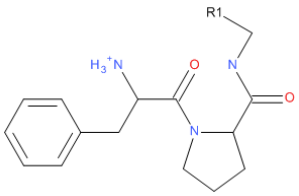	1		-8.46
	2	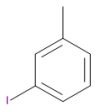	-8.25
	3	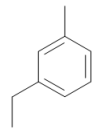	-7.86
	4	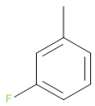	-7.48
	5	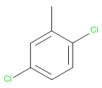	-9.18
	6		-8.22
	7	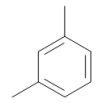	-8.32
	8	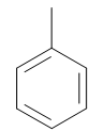	-7.58
	9		-8.89
	10	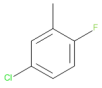	-8.91
	11	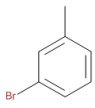	-8.56

Table A.4: Chemical structures and experimental binding affinities of MCL1 ligands. No error bars are available on the values used in this study.

Common scaffold	Ligand	R1	R2	R3	ΔG_{exp} (kcal/-mol)
	1	O		H	-8.24
	2	NH		H	-6.66
	3	NH		H	-6.88
	4	NH		H	-7.60
	5	NH		H	-8.81
	6	NH		H	-7.92
	8	O		Cl	-7.69
	9	NH		H	-6.58
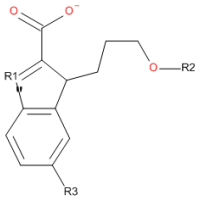	12	NH		Cl	-9.33
	13	NH		H	-6.62
	16	NH		H	-8.95
	17	NH		H	-7.85
	18	NH		Cl	-9.78
	32	NH		H	-5.78
	34	NCH_3		H	-9.26
	35	NH		Cl	-9.96
	38	NH		H	-8.95
	39	NH		H	-8.90
	41	NH	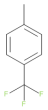	H	-6.87
	42	NH		H	-7.03

Table A.5: Chemical structures and experimental binding affinities of PTP1B ligands. No error bars are available on the values used in this study.

Common scaffold	Ligand	R1	R2	R3	ΔG_{exp} (kcal/mol)
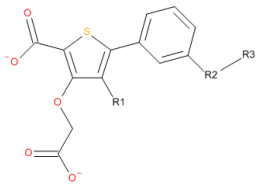	1	Br	NH		-7.72
	2	Br	NH	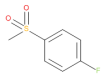	-8.65
	3	Br	$NHCH_2$	cyclohexyl	-9.11
	4	Br		$COOCH_3$	-8.72
	6	Cl		SO_2CH_2Ph	-12.47
	7	Br	$NHCH_2$	Ph	-8.61
	8	Br		SO_2CH_3	-10.01
	10	Br	OCH_2	Ph	-8.39
	11	Br	NH	cyclohexyl	-9.08
	12	Br	NH	OCH_2CH_3	-7.75
	13	Br	NH	cyclopentyl	-8.72
	14	Br		SO_2CH_2Ph	-11.42
	19	Br	NH	H	-7.85
	20	Br	NH	cycloheptyl	-9.41
	22	Br		$COCH_3$	-9.14
	23	Br	NH	3,3,5,5-tetramethylcyclohexyl	-10.12

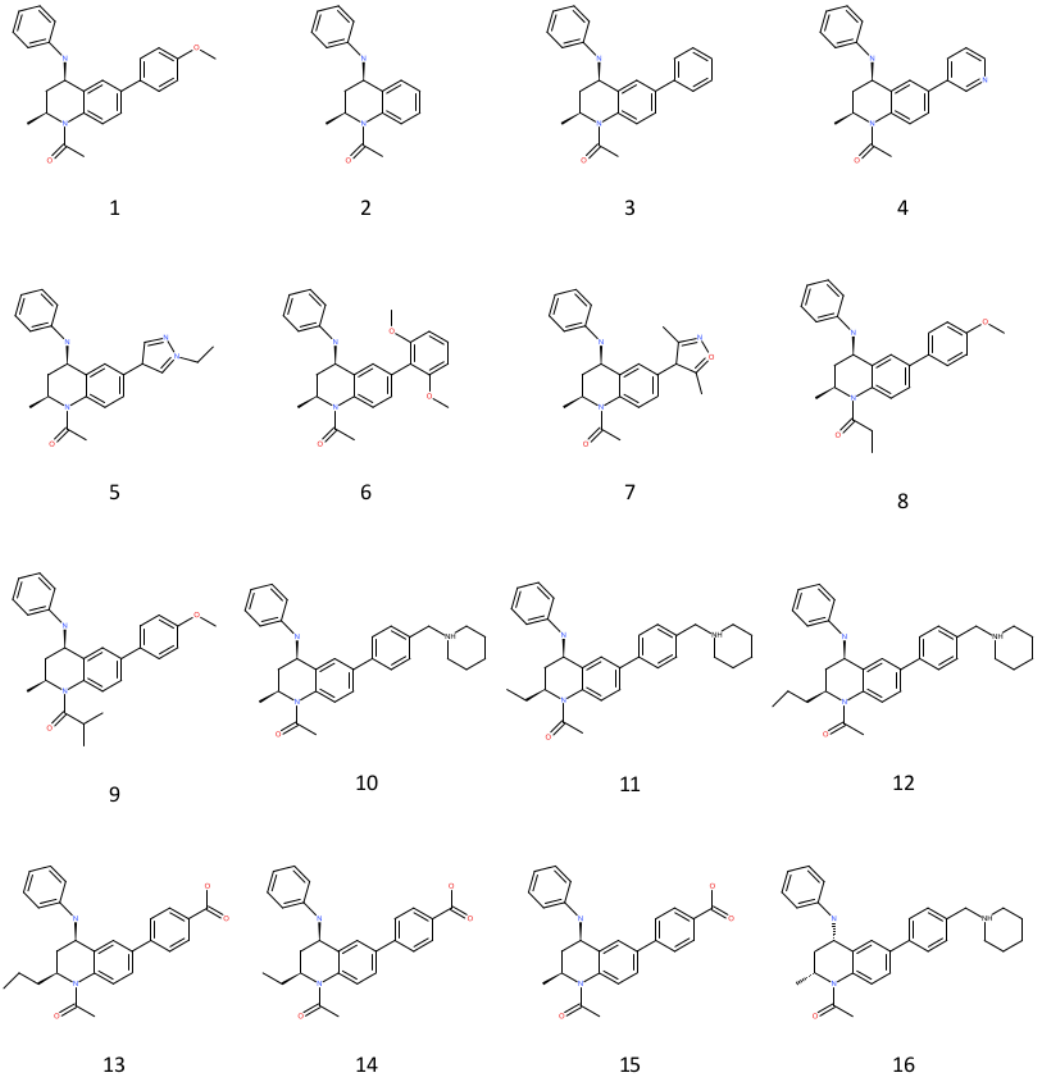

Figure A.1: Chemical structures of BRD4 ligands.

Table A.6: Chemical structures of TRKA ligands. All ligands have the same net neutral charges. The experimental TRKA inhibitory values (IC50) and the binding free energies derived from them are shown. Experimental IC50 measurements were conducted independently in two separate laboratories using an identical protocol25; Pfizer, Sandwich (UK) IC50 values are shown in black; TCG Lifescience (India) TrkA IC50 values are shown in blue.

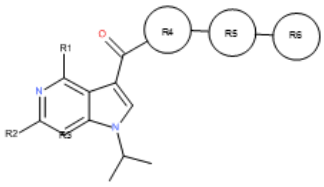

Compound	R1	R2	R3	R4	R5	R6	IC_{50} (nM)	ΔG (kcal/mol)
1	NH_2	H	N			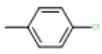	6.97 4.25	-11.20 -11.49
3	NH_2	H	N			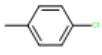	24.53	-10.45
4	H	H	N			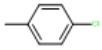	10.86	-10.93
6	NH_2	H	N			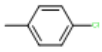	8.67	-11.07
7	H	H	CH			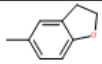	44.25	-10.09
8	H	H	CH			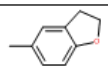	735.79	-8.42
11	H	H	N			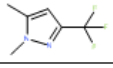	11.04 5.45	-10.92 -11.34
12	H	H	N			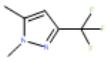	14.18	-10.77
13	H	H	N			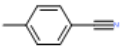	224.74	-9.13
16	H	H	N			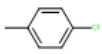	9800.00	-6.87
17	H	NH_2	N			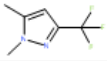	6.84 3.73	-11.21 -11.57
22	OH	H	N			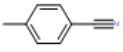	1756.36	-7.90
23	H	$NHCH_3$	N			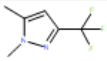	9.55	-11.01
24	H	OH	N				249.42	-9.06
26	H	H	N				20.53	-10.55
30	H	H	N				201.70 47.87	-9.19 -10.05

Table A.7: Graphical display of all the ligand transformations studied using TIES.

Protein system	Transformations
CDK2	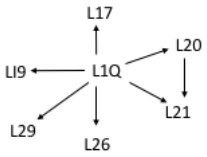
Thrombin	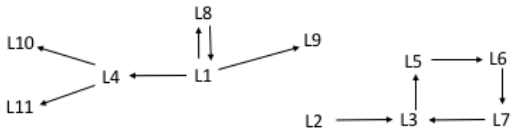
PTP1B	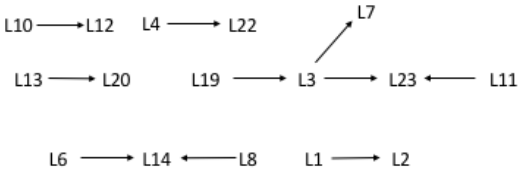
MCL1	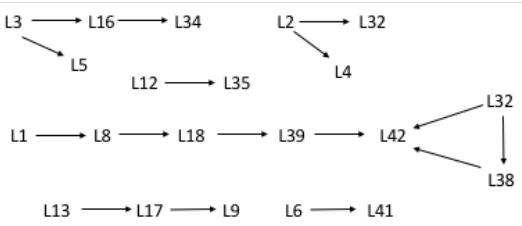
TYK2	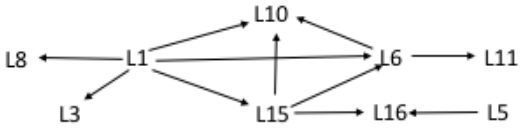
BRD4	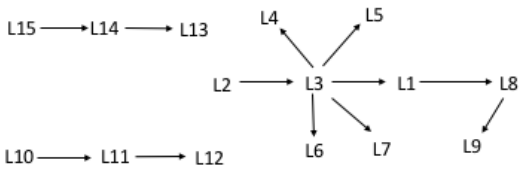
TRKA	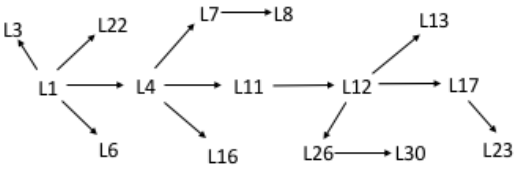

Table A.8: Free energy predictions for all complexes studied using 5 replicas for the four schemes (I to IV†). The largest values among all replicas are highlighted in **bold** and the smallest ones in *italics*. All values are in kcal/mol.

System	FE-type	Scheme	rep1	rep2	rep3	rep4	rep5	TIES-analysis
V561M mutant (forward) with PD173074	ΔG^{com}_{alch}	I	2.94	**3.12**	2.79	2.91	*2.41*	2.84(0.16)
		II	3.00	**3.16**	2.93	2.67	*2.20*	2.79(0.15)
		III	**2.40**	1.85	2.04	2.06	*1.78*	2.03(0.06)
		IV	**2.30**	1.87	2.00	2.11	*1.79*	2.01(0.05)
	ΔG^{pro}_{alch}	I	-0.75	**-0.45**	-0.80	-0.79	*-0.83*	-0.72(0.09)
		II	-0.71	**-0.60**	-0.83	*-0.92*	-0.72	-0.75(0.08)
		III	-1.25	*-1.30*	-1.26	-1.12	**-1.06**	-1.20(0.05)
		IV	*-1.31*	-1.26	-1.18	**-1.03**	-1.12	-1.18(0.04)
V561M mutant (reverse) with PD173074	ΔG^{com}_{alch}	I	1.86	**1.89**	1.69	*1.67*	1.86	1.79(0.10)
		II	1.77	1.85	*1.48*	1.58	**2.10**	1.76(0.09)
		III	*1.99*	2.39	2.09	**2.52**	2.32	2.26(0.07)
		IV	*2.00*	2.36	2.05	**2.51**	2.33	2.25(0.07)
	ΔG^{pro}_{alch}	I	**-0.53**	-0.89	-0.92	*-1.08*	-0.90	-0.86(0.08)
		II	**-0.66**	-0.79	*-1.07*	-1.04	-0.87	-0.89(0.08)
		III	-1.02	-1.32	**-0.92**	-1.18	*-1.35*	-1.16(0.07)
		IV	-1.06	-1.24	**-1.00**	-1.24	*-1.31*	-1.17(0.06)
V561M mutant (forward) with TKI258	ΔG^{com}_{alch}	III	*-1.73*	-1.52	**-1.05**	-1.22	-1.23	-1.35(0.07)
		IV	*-1.76*	-1.55	**-1.00**	-1.27	-1.26	-1.37(0.07)
L1-L9 with thrombin	ΔG^{com}_{alch}	III	**1.29**	*0.54*	0.86	1.06	1.04	0.96(0.09)
		IV	**1.22**	*0.54*	0.84	1.16	1.10	0.97(0.08)
	ΔG^{lig}_{alch}	III	1.61	**1.68**	1.60	*1.58*	1.66	1.63(0.04)
		IV	**1.68**	1.66	1.63	*1.60*	1.65	1.64(0.03)
L4-L11 with thrombin	ΔG^{com}_{alch}	III	-2.00	**-1.58**	-1.97	*-2.83*	-2.77	-2.23(0.13)
		IV	-1.95	**-1.59**	-2.00	*-2.86*	-2.80	-2.24(0.12)
	ΔG^{lig}_{alch}	III	*-1.29*	-1.05	-1.22	-1.26	**-1.01**	-1.17(0.04)
		IV	*-1.35*	-1.10	-1.21	-1.26	**-1.04**	-1.19(0.03)
L3-L6 with BRD4	ΔG^{com}_{alch}	III	*-4.73*	-4.17	**-4.14**	-4.34	-4.32	-4.34(0.08)
		IV	*-4.86*	-4.15	**-4.11**	-4.33	-4.30	-4.35(0.07)
	ΔG^{lig}_{alch}	III	**-5.18**	-5.63	-5.29	-5.58	*-5.74*	-5.48(0.06)
		IV	**-5.24**	-5.59	-5.34	-5.55	*-5.72*	-5.49(0.04)
L3-L7 with BRD4	ΔG^{com}_{alch}	III	*4.79*	4.89	5.00	**5.22**	4.90	4.96(0.08)
		IV	*4.72*	4.86	4.97	**5.21**	4.87	4.92(0.07)
	ΔG^{lig}_{alch}	III	5.27	5.19	*5.15*	**5.40**	5.17	5.23(0.06)
		IV	5.28	5.22	*5.03*	**5.39**	5.06	5.19(0.05)

† In scheme IV, the samples from states which are electrostatically fully decoupled from the state of interest are excluded from MBAR analysis. This is because the energies of such samples at the state of interest may approach infinitely high values due to overlapping atoms by virtue of the non-softcore electrostatic potential used in these simulations.

Bibliography

[1] Nature special. `http://www.nature.com/news/reproducibility-1.17552`. Accessed: 2017-09-26.

[2] M. Baker. 1,500 scientists lift the lid on reproducibility. *Nature*, 533:452–454, 2016.

[3] J. P. A. Ioannidis. Why most published research findings are false. *PLOS Medicine*, 2(8):e124, 08 2005.

[4] P. V. Coveney, E. R. Dougherty, and R. R. Highfield. Big data need big theory too. *Philosophical Transactions of the Royal Society of London A: Mathematical, Physical and Engineering Sciences*, 374(2080), 2016. ArticleID: 20160153.

[5] M. Baker. Reproducibility: Check your chemistry. *Nature*, 548:485–488, 2017.

[6] G. J. Lithgow, M. Driscoll, and P. Phillips. A long journey to reproducible results. *Nature*, 548:387–388, 2017.

[7] W. F. vanGunsteren, X. Daura, N. Hansen, A. E. Mark, C. Oostenbrink, S. Riniker, and L. J. Smith. Validation of molecular simulation: An overview of issues. *Angewandte Chemie International Edition*, 57(4):884–902, 2018.

[8] G. Sliwoski, S. Kothiwale, J. Meiler, and E. W. Lowe. Computational methods in drug discovery. *Pharmacological Reviews*, 66(1):334–395, 2014.

[9] D. L. Mobley and M. K. Gilson. Predicting binding free energies: Frontiers and benchmarks. *Annual Review of Biophysics*, 46(1):531–558, 2017.

[10] P. V. Coveney and S. Wan. On the calculation of equilibrium thermodynamic properties from molecular dynamics. *Physical Chemistry Chemical Physics*, 18:30236–30240, 2016.

[11] C. Abrams and G. Bussi. Enhanced sampling in molecular dynamics using metadynamics, replica-exchange, and temperature-acceleration. *Entropy*, 16(1):163–199, 2014.

[12] R. C. Bernardi, M. C. Melo, and K. Schulten. Enhanced sampling techniques in molecular dynamics simulations of biological systems. *Biochimica et Biophysica Acta (BBA) - General Subjects*, 1850(5):872–877, 2015. Recent developments of molecular dynamics.

[13] S. Marsili, G. F. Signorini, R. Chelli, M. Marchi, and P. Procacci. ORAC: A molecular dynamics simulation program to explore free energy surfaces in biomolecular systems at the atomistic level. *Journal of Computational Chemistry*, 31(5):1106–1116, 2010.

[14] D. J. Earl and M. W. Deem. Parallel tempering: Theory, applications, and new perspectives. *Physical Chemistry Chemical Physics*, 7:3910–3916, 2005.

[15] J. Kstner. Umbrella sampling. *Wiley Interdisciplinary Reviews: Computational Molecular Science*, 1(6):932–942, 2011.

[16] K. Ostermeir and M. Zacharias. Advanced replica-exchange sampling to study the flexibility and plasticity of peptides and proteins. *Biochimica et Biophysica Acta (BBA) - Proteins and Proteomics*, 1834(5):847–853, 2013. The emerging dynamic view of proteins:Protein plasticity in allostery,evolution and self-assembly.

[17] H. Fukunishi, O. Watanabe, and S. Takada. On the Hamiltonian replica exchange method for efficient sampling of biomolecular systems: Application to protein structure prediction. *The Journal of Chemical Physics*, 116(20):9058–9067, 2002.

[18] L. Wang, R. A. Friesner, and B. J. Berne. Replica exchange with solute scaling: A more efficient version of replica exchange with solute tempering (REST2). *The Journal of Physical Chemistry B*, 115(30):9431–9438, 2011.

[19] L. Wang, B. J. Berne, and R. A. Friesner. On achieving high accuracy and reliability in the calculation of relative proteinligand binding affinities. *Proceedings of the National Academy of Sciences*, 109(6):1937–1942, 2012.

[20] M. R. Shirts and J. D. Chodera. Statistically optimal analysis of samples from multiple equilibrium states. *The Journal of Chemical Physics*, 129(12):124105, 2008.

[21] A. P. Bhati, S. Wan, D. W. Wright, and P. V. Coveney. Rapid, accurate, precise, and reliable relative free energy prediction using ensemble based thermodynamic integration. *Journal of Chemical Theory and Computation*, 13(1):210–222, 2017.

[22] S. Wan, A. P. Bhati, S. J. Zasada, I. Wall, D. Green, P. Bamborough, and P. V. Coveney. Rapid and reliable binding affinity prediction of bromodomain inhibitors: A computational study. *Journal of Chemical Theory and Computation*, 13(2):784–795, 2017.

[23] S. Wan, A. P. Bhati, S. Skerratt, K. Omoto, V. Shanmugasundaram, S. K. Bagal, and P. V. Coveney. Evaluation and characterization of trk kinase inhibitors for the treatment of pain: Reliable binding affinity predictions from theory and computation. *Journal of Chemical Information and Modeling*, 57(4):897–909, 2017.

[24] J. Piehler. New methodologies for measuring protein interactions *in vivo* and *in vitro*. *Current Opinion in Structural Biology*, 15(1):4–14, 2005. Folding and binding / Protein-nucleic acid interactions.

[25] B. A. Shoemaker and A. R. Panchenko. Deciphering protein-protein interactions. Part I. Experimental techniques and databases. *PLOS Computational Biology*, 3(3):1–8, 03 2007.

[26] J. E. Ladbury and B. Z. Chowdhry. Sensing the heat: the application of isothermal titration calorimetry to thermodynamic studies of biomolecular interactions. *Chemistry & Biology*, 3(10):791–801, 1996.

[27] C. Yung-Chi and W. H. Prusoff. Relationship between the inhibition constant (Ki) and the concentration of inhibitor which causes 50 per cent inhibition (I50) of an enzymatic reaction. *Biochemical Pharmacology*, 22(23):3099–3108, 1973.

[28] D. A. McQuarrie. *Statistical Mechanics*. University Science Books, 2000.

[29] A. R. Leach. *Molecular modelling: Principles and applications*. Pearson education, 2001.

[30] D. Frenkel and B. Smit. *Understanding molecular simulation: From algorithms to applications*, volume 1. Academic press, 2001.

[31] M. P. Allen and D. J. Tildesley. *Computer simulation of liquids*. Oxford university press, 2017.

[32] L. Verlet. Computer "experiments" on classical fluids. I. Thermodynamical properties of Lennard-Jones molecules. *Physical Review*, 159:98–103, Jul 1967.

[33] D. A. Case, T. E. Cheatham, T. Darden, H. Gohlke, R. Luo, K. M. Merz, A. Onufriev, C. Simmerling, B. Wang, and R. J. Woods. The AMBER biomolecular simulation programs. *Journal of Computational Chemistry*, 26(16):1668–1688, 2005.

[34] L. Nilsson and M. Karplus. Empirical energy functions for energy minimization and dynamics of nucleic acids. *Journal of Computational Chemistry*, 7(5):591–616, 1986.

[35] T. A. Halgren. Merck molecular force field. I. Basis, form, scope, parameterization, and performance of MMFF94. *Journal of Computational Chemistry*, 17(5-6):490–519, 1996.

[36] J. Koehler, W. Saenger, and W. Van Gunsteren. A molecular dynamics simulation of crystalline α-cyclodextrin hexahydrate. *European Biophysics Journal*, 15(4):197–210, 1987.

[37] W. L. Jorgensen and J. Tirado-Rives. The OPLS [optimized potentials for liquid simulations] potential functions for proteins, energy minimizations for crystals of cyclic peptides and crambin. *Journal of the American Chemical Society*, 110(6):1657–1666, 1988.

[38] J. Hermans, H. J. Berendsen, W. F. Van Gunsteren, and J. P. Postma. A consistent empirical potential for water-protein interactions. *Biopolymers*, 23(8):1513–1518, 1984.

[39] N. L. Allinger. Conformational analysis. 130, MM2, a hydrocarbon force field utilizing V1 and V2 torsional terms. *Journal of the American Chemical Society*, 99:8127, 1977.

[40] N. L. Allinger, Y. H. Yuh, and J.-H. Lii. Molecular mechanics: The MM3 force field for hydrocarbons. 1. *Journal of the American Chemical Society*, 11(8551), 1989.

[41] J. Wang, R. M. Wolf, J. W. Caldwell, P. A. Kollman, and D. A. Case. Development and testing of a general AMBER force field. *Journal of Computational Chemistry*, 25(9):1157–1174, 2004.

[42] S. A. Adelman and J. D. Doll. Generalized Langevin equation approach for atom/solidsurface scattering: General formulation for classical scat-

tering off harmonic solids. *The Journal of Chemical Physics*, 64(6):2375–2388, 1976.

[43] S. A. Adelman. Generalized Langevin theory for manybody problems in chemical dynamics: General formulation and the equivalent harmonic chain representation. *The Journal of Chemical Physics*, 71(11):4471–4486, 1979.

[44] H. J. C. Berendsen, J. P. M. Postma, W. F. van Gunsteren, A. DiNola, and J. R. Haak. Molecular dynamics with coupling to an external bath. *The Journal of Chemical Physics*, 81(8):3684–3690, 1984.

[45] J. C. Phillips, R. Braun, W. Wang, J. Gumbart, E. Tajkhorshid, E. Villa, C. Chipot, R. D. Skeel, L. Kale, and K. Schulten. Scalable molecular dynamics with NAMD. *Journal of Computational Chemistry*, 26(16):1781–1802, 2005.

[46] P. P. Ewald. Die Berechnung optischer und elektrostatischer Gitterpotentiale. *Annalen der Physik*, 369(3):253–287, 1921.

[47] T. Darden, D. York, and L. Pedersen. Particle Mesh Ewald: An N.log(N) method for Ewald sums in large systems. *The Journal of Chemical Physics*, 98(12):10089–10092, 1993.

[48] H. Grubmüller, H. Heller, A. Windemuth, and K. Schulten. Generalized verlet algorithm for efficient molecular dynamics simulations with long-range interactions. *Molecular Simulation*, 6(1-3):121–142, 1991.

[49] J.-P. Ryckaert, G. Ciccotti, and H. J. Berendsen. Numerical integration of the Cartesian equations of motion of a system with constraints: molecular dynamics of n-alkanes. *Journal of Computational Physics*, 23(3):327–341, 1977.

[50] H. C. Andersen. Rattle: A "velocity" version of the shake algorithm

for molecular dynamics calculations. *Journal of Computational Physics*, 52(1):24–34, 1983.

[51] S. Miyamoto and P. A. Kollman. Settle: An analytical version of the SHAKE and RATTLE algorithm for rigid water models. *Journal of Computational Chemistry*, 13(8):952–962, 1992.

[52] V. Kräutler, W. F. van Gunsteren, and P. H. Hünenberger. A fast SHAKE algorithm to solve distance constraint equations for small molecules in molecular dynamics simulations. *Journal of Computational Chemistry*, 22(5):501–508, 2001.

[53] R. W. Zwanzig. High-temperature equation of state by a perturbation method. I. nonpolar gases. *The Journal of Chemical Physics*, 22(8):1420–1426, 1954.

[54] J. G. Kirkwood. Statistical mechanics of fluid mixtures. *The Journal of Chemical Physics*, 3(5):300–313, 1935.

[55] J. Valleau and G. Torrie. Modern theoretical chemistry. *A Guide to Monte Carlo for Statistical Mechanics*, 2:169–194, 1977.

[56] S. H. Northrup, M. R. Pear, C. Y. Lee, J. A. McCammon, and M. Karplus. Dynamical theory of activated processes in globular proteins. *Proceedings of the National Academy of Sciences*, 79(13):4035–4039, 1982.

[57] B. L. Tembe and J. A. McCammon. Ligand-receptor interactions. *Computers & Chemistry*, 8(4):281–283, 1984.

[58] W. L. Jorgensen and C. Ravimohan. Monte Carlo simulation of differences in free energies of hydration. *The Journal of Chemical Physics*, 83(6):3050–3054, 1985.

[59] K. M. Merz and P. A. Kollman. Free energy perturbation simulations of the inhibition of thermolysin: prediction of the free energy of binding of a

new inhibitor. *Journal of the American Chemical Society*, 111(15):5649–5658, 1989.

[60] W. L. Jorgensen, J. K. Buckner, S. Boudon, and J. Tirado-Rives. Efficient computation of absolute free energies of binding by computer simulations. Application to the methane dimer in water. *The Journal of Chemical Physics*, 89(6):3742–3746, 1988.

[61] D. A. Pearlman and B. G. Rao. Free energy calculations: methods and applications. *Encyclopedia of Computational Chemistry*, 1998.

[62] M. R. Reddy, M. D. Erion, and A. Agarwal. Free energy calculations: use and limitations in predicting ligand binding affinities. *Reviews in Computational Chemistry*, 16:217–304, 2000.

[63] C. F. Wong and J. A. McCammon. Dynamics and design of enzymes and inhibitors. *Journal of the American Chemical Society*, 108(13):3830–3832, 1986.

[64] P. A. Bash, U. C. Singh, R. Langridge, and P. A. Kollman. Free energy calculations by computer simulation. *Science*, 236:564, 1987.

[65] D. L. Beveridge and F. DiCapua. Free energy via molecular simulation: Applications to chemical and biomolecular systems. *Annual Review of Biophysics and Biophysical Chemistry*, 18(1):431–492, 1989.

[66] T. P. Lybrand. Computer simulation of biomolecular systems using molecular dynamics and free energy perturbation methods. *Reviews in Computational Chemistry, Volume 1*, pages 295–320, 1990.

[67] T. Straatsma and J. McCammon. Computational alchemy. *Annual Review of Physical Chemistry*, 43(1):407–435, 1992.

[68] P. Kollman. Free energy calculations: applications to chemical and biochemical phenomena. *Chemical Reviews*, 93(7):2395–2417, 1993.

[69] A. Warshel, H. Tao, M. Fothergill, and Z.-T. Chu. Effective methods for estimation of binding energies in computer-aided drug design. *Israel Journal of Chemistry*, 34(2):253–256, 1994.

[70] T. J. Marrone, J. M. Briggs, and, and J. A. McCammon. Structure-based drug design: computational advances. *Annual Review of Pharmacology and Toxicology*, 37(1):71–90, 1997.

[71] T. Steinbrecher and A. Labahn. Towards accurate free energy calculations in ligand protein-binding studies. *Current medicinal chemistry*, 17(8):767–785, 2010.

[72] Z. Cournia, B. Allen, and W. Sherman. Relative binding free energy calculations in drug discovery: Recent advances and practical considerations. *Journal of Chemical Information and Modeling*, 57(12):2911–2937, 2017.

[73] K. M. Merz. Limits of free energy computation for proteinligand interactions. *Journal of Chemical Theory and Computation*, 6(5):1769–1776, 2010.

[74] D. L. Mobley and K. A. Dill. Binding of small-molecule ligands to proteins: what you see is not always what you get. *Structure*, 17(4):489 – 498, 2009.

[75] C. D. Christ, A. E. Mark, and W. F. van Gunsteren. Basic ingredients of free energy calculations: A review. *Journal of Computational Chemistry*, 31(8):1569–1582, 2010.

[76] B. J. Williams-Noonan, E. Yuriev, and D. K. Chalmers. Free energy methods in drug design: Prospects of alchemical perturbation in medicinal chemistry. *Journal of Medicinal Chemistry*, 61(3):638–649, 2018.

[77] R. Abel, L. Wang, D. L. Mobley, and R. A. Friesner. A critical review of validation, blind testing, and real- world use of alchemical protein-ligand

binding free energy calculations. *Current Topics in Medicinal Chemistry*, 17(23):2577–2585, 2017.

[78] D. L. Mobley and M. K. Gilson. Predicting binding free energies: Frontiers and benchmarks. *Annual Review of Biophysics*, 46(1):531–558, 2017.

[79] N. Hansen and W. F. van Gunsteren. Practical aspects of free-energy calculations: A review. *Journal of Chemical Theory and Computation*, 10(7):2632–2647, 2014.

[80] H.-J. Böhm. The development of a simple empirical scoring function to estimate the binding constant for a protein-ligand complex of known three-dimensional structure. *Journal of Computer-Aided Molecular Design*, 8(3):243–256, 1994.

[81] A. N. Jain. Scoring noncovalent protein-ligand interactions: a continuous differentiable function tuned to compute binding affinities. *Journal of Computer-Aided Molecular Design*, 10(5):427–440, 1996.

[82] M. D. Eldridge, C. W. Murray, T. R. Auton, G. V. Paolini, and R. P. Mee. Empirical scoring functions: I. the development of a fast empirical scoring function to estimate the binding affinity of ligands in receptor complexes. *Journal of Computer-Aided Molecular Design*, 11(5):425–445, 1997.

[83] T. Debroise, E. I. Shakhnovich, and N. Chron. A hybrid knowledge-based and empirical scoring function for proteinligand interaction: Smog2016. *Journal of Chemical Information and Modeling*, 57(3):584–593, 2017.

[84] J. Åqvist, C. Medina, and J.-E. Samuelsson. A new method for predicting binding affinity in computer-aided drug design. *Protein Engineering, Design and Selection*, 7(3):385–391, 1994.

[85] P. A. Kollman, I. Massova, C. Reyes, B. Kuhn, S. Huo, L. Chong, M. Lee, T. Lee, Y. Duan, W. Wang, et al. Calculating structures and free energies of complex molecules: combining molecular mechanics and continuum models. *Accounts of Chemical Research*, 33(12):889–897, 2000.

[86] T. P. Straatsma, H. J. C. Berendsen, and J. P. M. Postma. Free energy of hydrophobic hydration: A molecular dynamics study of noble gases in water. *The Journal of Chemical Physics*, 85(11):6720–6727, 1986.

[87] T. P. Straatsma and H. J. C. Berendsen. Free energy of ionic hydration: Analysis of a thermodynamic integration technique to evaluate free energy differences by molecular dynamics simulations. *The Journal of Chemical Physics*, 89(9):5876–5886, 1988.

[88] N. Makri. The linear response approximation and its lowest order corrections: An influence functional approach. *The Journal of Physical Chemistry B*, 103(15):2823–2829, 1999.

[89] H. Gohlke, C. Kiel, and D. A. Case. Insights into protein-protein binding by binding free energy calculation and free energy decomposition for the Ras-Raf and Ras-RalGDS complexes. *Journal of Molecular Biology*, 330(4):891–913, 2003.

[90] J. Srinivasan, T. E. Cheatham, P. Cieplak, P. A. Kollman, and D. A. Case. Continuum solvent studies of the stability of DNA, RNA, and phosphoramidate-DNA helices. *Journal of the American Chemical Society*, 120(37):9401–9409, 1998.

[91] Y. N. Vorobjev, J. C. Almagro, and J. Hermans. Discrimination between native and intentionally misfolded conformations of proteins: ES/IS, a new method for calculating conformational free energy that uses both dynamics simulations with an explicit solvent and an implicit solvent continuum model. *Proteins: Structure, Function, and Bioinformatics*, 32(4):399–413, 1998.

[92] B. Jayaram, D. Sprous, M. Young, and D. Beveridge. Free energy analysis of the conformational preferences of A and B forms of DNA in solution. *Journal of the American Chemical Society*, 120(41):10629–10633, 1998.

[93] M. K. Gilson and B. Honig. Calculation of the total electrostatic energy of a macromolecular system: solvation energies, binding energies, and conformational analysis. *Proteins: Structure, Function, and Bioinformatics*, 4(1):7–18, 1988.

[94] W. C. Still, A. Tempczyk, R. C. Hawley, and T. Hendrickson. Semianalytical treatment of solvation for molecular mechanics and dynamics. *Journal of the American Chemical Society*, 112(16):6127–6129, 1990.

[95] W. Kauzmann. Some factors in the interpretation of protein denaturation. *Advances in Protein Chemistry*, 14:1–63, 1959.

[96] F. M. Richards. Areas, volumes, packing, and protein structure. *Annual Review of Biophysics and Bioengineering*, 6(1):151–176, 1977.

[97] D. Sitkoff, K. A. Sharp, and B. Honig. Accurate calculation of hydration free energies using macroscopic solvent models. *The Journal of Physical Chemistry*, 98(7):1978–1988, 1994.

[98] M. M. Teeter and D. A. Case. Harmonic and quasiharmonic descriptions of crambin. *The Journal of Physical Chemistry*, 94(21):8091–8097, 1990.

[99] N. Singh and A. Warshel. A comprehensive examination of the contributions to the binding entropy of proteinligand complexes. *Proteins: Structure, Function, and Bioinformatics*, 78(7):1724–1735, 2010.

[100] R. M. Levy, M. Karplus, J. Kushick, and D. Perahia. Evaluation of the configurational entropy for proteins: application to molecular dynamics simulations of an α-helix. *Macromolecules*, 17(7):1370–1374, 1984.

[101] B. Brooks and M. Karplus. Harmonic dynamics of proteins: normal modes and fluctuations in bovine pancreatic trypsin inhibitor. *Proceedings of the National Academy of Sciences*, 80(21):6571–6575, 1983.

[102] B. R. Brooks, D. Janežič, and M. Karplus. Harmonic analysis of large systems. I. Methodology. *Journal of Computational Chemistry*, 16(12):1522–1542, 1995.

[103] E. B. Wilson, J. C. Decius, and P. C. Cross. *Molecular vibrations*. McGraw-Hill, New York, 1955.

[104] J. M. Swanson, R. H. Henchman, and J. A. McCammon. Revisiting free energy calculations: a theoretical connection to MM/PBSA and direct calculation of the association free energy. *Biophysical Journal*, 86(1):67–74, 2004.

[105] D. W. Wright, B. A. Hall, O. A. Kenway, S. Jha, and P. V. Coveney. Computing clinically relevant binding free energies of HIV-1 protease inhibitors. *Journal of Chemical Theory and Computation*, 10(3):1228–1241, 2014.

[106] W. H. Press, B. P. Flannery, S. A. Teukolsky, W. T. Vetterling, et al. *Numerical recipes*, volume 3. Cambridge University Press, Cambridge, 1989.

[107] C. H. Bennett. Efficient estimation of free energy differences from Monte Carlo data. *Journal of Computational Physics*, 22:245–268, October 1976.

[108] M. R. Shirts and V. S. Pande. Comparison of efficiency and bias of free energies computed by exponential averaging, the Bennett acceptance ratio, and thermodynamic integration. *The Journal of Chemical Physics*, 122(14):144107, April 2005.

[109] N. D. Lu, J. K. Singh, and D. A. Kofke. Appropriate methods to combine forward and reverse free-energy perturbation averages. *Journal of Chemical Physics*, 118(7), 2003.

[110] A. M. Ferrenberg and R. H. Swendsen. Optimized Monte Carlo data analysis. *Physical Review Letters*, 63(12):1195–1198, September 1989.

[111] S. Kumar, J. M. Rosenberg, D. Bouzida, R. H. Swendsen, and P. A. Kollman. The weighted histogram analysis method for free-energy calculations on biomolecules. I. The method. *Journal of Computational Chemistry*, 13(8):1011–1021, October 1992.

[112] C. J. Woods, J. W. Essex, and M. A. King. Enhanced configurational sampling in binding free-energy calculations. *The Journal of Physical Chemistry B*, 107(49):13711–13718, 2003.

[113] S. W. Rick. Increasing the efficiency of free energy calculations using parallel tempering and histogram reweighting. *Journal of Chemical Theory and Computation*, 2(4):939–946, 2006.

[114] J. D. Chodera, W. C. Swope, J. W. Pitera, C. Seok, and K. A. Dill. Use of the weighted histogram analysis method for the analysis of simulated and parallel tempering simulations. *Journal of Chemical Theory and Computation*, 3(1):26–41, 2007.

[115] M. Zacharias, T. P. Straatsma, and J. A. McCammon. Separation-shifted scaling, a new scaling method for Lennard-Jones interactions in thermodynamic integration. *The Journal of Chemical Physics*, 100(12):9025–9031, 1994.

[116] T. C. Beutler, A. E. Mark, R. C. van Schaik, P. R. Gerber, and W. F. van Gunsteren. Avoiding singularities and numerical instabilities in free energy calculations based on molecular simulations. *Chemical Physics Letters*, 222(6):529–539, 1994.

[117] V. Gapsys, D. Seeliger, and B. L. de Groot. New soft-core potential function for molecular dynamics based alchemical free energy calculations. *Journal of Chemical Theory and Computation*, 8(7):2373–2382, 2012.

[118] W. L. Jorgensen, J. K. Buckner, S. Boudon, and J. TiradoRives. Efficient computation of absolute free energies of binding by computer simulations. Application to the methane dimer in water. *The Journal of Chemical Physics*, 89(6):3742–3746, 1988.

[119] M. Gilson, J. Given, B. Bush, and J. McCammon. The statistical-thermodynamic basis for computation of binding affinities: a critical review. *Biophysical Journal*, 72(3):1047–1069, 1997.

[120] S. Boresch, F. Tettinger, M. Leitgeb, and M. Karplus. Absolute binding free energies: A quantitative approach for their calculation. *The Journal of Physical Chemistry B*, 107(35):9535–9551, 2003.

[121] Y. Deng and B. Roux. Computations of standard binding free energies with molecular dynamics simulations. *The Journal of Physical Chemistry B*, 113(8):2234–2246, 2009.

[122] J. Wang, Y. Deng, and B. Roux. Absolute binding free energy calculations using molecular dynamics simulations with restraining potentials. *Biophysical Journal*, 91(8):2798–2814, 2006.

[123] J. N. Onuchic, Z. Luthey-Schulten, and P. G. Wolynes. Theory of protein folding: The energy landscape perspective. *Annual Review of Physical Chemistry*, 48(1):545–600, 1997.

[124] Y. Duan and P. A. Kollman. Pathways to a protein folding intermediate observed in a 1-microsecond simulation in aqueous solution. *Science*, 282(5389):740–744, 1998.

[125] C. Bergonzo, N. M. Henriksen, D. R. Roe, J. M. Swails, A. E. Roitberg, and T. E. Cheatham. Multidimensional replica exchange molecular dy-

namics yields a converged ensemble of an RNA tetranucleotide. *Journal of Chemical Theory and Computation*, 10(1):492–499, 2014.

[126] G. Torrie and J. Valleau. Nonphysical sampling distributions in Monte Carlo free-energy estimation: Umbrella sampling. *Journal of Computational Physics*, 23(2):187–199, 1977.

[127] A. Laio and M. Parrinello. Escaping free-energy minima. *Proceedings of the National Academy of Sciences*, 99(20):12562–12566, 2002.

[128] S. Izrailev, S. Stepaniants, B. Isralewitz, D. Kosztin, H. Lu, F. Molnar, W. Wriggers, and K. Schulten. Steered molecular dynamics. *Computational Molecular Dynamics: Challenges, Methods, Ideas*, 4:39–65, 1999.

[129] B. Isralewitz, M. Gao, and K. Schulten. Steered molecular dynamics and mechanical functions of proteins. *Current Opinion in Structural Biology*, 11(2):224–230, 2001.

[130] E. Carter, G. Ciccotti, J. T. Hynes, and R. Kapral. Constrained reaction coordinate dynamics for the simulation of rare events. *Chemical Physics Letters*, 156(5):472–477, 1989.

[131] E. Darve, D. Rodrguez-Gmez, and A. Pohorille. Adaptive biasing force method for scalar and vector free energy calculations. *The Journal of Chemical Physics*, 128(14):144120, 2008.

[132] J. Hermans. Simple analysis of noise and hysteresis in (slow-growth) free energy simulations. *The Journal of Physical Chemistry*, 95(23):9029–9032, 1991.

[133] D. A. Hendrix and C. Jarzynski. A fast growth method of computing free energy differences. *The Journal of Chemical Physics*, 114(14):5974–5981, 2001.

[134] Y. Miao, V. A. Feher, and J. A. McCammon. Gaussian accelerated molecular dynamics: Unconstrained enhanced sampling and free energy

calculation. *Journal of Chemical Theory and Computation*, 11(8):3584–3595, 2015.

[135] H. Xiong, A. Crespo, M. Marti, D. Estrin, and A. E. Roitberg. Free energy calculations with non-equilibrium methods: Applications of the Jarzynski relationship. *Theoretical Chemistry Accounts*, 116(1):338–346, Aug 2006.

[136] M. Souaille and B. Roux. Extension to the weighted histogram analysis method: Combining umbrella sampling with free energy calculations. *Computer Physics Communications*, 135(1):40–57, 2001.

[137] A. Cavalli, A. Spitaleri, G. Saladino, and F. L. Gervasio. Investigating drugtarget association and dissociation mechanisms using metadynamics-based algorithms. *Accounts of Chemical Research*, 48(2):277–285, 2015.

[138] Y. Sakai, A. Kawaguchi, K. Nagata, and T. Hirokawa. Analysis by metadynamics simulation of binding pathway of influenza virus m2 channel blockers. *Microbiology and Immunology*, 62(1):34–43, 2018.

[139] N. Saleh, P. Ibrahim, G. Saladino, F. L. Gervasio, and T. Clark. An efficient metadynamics-based protocol to model the binding affinity and the transition state ensemble of g-protein-coupled receptor ligands. *Journal of Chemical Information and Modeling*, 57(5):1210–1217, 2017.

[140] V. Limongelli, M. Bonomi, and M. Parrinello. Funnel metadynamics as accurate binding free-energy method. *Proceedings of the National Academy of Sciences*, 110(16):6358–6363, 2013.

[141] Y. Okamoto. Generalized-ensemble algorithms: enhanced sampling techniques for Monte Carlo and molecular dynamics simulations. *Journal of Molecular Graphics and Modelling*, 22(5):425–439, 2004. Conformational Sampling.

[142] U. H. E. Hansmann and Y. Okamoto. Generalized-ensemble Monte Carlo method for systems with rough energy landscape. *Physics Review E*, 56:2228–2233, Aug 1997.

[143] E. Marinari and G. Parisi. Simulated tempering: A new Monte Carlo scheme. *Europhysics Letters*, 19(6):451, 1992.

[144] A. P. Lyubartsev, A. A. Martsinovski, S. V. Shevkunov, and P. N. VorontsovVelyaminov. New approach to Monte Carlo calculation of the free energy: Method of expanded ensembles. *The Journal of Chemical Physics*, 96(3):1776–1783, 1992.

[145] Y. Sugita and Y. Okamoto. Replica-exchange molecular dynamics method for protein folding. *Chemical Physics Letters*, 314(1):141–151, 1999.

[146] R. H. Swendsen and J.-S. Wang. Replica Monte Carlo simulation of spin-glasses. *Physical Review Letters*, 57:2607–2609, Nov 1986.

[147] C. Geyer. Computing science and statistics proceedings of the 23 symposium on the interface; American Statistical Association: New York, 1991; p 156.

[148] U. H. Hansmann. Parallel tempering algorithm for conformational studies of biological molecules. *Chemical Physics Letters*, 281(1):140–150, 1997.

[149] M. Falcioni and M. W. Deem. A biased Monte Carlo scheme for zeolite structure solution. *The Journal of Chemical Physics*, 110(3):1754–1766, 1999.

[150] N. Metropolis, A. W. Rosenbluth, M. N. Rosenbluth, A. H. Teller, and E. Teller. Equation of state calculations by fast computing machines. *The Journal of Chemical Physics*, 21(6):1087–1092, 1953.

[151] V. I. Manousiouthakis and M. W. Deem. Strict detailed balance is unnecessary in Monte Carlo simulation. *The Journal of Chemical Physics*, 110(6):2753–2756, 1999.

[152] N. Rathore, M. Chopra, and J. J. de Pablo. Optimal allocation of replicas in parallel tempering simulations. *The Journal of Chemical Physics*, 122(2):024111, 2005.

[153] M. Cecchini, F. Rao, M. Seeber, and A. Caflisch. Replica exchange molecular dynamics simulations of amyloid peptide aggregation. *The Journal of Chemical Physics*, 121(21):10748–10756, 2004.

[154] A. Kone and D. A. Kofke. Selection of temperature intervals for parallel-tempering simulations. *The Journal of Chemical Physics*, 122(20):206101, 2005.

[155] D. A. Kofke. On the acceptance probability of replica-exchange Monte Carlo trials. *The Journal of Chemical Physics*, 117(15):6911–6914, 2002.

[156] A. Patriksson and D. van der Spoel. A temperature predictor for parallel tempering simulations. *Physical Chemistry Chemical Physics*, 10:2073–2077, 2008.

[157] H. G. Katzgraber, S. Trebst, D. A. Huse, and M. Troyer. Feedback-optimized parallel tempering Monte Carlo. *Journal of Statistical Mechanics: Theory and Experiment*, 2006(03):P03018, 2006.

[158] C. Predescu, M. Predescu, and C. V. Ciobanu. On the efficiency of exchange in parallel tempering Monte Carlo simulations. *The Journal of Physical Chemistry B*, 109(9):4189–4196, 2005.

[159] Q. Yan and J. J. de Pablo. Hyper-parallel tempering Monte Carlo: Application to the Lennard-Jones fluid and the restricted primitive model. *The Journal of Chemical Physics*, 111(21):9509–9516, 1999.

[160] Q. Yan and J. J. de Pablo. Hyperparallel tempering Monte Carlo simulation of polymeric systems. *The Journal of Chemical Physics*, 113(3):1276–1282, 2000.

[161] Y. Sugita, A. Kitao, and Y. Okamoto. Multidimensional replica-exchange method for free-energy calculations. *The Journal of Chemical Physics*, 113(15):6042–6051, 2000.

[162] K. Murata, Y. Sugita, and Y. Okamoto. Free energy calculations for DNA base stacking by replica-exchange umbrella sampling. *Chemical Physics Letters*, 385(1):1–7, 2004.

[163] W. Jiang, M. Hodoscek, and B. Roux. Computation of absolute hydration and binding free energy with free energy perturbation distributed replica-exchange molecular dynamics. *Journal of Chemical Theory and Computation*, 5(10):2583–2588, 2009.

[164] A. Mitsutake and Y. Okamoto. Replica-exchange simulated tempering method for simulations of frustrated systems. *Chemical Physics Letters*, 332(1):131–138, 2000.

[165] Y. Sugita and Y. Okamoto. Replica-exchange multicanonical algorithm and multicanonical replica-exchange method for simulating systems with rough energy landscape. *Chemical Physics Letters*, 329(3):261–270, 2000.

[166] A. Mitsutake, Y. Sugita, and Y. Okamoto. Generalized-ensemble algorithms for molecular simulations of biopolymers. *Peptide Science*, 60(2):96–123, 2001.

[167] R. Faller, Q. Yan, and J. J. de Pablo. Multicanonical parallel tempering. *The Journal of Chemical Physics*, 116(13):5419–5423, 2002.

[168] A. Mitsutake, Y. Sugita, and Y. Okamoto. Replica-exchange multicanonical and multicanonical replica-exchange Monte Carlo simulations

of peptides. I. Formulation and benchmark test. *The Journal of Chemical Physics*, 118(14):6664–6675, 2003.

[169] A. Mitsutake, Y. Sugita, and Y. Okamoto. Replica-exchange multicanonical and multicanonical replica-exchange Monte Carlo simulations of peptides. II. Application to a more complex system. *The Journal of Chemical Physics*, 118(14):6676–6688, 2003.

[170] C. Chen, Y. Xiao, and Y. Huang. Improving the replica-exchange molecular-dynamics method for efficient sampling in the temperature space. *Physical Review E*, 91:052708, May 2015.

[171] C. Chen and Y. Huang. Walking freely in the energy and temperature space by the modified replica exchange molecular dynamics method. *Journal of Computational Chemistry*, 37(17):1565–1575, 2016.

[172] J. Kim, J. E. Straub, and T. Keyes. Replica exchange statistical temperature molecular dynamics algorithm. *The Journal of Physical Chemistry B*, 116(29):8646–8653, 2012.

[173] R. Urano and Y. Okamoto. New implementations of replica-exchange method for simulations of complex systems: Designed-walk and deterministic replica-exchange methods. *Physics Procedia*, 68:100–104, 2015. Proceedings of the 28th Workshop on Computer Simulation Studies in Condensed Matter Physics (CSP2015).

[174] M. Kouza and U. H. E. Hansmann. Velocity scaling for optimizing replica exchange molecular dynamics. *The Journal of Chemical Physics*, 134(4):044124, 2011.

[175] X. Cheng, G. Cui, V. Hornak, and C. Simmerling. Modified replica exchange simulation methods for local structure refinement. *The Journal of Physical Chemistry B*, 109(16):8220–8230, 2005.

[176] J. Hritz and C. Oostenbrink. Hamiltonian replica exchange molecular dynamics using soft-core interactions. *The Journal of Chemical Physics*, 128(14):144121, 2008.

[177] R. Affentranger, I. Tavernelli, and E. E. Di Iorio. A novel Hamiltonian replica exchange MD protocol to enhance protein conformational space sampling. *Journal of Chemical Theory and Computation*, 2(2):217–228, 2006.

[178] S. Jang, S. Shin, and Y. Pak. Replica-exchange method using the generalized effective potential. *Physics Review Letters*, 91:058305, Aug 2003.

[179] S. G. Itoh, H. Okumura, and Y. Okamoto. Replica-exchange method in van der Waals radius space: Overcoming steric restrictions for biomolecules. *The Journal of Chemical Physics*, 132(13):134105, 2010.

[180] M. Fajer, D. Hamelberg, and J. A. McCammon. Replica-exchange accelerated molecular dynamics (REXAMD) applied to thermodynamic integration. *Journal of Chemical Theory and Computation*, 4(10):1565–1569, 2008.

[181] D. R. Roe, C. Bergonzo, and T. E. Cheatham. Evaluation of enhanced sampling provided by accelerated molecular dynamics with Hamiltonian replica exchange methods. *The Journal of Physical Chemistry B*, 118(13):3543–3552, 2014.

[182] W. Jiang and B. Roux. Free energy perturbation Hamiltonian replica-exchange molecular dynamics (FEP/H-REMD) for absolute ligand binding free energy calculations. *Journal of Chemical Theory and Computation*, 6(9):2559–2565, 2010.

[183] P. Liu, B. Kim, R. A. Friesner, and B. J. Berne. Replica exchange with solute tempering: A method for sampling biological systems in explicit water. *Proceedings of the National Academy of Sciences of the United States of America*, 102(39):13749–13754, 2005.

[184] X. Huang, M. Hagen, B. Kim, R. A. Friesner, R. Zhou, and B. J. Berne. Replica exchange with solute tempering: Efficiency in large scale systems. *The Journal of Physical Chemistry B*, 111(19):5405–5410, 2007.

[185] S. L. C. Moors, S. Michielssens, and A. Ceulemans. Improved replica exchange method for native-state protein sampling. *Journal of Chemical Theory and Computation*, 7(1):231–237, 2011.

[186] T. Terakawa, T. Kameda, and S. Takada. On easy implementation of a variant of the replica exchange with solute tempering in GROMACS. *Journal of Computational Chemistry*, 32(7):1228–1234, 2011.

[187] C. J. Woods, J. W. Essex, and M. A. King. The development of replica-exchange-based free-energy methods. *The Journal of Physical Chemistry B*, 107(49):13703–13710, 2003.

[188] I. V. Khavrutskii and A. Wallqvist. Improved binding free energy predictions from single-reference thermodynamic integration augmented with Hamiltonian replica exchange. *Journal of Chemical Theory and Computation*, 7(9):3001–3011, 2011.

[189] D. K. Shenfeld, H. Xu, M. P. Eastwood, R. O. Dror, and D. E. Shaw. Minimizing thermodynamic length to select intermediate states for free-energy calculations and replica-exchange simulations. *Physics Review E*, 80:046705, Oct 2009.

[190] M. P. Luitz and M. Zacharias. Role of tyrosine hot-spot residues at the interface of colicin E9 and immunity protein 9: A comparative free energy simulation study. *Proteins: Structure, Function, and Bioinformatics*, 81(3):461–468, 2013.

[191] Y. Meng, D. Sabri Dashti, and A. E. Roitberg. Computing alchemical free energy differences with Hamiltonian replica exchange molecular dynamics (H-REMD) simulations. *Journal of Chemical Theory and Computation*, 7(9):2721–2727, 2011.

[192] D. Min, H. Li, G. Li, R. Bitetti-Putzer, and W. Yang. Synergistic approach to improve "alchemical" free energy calculation in rugged energy surface. *The Journal of Chemical Physics*, 126(14):144109, 2007.

[193] T. Rodinger, P. L. Howell, and R. Poms. Calculation of absolute protein-ligand binding free energy using distributed replica sampling. *The Journal of Chemical Physics*, 129(15):155102, 2008.

[194] M. Lapelosa, E. Gallicchio, and R. M. Levy. Conformational transitions and convergence of absolute binding free energy calculations. *Journal of Chemical Theory and Computation*, 8(1):47–60, 2012.

[195] L. Wang, Y. Deng, J. L. Knight, Y. Wu, B. Kim, W. Sherman, J. C. Shelley, T. Lin, and R. Abel. Modeling local structural rearrangements using FEP/REST: Application to relative binding affinity predictions of CDK2 inhibitors. *Journal of Chemical Theory and Computation*, 9(2):1282–1293, 2013.

[196] L. Wang, Y. Wu, Y. Deng, B. Kim, L. Pierce, G. Krilov, D. Lupyan, S. Robinson, M. K. Dahlgren, J. Greenwood, D. L. Romero, C. Masse, J. L. Knight, T. Steinbrecher, T. Beuming, W. Damm, E. Harder, W. Sherman, M. Brewer, R. Wester, M. Murcko, L. Frye, R. Farid, T. Lin, D. L. Mobley, W. L. Jorgensen, B. J. Berne, R. A. Friesner, and R. Abel. Accurate and reliable prediction of relative ligand binding potency in prospective drug discovery by way of a modern free-energy calculation protocol and force field. *Journal of the American Chemical Society*, 137(7):2695–2703, 2015.

[197] A. Elofsson and L. Nilsson. How consistent are molecular dynamics simulations?: Comparing structure and dynamics in reduced and oxidized escherichia coli thioredoxin. *Journal of Molecular Biology*, 233(4):766 – 780, 1993.

[198] L. S. D. Caves, J. D. Evanseck, and M. Karplus. Locally accessible

conformations of proteins: Multiple molecular dynamics simulations of crambin. *Protein Science*, 7(3):649–666, 1998.

[199] S. K. Sadiq, D. W. Wright, O. A. Kenway, and P. V. Coveney. Accurate ensemble molecular dynamics binding free energy ranking of multidrug-resistant HIV-1 proteases. *Journal of Chemical Information and Modeling*, 50(5):890–905, 2010.

[200] H. Fujitani, Y. Tanida, M. Ito, G. Jayachandran, C. D. Snow, M. R. Shirts, E. J. Sorin, and V. S. Pande. Direct calculation of the binding free energies of fkbp ligands. *The Journal of Chemical Physics*, 123(8):084108, 2005.

[201] S. Genheden and U. Ryde. How to obtain statistically converged MM/GBSA results. *Journal of Computational Chemistry*, 31(4):837–846, 2010.

[202] B. Zagrovic and W. F. van Gunsteren. Computational analysis of the mechanism and thermodynamics of inhibition of phosphodiesterase 5A by synthetic ligands. *Journal of Chemical Theory and Computation*, 3(1):301–311, 2007.

[203] S. Genheden and U. Ryde. A comparison of different initialization protocols to obtain statistically independent molecular dynamics simulations. *Journal of Computational Chemistry*, 32(2):187–195, 2011.

[204] M. Lawrenz, R. Baron, and J. A. McCammon. Independent-trajectories thermodynamic-integration free-energy changes for biomolecular systems: Determinants of H5N1 avian influenza virus neuraminidase inhibition by peramivir. *Journal of Chemical Theory and Computation*, 5(4):1106–1116, 2009.

[205] A. A. Gorfe, P. Ferrara, A. Caflisch, D. N. Marti, H. R. Bosshard, and I. Jelesarov. Calculation of protein ionization equilibria with conformational sampling: pka of a model leucine zipper, gcn4 and barnase. *Proteins: Structure, Function, and Bioinformatics*, 46(1):41–60.

[206] E. C. Sherer and C. J. Cramer. Internal loophelix coupling in the dynamics of the rna duplex (gc*c*aguucgcuggc)2. *The Journal of Physical Chemistry B*, 106(19):5075–5085, 2002.

[207] A. E. Loccisano, O. Acevedo, J. DeChancie, B. G. Schulze, and J. D. Evanseck. Enhanced sampling by multiple molecular dynamics trajectories: carbonmonoxy myoglobin 10 μs a0 a13 transition from ten 400 picosecond simulations. *Journal of Molecular Graphics and Modelling*, 22(5):369 – 376, 2004. Conformational Sampling.

[208] A. N. Koller, H. Schwalbe, and H. Gohlke. Starting structure dependence of nmr order parameters derived from md simulations: Implications for judging force-field quality. *Biophysical Journal*, 95(1):L04 – L06, 2008.

[209] F. Manzoni and U. Ryde. Assessing the stability of free-energy perturbation calculations by performing variations in the method. *Journal of Computer-Aided Molecular Design*, 32(4):529–536, Apr 2018.

[210] P. Auffinger, S. Louise-May, and E. Westhof. Multiple molecular dynamics simulations of the anticodon loop of tRNAAsp in aqueous solution with counterions. *Journal of the American Chemical Society*, 117(25):6720–6726, 1995.

[211] M. Lawrenz, R. Baron, Y. Wang, and J. A. McCammon. *Independent-Trajectory Thermodynamic Integration: A Practical Guide to Protein-Drug Binding Free Energy Calculations Using Distributed Computing*, pages 469–486. Springer New York, New York, NY, 2012.

[212] S. Wan, B. Knapp, D. W. Wright, C. M. Deane, and P. V. Coveney. Rapid, precise, and reproducible prediction of peptide-MHC binding affinities from molecular dynamics that correlate well with experiment. *Journal of Chemical Theory and Computation*, 11(7):3346–3356, 2015.

[213] S. Wan and P. V. Coveney. Rapid and accurate ranking of binding affinities of epidermal growth factor receptor sequences with selected

lung cancer drugs. *Journal of the Royal Society Interface*, 8(61):1114–1127, 2011.

[214] T. D. Bunney, S. Wan, N. Thiyagarajan, L. Sutto, S. V. Williams, P. Ashford, H. Koss, M. A. Knowles, F. L. Gervasio, P. V. Coveney, and M. Katan. The effect of mutations on drug sensitivity and kinase activity of fibroblast growth factor receptors: a combined experimental and theoretical study. *EBioMedicine*, 2(3):194–204, 2015.

[215] S. Genheden, I. Nilsson, and U. Ryde. Binding affinities of factor xa inhibitors estimated by thermodynamic integration and mm/gbsa. *Journal of Chemical Information and Modeling*, 51(4):947–958, 2011. PMID: 21417269.

[216] I. R. Hardcastle, C. E. Arris, J. Bentley, F. T. Boyle, Y. Chen, N. J. Curtin, J. A. Endicott, A. E. Gibson, B. T. Golding, R. J. Griffin, P. Jewsbury, J. Menyerol, V. Mesguiche, D. R. Newell, M. E. M. Noble, D. J. Pratt, L.-Z. Wang, and H. J. Whitfield. N2-substituted O6-cyclohexylmethylguanine derivatives: Potent inhibitors of cyclin-dependent kinases 1 and 2. *Journal of Medicinal Chemistry*, 47(15):3710–3722, 2004.

[217] T. Steinmetzer and J. Sturzebecher. Progress in the development of synthetic thrombin inhibitors as new orally active anticoagulants. *Current Medicinal Chemistry*, 11(17):2297–2321, 2004.

[218] J. Liang, V. Tsui, A. V. Abbema, L. Bao, K. Barrett, M. Beresini, L. Berezhkovskiy, W. S. Blair, C. Chang, J. Driscoll, C. Eigenbrot, N. Ghilardi, P. Gibbons, J. Halladay, A. Johnson, P. B. Kohli, Y. Lai, M. Liimatta, P. Mantik, K. Menghrajani, J. Murray, A. Sambrone, Y. Xiao, S. Shia, Y. Shin, J. Smith, S. Sohn, M. Stanley, M. Ultsch, B. Zhang, L. C. Wu, and S. Magnuson. Lead identification of novel and

selective TYK2 inhibitors. *European Journal of Medicinal Chemistry*, 67:175–187, 2013.

[219] J. Liang, A. van Abbema, M. Balazs, K. Barrett, L. Berezhkovsky, W. Blair, C. Chang, D. Delarosa, J. DeVoss, J. Driscoll, C. Eigenbrot, N. Ghilardi, P. Gibbons, J. Halladay, A. Johnson, P. B. Kohli, Y. Lai, Y. Liu, J. Lyssikatos, P. Mantik, K. Menghrajani, J. Murray, I. Peng, A. Sambrone, S. Shia, Y. Shin, J. Smith, S. Sohn, V. Tsui, M. Ultsch, L. C. Wu, Y. Xiao, W. Yang, J. Young, B. Zhang, B.-y. Zhu, and S. Magnuson. Lead optimization of a 4-aminopyridine benzamide scaffold to identify potent, selective, and orally bioavailable TYK2 inhibitors. *Journal of Medicinal Chemistry*, 56(11):4521–4536, 2013.

[220] A. Friberg, D. Vigil, B. Zhao, R. N. Daniels, J. P. Burke, P. M. Garcia-Barrantes, D. Camper, B. A. Chauder, T. Lee, E. T. Olejniczak, and S. W. Fesik. Discovery of potent myeloid cell leukemia 1 (mcl-1) inhibitors using fragment-based methods and structure-based design. *Journal of Medicinal Chemistry*, 56(1):15–30, 2013.

[221] D. P. Wilson, Z.-K. Wan, W.-X. Xu, S. J. Kirincich, B. C. Follows, D. Joseph-McCarthy, K. Foreman, A. Moretto, J. Wu, M. Zhu, E. Binnun, Y.-L. Zhang, M. Tam, D. V. Erbe, J. Tobin, X. Xu, L. Leung, A. Shilling, S. Y. Tam, T. S. Mansour, and J. Lee. Structure-based optimization of protein tyrosine phosphatase 1B inhibitors: From the active site to the second phosphotyrosine binding site. *Journal of Medicinal Chemistry*, 50(19):4681–4698, 2007.

[222] H. M. Berman, J. Westbrook, Z. Feng, G. Gilliland, T. N. Bhat, H. Weissig, I. N. Shindyalov, and P. E. Bourne. The protein data bank. *Nucleic Acids Research*, 28:235242, 2000.

[223] K. Lindorff-Larsen, S. Piana, K. Palmo, P. Maragakis, J. L. Klepeis, R. O. Dror, and D. E. Shaw. Improved side-chain torsion potentials for

the AMBER ff99SB protein force field. *Proteins: Structure, Function, and Bioinformatics*, 78(8):1950–1958, 2010.

[224] W. L. Jorgensen, J. Chandrasekhar, J. D. Madura, R. W. Impey, and M. L. Klein. Comparison of simple potential functions for simulating liquid water. *The Journal of Chemical Physics*, 79(2):926–935, 1983.

[225] D. A. Pearlman. A comparison of alternative approaches to free energy calculations. *The Journal of Physical Chemistry*, 98(5):1487–1493, 1994.

[226] S. Wan, P. V. Coveney, and D. R. Flower. Molecular basis of peptide recognition by the TCR: Affinity differences calculated using large scale computing. *The Journal of Immunology*, 175(3):1715–1723, 2005.

[227] B. K. Øksendal. *Stochastic differential equations : An introduction with applications*. Universitext. Springer, Berlin, Heidelberg, New York, 1998. Corrected second printing 2000.

[228] C. Kramer, G. Dahl, C. Tyrchan, and J. Ulander. A comprehensive company database analysis of biological assay variability. *Drug Discovery Today*, 21(8):1213–1221, 2016.

[229] J. D. Chodera and D. L. Mobley. Entropy-enthalpy compensation: Role and ramifications in biomolecular ligand recognition and design. *Annual Review of Biophysics*, 42(1):121–142, 2013.

[230] T.-S. Lee, Y. Hu, B. Sherborne, Z. Guo, and D. M. York. Toward fast and accurate binding affinity prediction with pmemdgti: An efficient implementation of gpu-accelerated thermodynamic integration. *Journal of Chemical Theory and Computation*, 13(7):3077–3084, 2017.

[231] A. P. Bhati, S. Wan, Y. Hu, B. Sherborne, and P. V. Coveney. Uncertainty quantification in alchemical free energy methods. *Journal of Chemical Theory and Computation*, 2018. Just Accepted Manuscript.

[232] S. Jo and W. Jiang. A generic implementation of replica exchange with solute tempering (REST2) algorithm in NAMD for complex biophysical simulations. *Computer Physics Communications*, 197(Supplement C):304–311, 2015.

[233] G. J. Rocklin, D. L. Mobley, K. A. Dill, and P. H. Hünenberger. Calculating the binding free energies of charged species based on explicit-solvent simulations employing lattice-sum methods: An accurate correction scheme for electrostatic finite-size effects. *The Journal of Chemical Physics*, 139(18):184103, 2013.

[234] M. A. Olsson, A. T. García-Sosa, and U. Ryde. Binding affinities of the farnesoid X receptor in the D3R grand challenge 2 estimated by free-energy perturbation and docking. *Journal of Computer-Aided Molecular Design*, pages https://doi.org/10.1007/s10822–017–0056–z, Sep 2017. online article.

[235] C. Lozzio and B. Lozzio. Human chronic myelogenous leukemia cell-line with positive Philadelphia chromosome. *Blood*, 45(3):321–334, 1975.

[236] J. Zhang, P. L. Yang, and N. S. Gray. Targeting cancer with small molecule kinase inhibitors. *Nature Reviews Cancer*, 9(1):28–39, 2009.

[237] T. O'Hare, C. A. Eide, and M. W. Deininger. Bcr-Abl kinase domain mutations, drug resistance, and the road to a cure for chronic myeloid leukemia. *Blood*, 110(7):2242–2249, 2007.

[238] S. G. Deeks, M. Smith, M. Holodniy, and J. O. Kahn. HIV-1 protease inhibitors: A review for clinicians. *JAMA*, 277(2):145–153, 1997.

[239] S. K. Sadiq, D. Wright, S. J. Watson, S. J. Zasada, I. Stoica, and P. V. Coveney. Automated molecular simulation based binding affinity calculator for ligand-bound HIV-1 proteases. *Journal of Chemical Information and Modeling*, 48(9):1909–1919, 2008.

[240] S. Redaelli, L. Mologni, R. Rostagno, R. Piazza, V. Magistroni, M. Ceccon, M. Viltadi, D. Flynn, and C. Gambacorti-Passerini. Three novel patient-derived BCR/ABL mutants show different sensitivity to second and third generation tyrosine kinase inhibitors. *American Journal of Hematology*, 87(11), 2012.

[241] D. Groen, A. P. Bhati, J. Suter, J. Hetherington, S. J. Zasada, and P. V. Coveney. Fabsim: Facilitating computational research through automation on large-scale and distributed e-infrastructures. *Computer Physics Communications*, 207(Supplement C):375–385, 2016.

[242] *https://github.com/djgroen/FabSim*.

[243] *https://blog.sciencemuseum.org.uk/supercomputer-bid-to-create-the-first-truly-personalised-medicine*.

[244] S. Lovera, L. Sutto, R. Boubeva, L. Scapozza, N. Dlker, and F. L. Gervasio. The different flexibility of c-src and c-abl kinases regulates the accessibility of a druggable inactive conformation. *Journal of the American Chemical Society*, 134(5):2496–2499, 2012.

[245] W. L. Jorgensen, J. K. Buckner, S. Boudon, and J. T. Rives. Efficient computation of absolute free energies of binding by computer simulations. Application to the methane dimer in water. *The Journal of Chemical Physics*, 89(6):3742–3746, 1988.

[246] M. Aldeghi, A. Heifetz, M. J. Bodkin, S. Knapp, and P. C. Biggin. Accurate calculation of the absolute free energy of binding for drug molecules. *Chemical Science*, 7:207–218, 2016.